北海道工業開発試験所報告

REPORTS OF THE GOVERNMENT INDUSTRIAL DEVELOPMENT LABORATORY, HOKKAIDO

第23号　　昭和56年3月

目　　次

工業技術院

北海道工業開発試験所

HDOによる水吸着系の赤外研究
Ⅳ. La-Y型ゼオライト

日野雅夫・平間康子

1. 緒　　言

著者らは，これまでのHDOによる水吸着系のの赤外による一連の研究[1)~3)]において，Na-X，Y，A型ゼオライト及びZn-Y型ゼオライトの水吸着系スペクトルを解析し，各吸収帯の帰属ならびに吸着水の状態とそのサイトの種類について考察を行ってきた。第Ⅱ報[2)]において，共通な1価カチオン，Na^+を含み，類似した結晶構造を持つNa-XとNa-Y，及び結晶構造を異にするNa-Aゼオライトの吸着系スペクトルとそれらの結晶構造を比較検討し，TypeⅠの吸吸着水はサイトSⅢ，TypeⅡのそれはサイトSⅡにそれぞれ存在するNaイオンに吸着しているのであろうと推定した。しかし，第3報[3)]に示されたように，Na^+を含まず，またサイトSⅡにはカチオンが存在しないとされているZn-Yの系にも，TypeⅠ吸着水が見られた。

本報は，3価カチオン置換Y型ゼオライトの一例であるLa-Yの系について解析し，そのスペクトルの帰属を行うとともに，これまで得られた各種ゼオライトの系についての結果と比較検討することにより，吸着水のサイトについて，統一的な説明を試みることを目的としている。

2. 実験方法

2・1　試薬，試料および実験操作

La-Y：前報[3)]のと同一のLinde Molecular Sieves SK-40，20gに$LaCl_3\cdot 7H_2O$の10%水溶液（完全に溶解させるため少量の塩酸を加えpH＝5.3とした）400mlを加え、これを80℃で48h加熱撹拌する操作を新しい$LaCl_3$溶液と交換しながら3回くり返した。その後Cl^-イオンが検出されなくなるまで脱イオン蒸留水で洗浄した。

Laの定量分析：得られたLa-Yのイオン交換率を求めるため，蛍光X線分析法でLaの定量分析を行った。標準試料として既知量のLa_2O_3を一定量のSK—40に混合したものをつくり．LaのLα線（82.935°）を用いて検量線を作成した。その際，測定試料錠剤の作成条件などの不一致によるピーク強度のばらつきは，試料に含まれるSiのピーク強度を規準として補正した。このようにして得られた検量線は原点を通る直線となった。この検量線を用いてLa-Yを分析した結果，La/La-Y＝0.1647g/gが得られた。この値を，SK—40中のNaイオン3個につき1個のLaイオンが置換するものとして計算される値と比較した結果，SK—40のNaはほぼ93%，Laと置換していることがわかった。なお，試料中の水分量は，別に500℃排気により実測した重量減少量25%とした。

X線回析：得られた試料のX線回析を測定した結果，Y型ゼオライトの結晶構造が完全に保たれており，また結晶性は極めて良好であることが確認された。

HDO吸着系の測定：HDO吸着系のOH伸縮領域の測定には$H_2O:D_2O$＝1：5モル比の混合水（この組成は，およそ$H_2O:HDO:D_2O$=1：10：25）を用い，OD領域の測定には$H_2O:D_2O$＝7：1混合水（$H_2O:HDO:D_2O$=49：14：1）を用いた。

赤外吸収スペクトルの測定：DIGILAB，FTS-15B型を用いた。

その他の試薬，実験操作法は前報[3)]と同じであった。

3. 実験結果

3・1・吸着過程のスペクトル

3・1・1　H_2O, D_2O 系

Fig.1および2に，それぞれH_2O及びD_2Oの吸着過程のスペクトル変化を示した。図に見るように，水（H_2O, D_2O)の吸着によってOH(D)伸縮領域にはb，c，d，f，gの5本の吸収が，またOH変角領域には，h，jの2本の吸収が現われた。b，c，d，f，gの各吸収は，H_2O

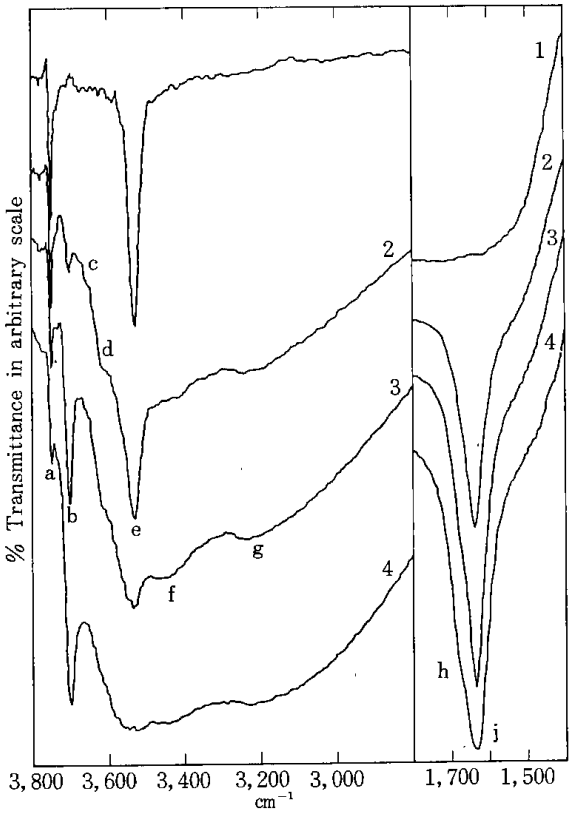

Fig. 1 Spectra of the H_2O system in the adsorption process

[1] Evacuated at 500°C for 3h. [2] 10.0, [3] 19.9, [4] 39.9 ml (stp)/g of H_2O vapor were readsorbed. Sample piece thickness 10mg/cm². Spectra were obtained by rationing the observed spectra against that of the LaY-D_2O system after 500°C evacuation.

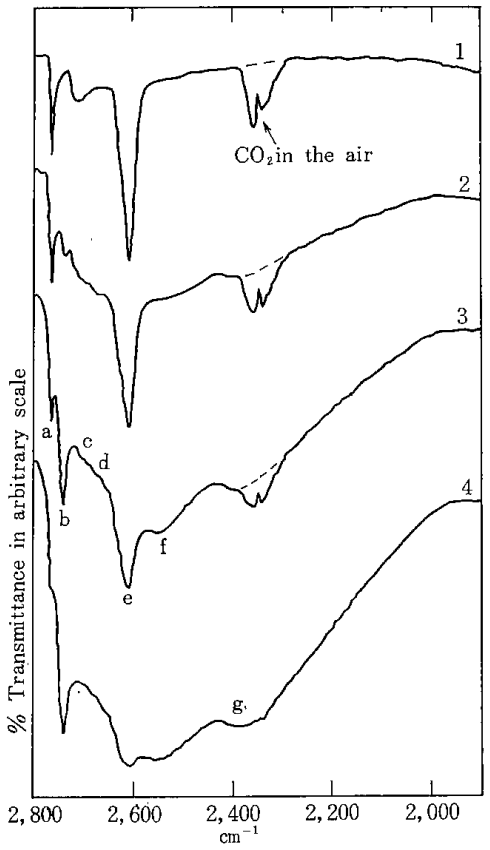

Fig. 2 Spectra of the D_2O system in the adsorption process.

[1] Evacuated at 500°C for 3h. [2] 8.6, [3] 17.2, [4] 34.4 ml (stp)/g of D_2O vapor were readsorbed. Sample piece thickness 10 mg/cm². Spectra were obtained by rationing the observed spectra against that of the LaY-H_2O system after 500°C evacuation.

系及びD_2O系におけるそれらの吸収の波数値の比が，およそ1.36であることから，それぞれに対応させ得るものであり，すべてOH(D)振動によるものである。a吸収は前報[1)~3)]に示したように，ゼオライトに不純物として含まれるSiO_2の構造OH基によるものである。吸収eについては，これまで多くの研究があり，ゼオライト格子の酸素O_3に形成されたO_3-Hによるもの[4),5)]あるいはO_2-H，O_3-H，O_4-Hが関与しているものとされている[6)]。

吸収帯の実測波数値を，他の系のそれらとともにTable 1に示した。

3・1・2 HDO系

Fig. 3にHDO吸着系のOD伸縮および変角領域のスペクトルを示した。D_2O系のスペクトルと比較すると，明らかにg吸収が消失していることがわかる。この事実は前報[1),2)]で見られたH_2O

Table 1. Summery of the IR bands of La-Y zeolite-water system

Band sign	D_2O system (cm^{-1})	H_2O system (cm^{-1})	HDO system (cm^{-1}) Stretching regions OD	OH	Deformation region
		[in the adsorptin process]			
a	2763	3748	2763	3748	
b	2740	3700	2716	3695	
c	2700	3655	2698	?	
d	2667	3610	?	?	
e	2610	3535	2610	3535	
f	2550	3450	2550	3470	
g	2380	3200	—	—	
h		1675			
j		1638			
k					1460
l					1426
		[in the desorption process]			
a	2763	3748	2763	3748	
b	2740	3698	2716	3695	
c	2710	?	2710	3655	
d	2685	3620	2685	3610	
e	2610	3535	2610	3535	
f	2550	?	2550	3470	
g	2380	3200	—	—	
h		1675			
j		1638			
k					1460
l					1426
m					1440
n	2520	3400	2530	3400	

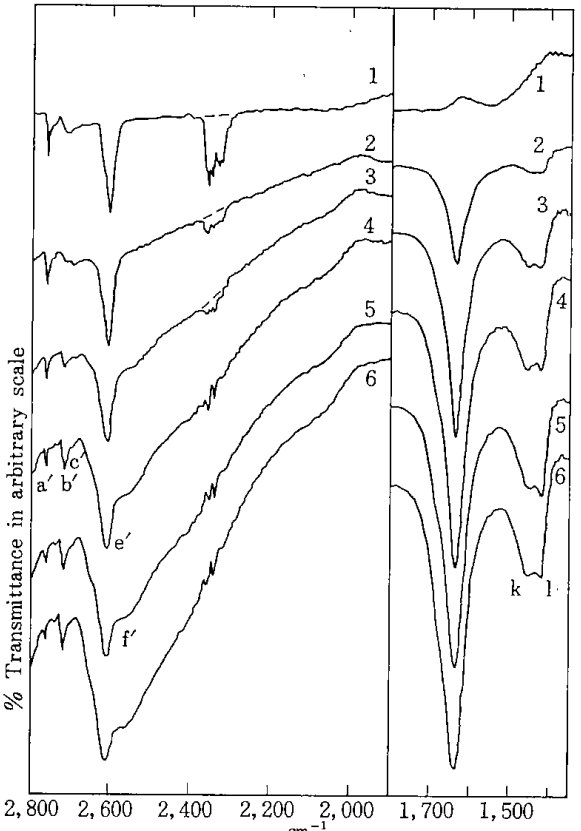

Fig. 3 Spectra in the OD stretching and deformation regions of the HDO system in the adsorption process.

[1] Evacuated at 500°C for 1h. [2] 8.9, [3] 17.8, [4] 26.7, [5] 35.5, [6] 44.4 ml(stp)/g of the vapor of H_2O-D_2O 7 to 1 mixed water were readsorbed. Sample piece thickness 10 mg/cm². Spectra were obtained by rationing the observed spectra against that of the sample after 500°C, 3h, evacuation.

系の3,200cm⁻¹近辺，D_2O 系2,400cm⁻¹近辺の吸収についての結果と同一であり，同様に吸着水の変角振動 h，j の倍音であることがわかる。b 吸収も前報[1)~3)]での相当する吸収と同様に低波数シフト (24cm⁻¹) を示し，2,716cm⁻¹ に現われた (b′)。c′ は c と同一波数を示しており，構造 OH によるものである。d に対応する吸収は認められない。a′，e′ は D_2O 系の対応する吸収 a，e とまったく同一波数を示しており，3・1・1 に述べた帰属が支持される。

変角振動領域には，明らかに2本の吸収（k，l）が認められ，この2本の吸収の相対的強度比は吸着量に依存せず，ほぼ一定していることがわかる。2,080cm⁻¹近辺の微弱な吸収は，Na-X および Na-A[1)] の HDO 系で，それぞれ2,120，2,140cm⁻¹ に見られたものと同種のものであり，共存する吸着 H_2O の何らかの結合音によるものであろう。

3・2 脱離過程のスペクトル

3・2・1 D_2O 系

Fig. 4 に D_2O 吸着系の脱離過程におけるスペクトル変化を示した。伸縮領域の b 吸収が，90℃，1.5h の排気でほぼ完全に消失しているのがわかる。同時に，2,550 cm⁻¹ に極大を特つ f 呼吸が強度減少を示し，その結果 2,520cm⁻¹ 近辺に極大を示し，2,800cm⁻¹ から2,000cm⁻¹ に至る巾の広い吸収 (n) が存在しているのが認められる。

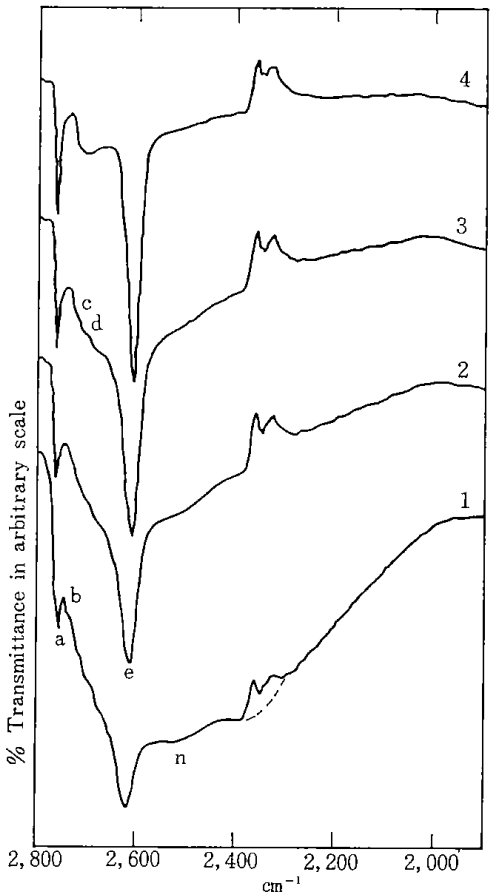

Fig. 4 Specta of the D_2O system in the desorption process.

Evacuated at [1] 90°C for 1.5h, [2] 200°C for 1h, [3] 300°C for 45 min, [4] 500°C for 1h after exposure to the D_2O vapor. Sample thickness 10mg/cm². Spectra were obtained by rationing the observed spectra against that of the La Y-H_2O system after 500°C evacuation.

3・2・2 HDO 系

Fig. 5 は HDO 系の脱離過程における OD 伸縮及び変角振動領域のスペクトルである。変角領域中の 1,640 cm⁻¹ 近辺の吸収（h，j）は共存する

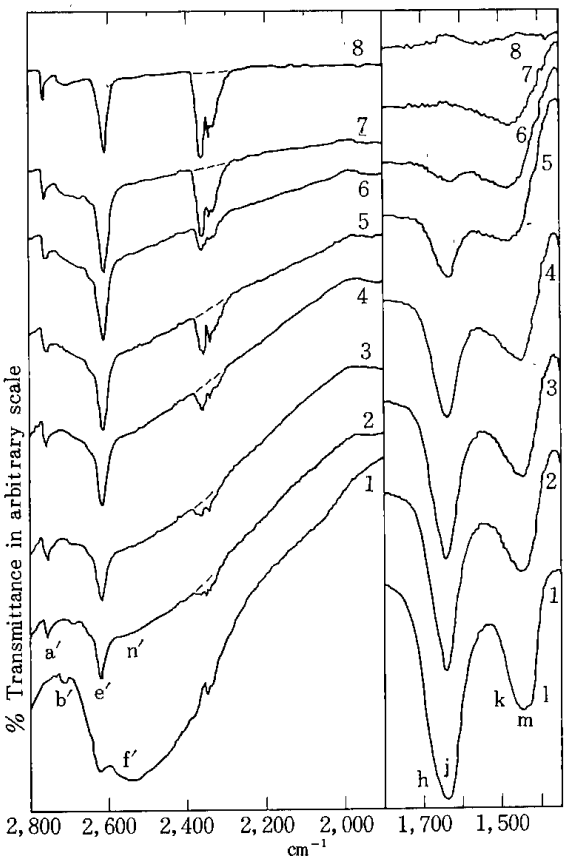

Fig. 5 **Spectra in the OD stretching and defomation regions of the HDO system in the desorption process.**

Evacuated at [1] room temperature for 15 min, [2] 90° C for 15 min, [3] 90° C for 45 min, [4] 120° C for 1 h, [5] 165° C for 30 min, [6] 200° C for 1 h, [7] 300° C for 45 min, [8] 500° C for 1 h after exposure to the vapor of the H_2O-D_2O 7 to 1 mixed water. Sample piece thickness 10 mg/cm². Spectra were obtained by rationing the observed spectra against that of the sample after 500° C, 3 h, evacuation.

H_2Oによるものであり，1,440cm^{-1}近辺のそれら(k, m, l）がHDOによるものである。90℃排気により，D_2O系の場合と同様にb′が完全に消失し，f′の強度が減少し，2,530cm^{-1}近辺に極大を持つと見られる巾の広い吸収（n′）が現われている。HDO変角領域では，室温排気でh，lの中間の位置に明らかにもう1本の吸収m（1,440cm^{-1}）があることがわかる。加熱排気により，これらの吸収のうちk，lが比較的優先的に消失し，mが残留していくのが特徴的である。また、その際共存するH_2Oによる吸収では1,675cm^{-1}近辺の膨らみ（h）が消失し，対称性の良いただ1本の吸収（j）に変化していくのがわかる。3・1・2ではdに対応するd′吸収が認められなかったが，ここでは，d′がdと同波数の位置に認められた。

4. 考　　察

La-Yの水吸着系にも，吸着型の異る2種類の吸着水のあることが明らかである。その1つは，吸収b，f，h（HDO系ではb′，f′，及びk，l）を与えるものであり，これは前報[1)~3)]で見られているType Ⅰの吸着水と同種のものである。他の1つは，nとj（n′とm）を与えるもので，同じく前報でのType Ⅱ（C_{2v}）に類似したものである。吸収nは，たぶん巾の広いν_3とν_1振動が重なっているのであろう。

さきに[2)]，Type Ⅰの吸着水はゼオライト結晶構造を構成するソーダライト構造の4員環の中心（サイトSⅢ）に位置するNaイオンに吸着しているのであろうと示唆した。しかし，第Ⅲ報で示したように，Zn-Yの系にもこの型の吸着水のあることが明らかであり，また本報でLa-Y系についても同様であることがわかった。

本報で用いたYゼオライト(Si/Al=2.3)に含まれるカチオンの数は，1価の場合結晶構造1ユニットセル当り58個であり，Rabo ら[7)]にしたがえば，これらのカチオンは3種類のサイトSⅠ，SⅡ，SⅢにおのおの16，32，10個ずつ位置していることになる。このイオンが多価イオンと交換される際，電気的中性を保つためにイオン数は交換イオンの電荷に応じて減少する。すなわち，2価イオンでは1/2に，3価イオンでは1/3になる。これらのイオンは3種類のサイトのうち，エネルギー的に安定な方から順に，つまりSⅠ，SⅡ，SⅢの順に，配置される。ただし，SⅠは16，SⅡは32で満席である。この機構にしたがってイオン交換されるものとすれば，Zn-YのカチオンはSⅠに16個，SⅡに13個存在し，SⅢは空席となる。La-YではSⅠに16，SⅡに3個，SⅢは同じく空席になる。

われわれが用いたZn-Y，La-Yはイオン交換率がそれぞれ98%，93%であった。この場合，1ユニットセル当りZn-Yでは1個の，La-Yでは4個のNaイオンが未交換のまま残されていることになる。Na-Yの3種類のサイトを占めるカチオンについての交換の難易性の順位は明らかではない。しかし，SⅢより安定であるとされるSⅡに

は空席が，Zn-Yでは19個，La-Yでは29個残されている。したがって，このカチオンの多くはたぶんSⅡにあり，一部はSⅠに残されている可能性もあるものと考えられる。このように，用いたZn-YおよびLa-YのSⅢは，空席になっているものと考えて良いであろう。

さきに，Na-X，Na-YではType Ⅰ吸着水がSⅢに位置するNa^+イオンに吸着しているものとして良く説明がついたが，同じ型の吸着水が明らかに認められるZn-Y，La-YではSⅢにNa^+イオンもその他のカチオンも存在しない。この矛盾は以下に述べるように，Zn-Y，La-Yの場合はこの吸着水が空席のSⅢに位置していると考えると説明がつく。

まず，きわめて非対称的な点で特異なこの吸着水の形態は，吸着サイトの幾可学性によるものであろう。そうするとNa-X，Na-Yの場合にこの吸着サイトはSⅢ—この場合そこにはNa^+イオンが存在するが—であると考えられたのでZn-Y，La-Yの場合もAl，Si特にOの位置関係がSⅢと同等な幾可学性を持つ位置であろうと考えられるが，Y型ゼオライトには，そのような位置はこのカチオンサイトSⅢ以外にはない。

Type Ⅰ 吸着水がSⅢに位置しているものとすると，1価カチオン型X，Yゼオライトの場合，そこに存在するカチオンの数および電気的性質の影響が，直接的にその吸着水に現われても良いはずである。第Ⅱ報において，90℃排気後に残留するType Ⅰ吸着水による吸収の強度が，Na-XおよびNa-Y吸着系において，それらのSⅢに位置すると考えられるNaイオンの数の比に，ほぼ見合うことを示した。Ward[4]は，一連のY型ゼオライトについてH_2O吸着系のIRによる研究を報告している。その中で，本報のb吸収に相当する吸収がすべての1価および2価カチオン型ゼオライトで，H_2Oの再吸着時に認められることを示しているが，1価カチオン型の場合その波数はカチオンによって大巾に異なり，かつカチオンのイオン化ポテンシャルおよびイオン半径との間に直線関係のあることを見出している。

一方，多価カチオン型の場合は，SⅢにはカチオンが存在しないので，カチオンの影響を直接的には受けないであろう。2価カチオンゼオライトの場合，Wardはこの吸収の波数には1価カチオン型で見られたようなカチオンへの著しい依存性は見られないことを示している。すなわち，1価カチオン型では最高値が3,718cm^{-1} (Li,第1イオン化ポテンシャル5.39eV，イオン半径0.73Å)，最低値は3,640cm^{-1} (Cs，3.89eV，1.84Å)であったのに対して，2価型ではそれぞれ3,700cm^{-1} (Ba，第2イオン化ポテンシャル10.00eV，1.50Å)，3,688cm^{-1} (Mg，15.00eV，0.63Å)であり，イオン化ポテンシャルならびにイオン半径に大きな差があるにもかかわらず，波数差はわずかに12cm^{-1}の範囲内にあった。波数とカチオンの性質間にも顕著な相関性は認められず，またイオン化ポテンシャルに対してプロットした点は1価カチオンで見られる直線から大きくはずれている。次に，この吸着水が空席のSⅢに吸着しているものとすれば，3価カチオン型ゼオライトにも，その吸収が現われるはずである。Wardは1種類の稀土類置換ゼオライトについても測定しており，そこでは，bに相当する吸収が認められない。しかし本報で示したように，La-Yでも明らかにこの吸収の現われることが確認された。その波数値は3,700cm^{-1}であったが，La^{3+}イオンの電気的性質が1価，2価カチオンと著しく相違することを考慮するならば，この波数値はLa^{3+}イオンの性質を直接的に反映しているものとは考えられない。つまり，この場合もType Ⅰ吸着水との相互作用は2価カチオンの場合と同様に二次的なものであろう。

著者らが，さきに示したように，Na-X，Na-Yでは90℃排気後，この吸着水はかなりの量残留したが，Zn-Y，La-Yでは同条件の排気でほとんど残らなかった。この事実は，空席の場合，吸着力に大きく関与するものは格子酸素原子に局在する陰荷電であり，そこにカチオンが存在する場合は，さらに局在する陽荷電が加わるためであろう。

Wardはb吸収が吸着水によるものと考えてはいるが，それに対応して観測されるはずのν_1振動の帰属はしておらず，本報のf，gに相当する吸収は，それぞれ異なった格子酸素原子上のOH基，あるいは異なったサイトに位置するカチオンへの吸着水によるものとしている。また，1価カチオン型と2価カチオン型ゼオライトに見られるb吸収は，カチオンの性質への依存性の程度の違いから必ずしも同じ型の吸着水とは考えていない。著者らはこれまで示した結果と考察から，この吸収はすべて同種の吸着水，Type Ⅰ，のν_3振動であ

り，この吸着水はサイトSⅢに位置しているものと考える。

Type Ⅱ吸着水については，対称性が同じくC_{2v}である点でこれに類似したNa-X，Na-Y，Na-Aにおける吸着水が，SⅡに位置しているのであろうと前報で示唆した。この吸着型は，Type Ⅰの場合と同様に，サイトの幾何学性に依存するものと考えられるので，La-Y及びZn-Yにおける Type Ⅱ吸着水も同じくSⅡに位置するものと推定することができる。そのように考えると，SⅡには，いずれのゼオライトにおいてもカチオンが存在するので，その影響が現われてもよいはずである。また，Type Ⅰ吸着水とType Ⅱ吸着水との間に，Zn-Y及びLa-Yではかなりの相違があってもよいはずであり，一方Na型ゼオライトでは，それほど著しい差異はなくてもよいはずである。Type Ⅱ吸着水によるH_2O変角振動において，Na-X系では1,650cm^{-1}，Na-Y 1,645cm^{-1}，Zn-Y 1,610cm^{-1}，La-Y 1,638cm^{-1}とNa型ではほぼ等しく，1価～多価カチオン型間には明らかな相違が見られた。また，H_2O吸着系スペクトルにおいて，Na-X，Na-Yでは変角振動がただ1本(Type ⅠとType Ⅱによるそれらが，ほぼ同波数で重なっている)であったが，Zn-Y，La-Yでは明らかに波数の異なる2本の吸収が認められた。しかし，HDO系の変角振動では，Zn-YとLa-Y間に相違があるが，Na-YとLa-Yではほぼ一致しており，カチオンの性質との相関は不明である。Type Ⅱ吸着水の吸着サイトを明らかにするには，さらに多くのデータを必要とするであろう。

Literature cited

1) Masao Hino, Bull. Chem. Soc. Jpn., **50**, 574 (1977)
2) Masao Hino and Yasuko Mikami, Bull. Chem. Soc. Jpn., **52**, 2099 (1979)
3) 日野雅夫，平間康子，北海道工業開発試験所報告，No.19, p.19 (1979)
4) J. W. Ward, J. Phys. Chem., **72**, 4211, (1968)
5) J. W. Ward, J. Phys. Chem., **73**, 2086, (1969). J. W. Ward and R. C. Hansford, J. Catalysis, **13**, 364 (1969)
6) P. A. Jacobs and J. B. Uytterhoeven, J. Chem. Soc. Faraday Trans. Ⅰ, 359 (1973)
7) J. A. Rabo, C. L. Angell, P. H. Kasai and Verner Schomaker, Chem. Eng. Prog. 63 Symposium Series, No. **73**, 31 (1967)

Infrared Studies on Water Adsorption Systems with the Use of HDO. Ⅳ. La-Y Zeolite

Masao HINO and Yasuko HIRAMA

Infrared spectra of the adsorption systems of La-Y zeolite, one of trivalent cationic Y zeolite, with H_2O, D_2O and HDO were measured in the adsorption and desorption processes. The results showed that there were two types of adsorbed water analogous to those on the systems of other types of Y zeolite. One of them which gives bands at 3700, 3450 and 1675cm^{-1}, is of the asymmetric type, Type Ⅰ. The other, giving bands at ca. 3400 and 1638 cm^{-1}, is of the symmetric mode, Type Ⅱ. It was concluded that the present Type Ⅰ water as well as that of on the Zn-Y system was adsorbed on the vacant cation site SⅢ, while those of the Na type zeolites are adsorbed on the similar site on which the cations are situated. Other bands at 3748, 3655, 3610 and 3535 cm^{-1} were assigned to be arisen from the structural OH groups of the zeolite.

PRODUCTION OF HIGH QUALITY ADSORBENTS FROM TROPICAL PLANTS

TABLE OF CONTENTS

I. Production of Powdered Activated Carbon

A series of basic experiments on the production of activated carbon from tropical woods including a wood waste was carried out using fluidized bed reactors. The raw materials selected by NIST, the counter part institute, from the view point of utilization of unutilized woods and wood wastes consist of 12 species of woods and a coconut's waste (Coir-Dust). The production process employed includes (1)preparation of samples, (2) carbonization of samples, and (3) activation of the chars under an atmosphere of super heat steam. The screened raw materials of particle size ranging from 0.25mm to 2.0mm were used for the tests. The sample which was initialy fed into an inner heat type reactor in which temperature was held at approximetely 420°C with an electric heater began to evolve heat by the exothermic decomposition so that successively fed sample could be carbonized with the heat without any other heat source. All of the chars were activated batch wise in an external heat type reactor to know the characteristics of the reaction and of the activated products. A comparative activation test was carried out in an inner heat type reactor using a selected char. The adsorptive capacities of the activated products from both reactors attained maximum values at the yield rate of approximetely 30% under temperature ranging from 800°C to 900°C. These values, which are as high as commercialized carbons were as follows: internal surface area, 1000-1500m^2/g; methylene blue adsorptive value, 270-370 mg M.B./g products; iodine adsorptive value, 1000-1200mg/g. It was found from the results of the study that the fluidized bed process showed the following advantages for the production of high quality adosorbents from tropical woods: (1) The successful carbonization in the inner heat type reactor indicates that considerable saving in energy consumption could be realized as with other external heat type reactors. (2) The methylene blue adsorptive value for the different particle sizes of the activated products are almost the same. This indicates that the fluidized bed can produce more uniform products. (3) The chars and the activated products were both obtained within 45 minutes using the respective fluidized bed reactors. Other existing processes, rotary kiln for example, require at least several hours for each products. Thus, the fluidized bed offers great advantages however, further research and development on a polwt scale should be done for the practical application of the results.

Part 1. Carbonization Step

Kazuhiko NIIKAWA, Hideo HOSODA

1 1 Raw Materials

The raw materials were selected by NIST and consist of 12 wood species including coconut's waste (Coir-Dust) as listed in Table 1.

1 2 Analytical Procedure

The analytical methods employed were in accordance with the Japan Industrial Standard (JIS) procedure or with slight modification thereof.

1) Proximate analysis :

Moisture and ash content, volatile combustible materials and fix carbon in the raw materials, chars and activated carbon products were determined.

Table 1. Wood Species

Common names	Botanical names
Apitong	Dipterocarpus grandiflorus Blanco
Mayapis	Shorea squamata (Turez) Dyer.
Tangile	Shorea polysperma (Blanco) Merr.
Palosapis	Anisoptea thurifera (Blanco) Vid.
Bagtikan	Parashorea plicate Brandis
Yakal	Shorea astylosa Foxw.
Malabayabas	Tristania decorticate Merr.
Kaatoan Baugkal	Anthocephalus chinensis Lamk
Bakauan	Rhizophara
Ipil-Ipil	Istsia bejuga (Coleber.) O. Ktze.
KaKauate	-
Coconut	Cocus hucitera

Sample Preparation

All raw materials were chipped, crushed and screened to obtain small particle sizes ranging from 0.25mm to 2.0mm, the optimum particle size range for fluidizing bed. The screened samples were dried in a drying oven at 105°C for 24 hours.

Carbonization Process

Carbonization of the dried samples was carried out in a continuous fluidized bed reactor as shown in the schematic diagram in Figure 1.

The reactor, made of stainless steel with 155mm diameter and 750 mm in height has a screw feeder which can control feed velocity of the sample automatically to keep constant temperature in the reactor and an agitator at a rotation speed of 16 rpm.

Air is fed into the reactor with a blower which can control feed velocity automatically and flows up through a perforated plate with a perforation ratio of 0.5% located just below the screw feeder. In the beginning of the carbonization, suitable amount of sample was perviously fed into the reactor to make a fixed bed with a height nearly double that of the bed's diameter and then is heated with an electric heater fixed at the external surface of the reactor. When the temperature of the bed rises to nearly 400°C, sample begins to decompose and reacts rapidly with oxygen in the air to produce heat enough to carbonize the sample without any other heat source, so carbonization proceeds continuously at an almost constant temperature by varying feed rate of sample.

Table 2. Proximate Analysis of Wood Materials

Sample Spicies	Moisture (wt.%)	Ash (wt.%)	VCM (wt.%)	FC (wt.%)
Malabayabas	11.16	0.41	77.72	10.72
Kakauate	10.72	0.87	75.92	12.49
Bakauan	10.66	1.12	74.30	13.92
Coir-Dust	15.93	6.44	53.97	23.66
Ipil-ipil	21.07	0.28	71.18	7.47
Mayapis	12.48	0.03	80.10	7.39
K. Bangkal	11.68	0.76	77.18	10.37
Apitong	7.41	3.69	23.94	66.96
Kakauate	6.88	6.08	20.45	66.59
Palosapis	7.28	3.87	18.75	70.10
Tangile	9.42	1.46	24.90	64.22

VCM : Volatile Combustible Matter FC : Fixed Carbon

EXPERIMENTAL RESULTS AND DISCUSSION

1•5 Characteristics of Raw Materials

Table 2 shows the result of proximate analysis of the prepared raw materials. Most of the samples showed common characteristics as in other wooden materials; low ash and fixed carbon contents and high volatile matter and moisture contents.

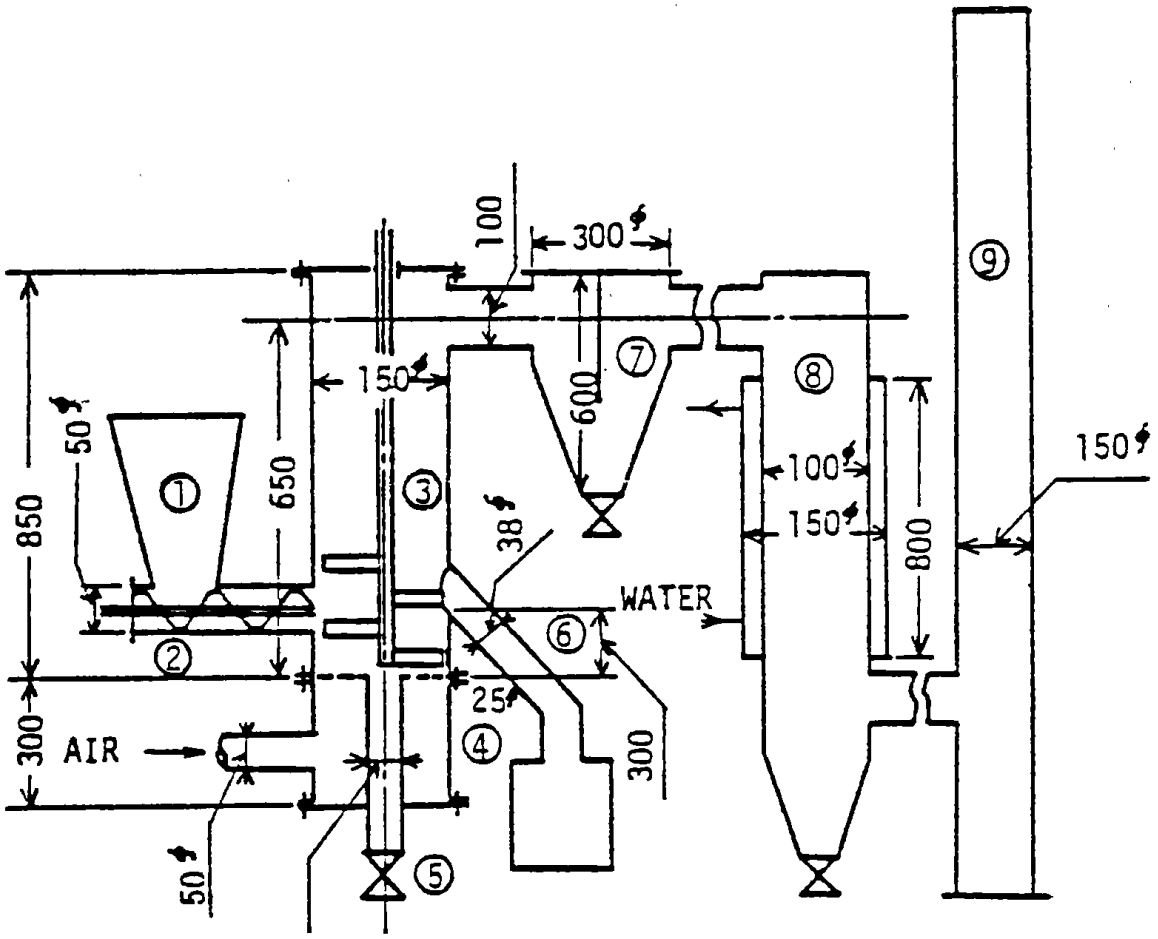

1 - Hopper
2 - Screw feeder
3 - Stirred fluidized bed
4 - Perforated plate
5 - Char take-off valve
6 - Over flow pipe of char
7 - Dust collector
8 - Heat exchanger
9 - Stack

Fig. 1. Inner Heat type Continuous flow Reactor for Carbonization

Change in sample weight with increase in temperature was measured using a thermal balance and a typical curve plotting the value of derivative of weight [w] with respect to temperature [t] is shown in Figure 2·1 — 2·9.

Area of sharp curve divided by the temperature range from nearly 200°C to 400°C corresponds to the amount of the volatile matter which consists mainly of primary tars reacting with oxygen rapidly to produce heat. Therefore, it is considered that optimum carbonization temperature is in the range of slightly beyond the highest peak when an inner heat type reactor is employed.

According with the weight decrease curves, carbonization temperature was established to be between 420°C and 430°C for all the chars, which could be carbonized successfully in the continuous fluidized bed reactor as shown in Table 3. The yield rate of chars was in the range from 10% to 20% except for Coir-Dust, (30%).

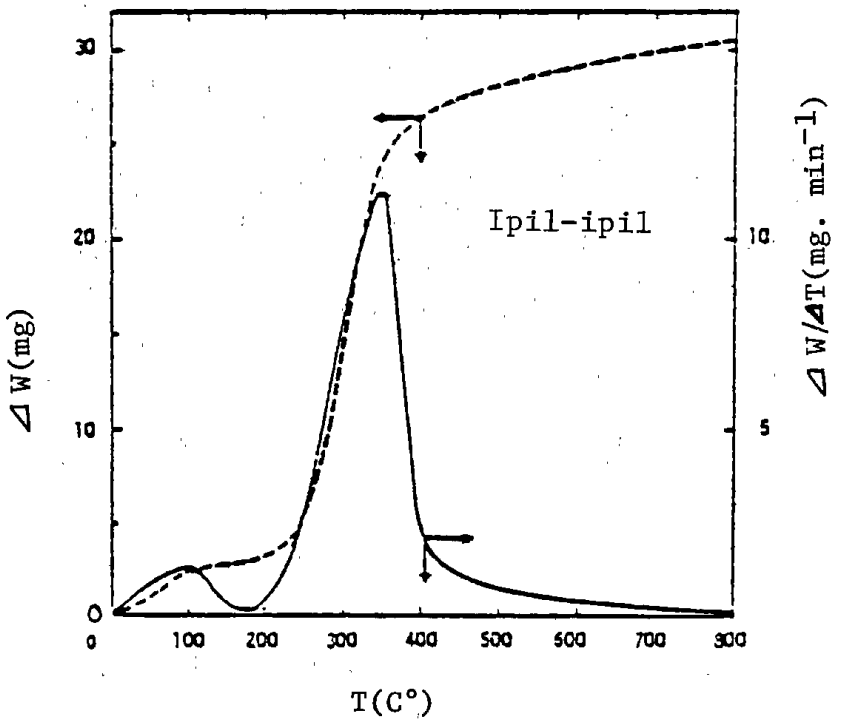

Fig. 2·1 Typical curve of Thermo Gravimetry for the Raw Materials.
Solid line is plot of slope of dotted line.

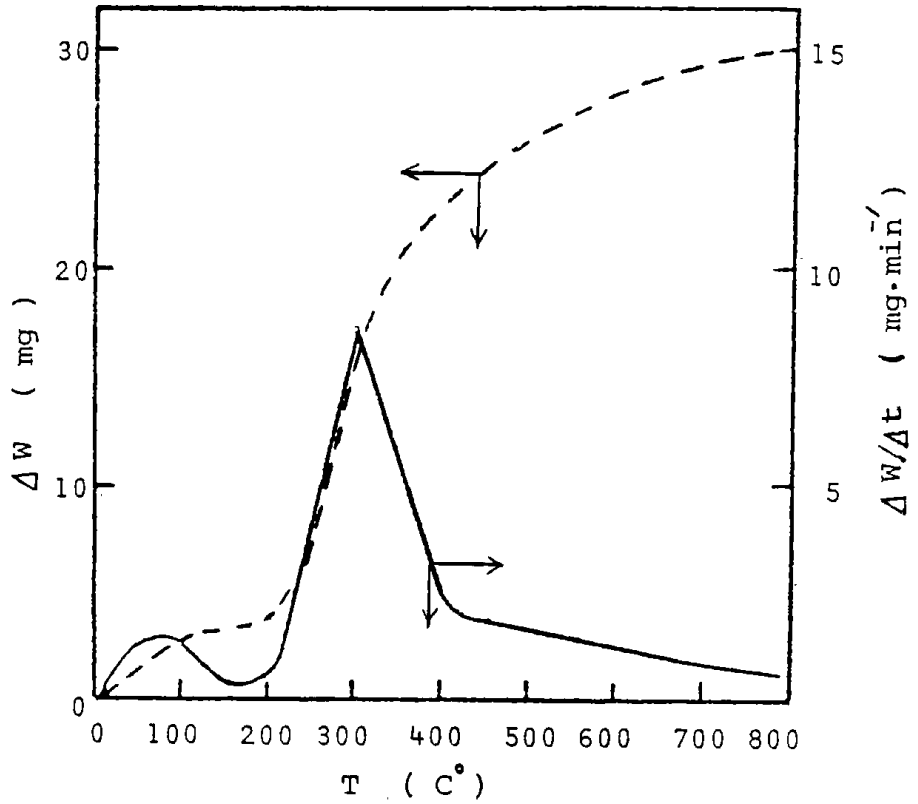

Fig. 2•2 T.G. Curve of Kaatoan-Bangkal

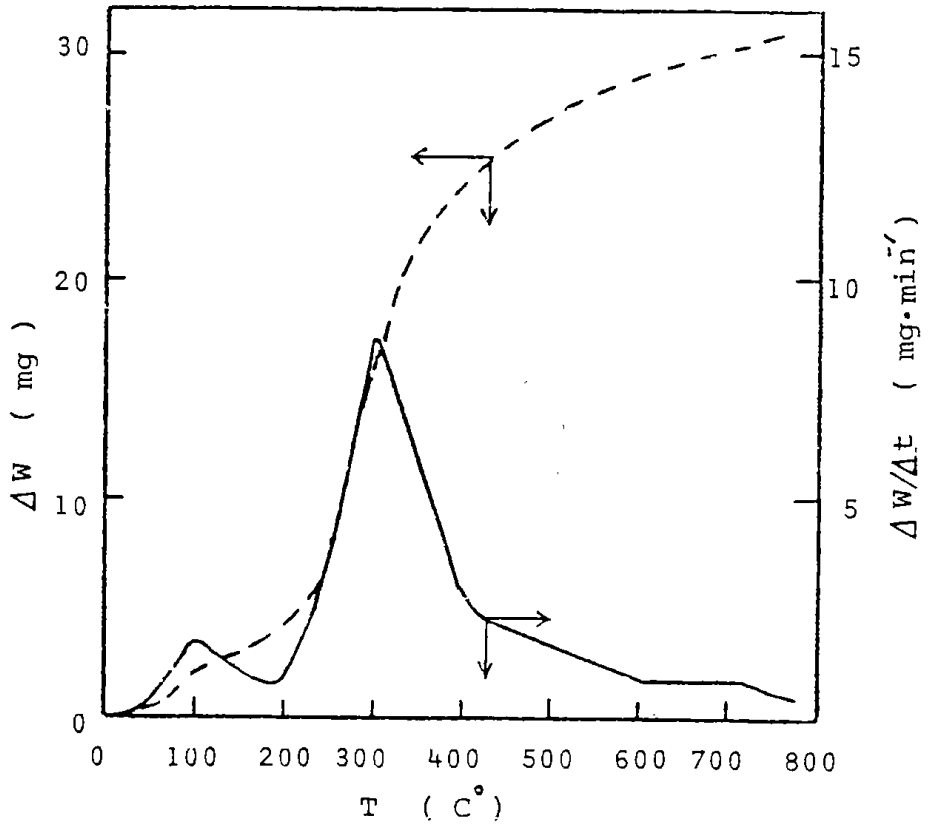

Fig. 2•3 T.G. Curve of Kakauate

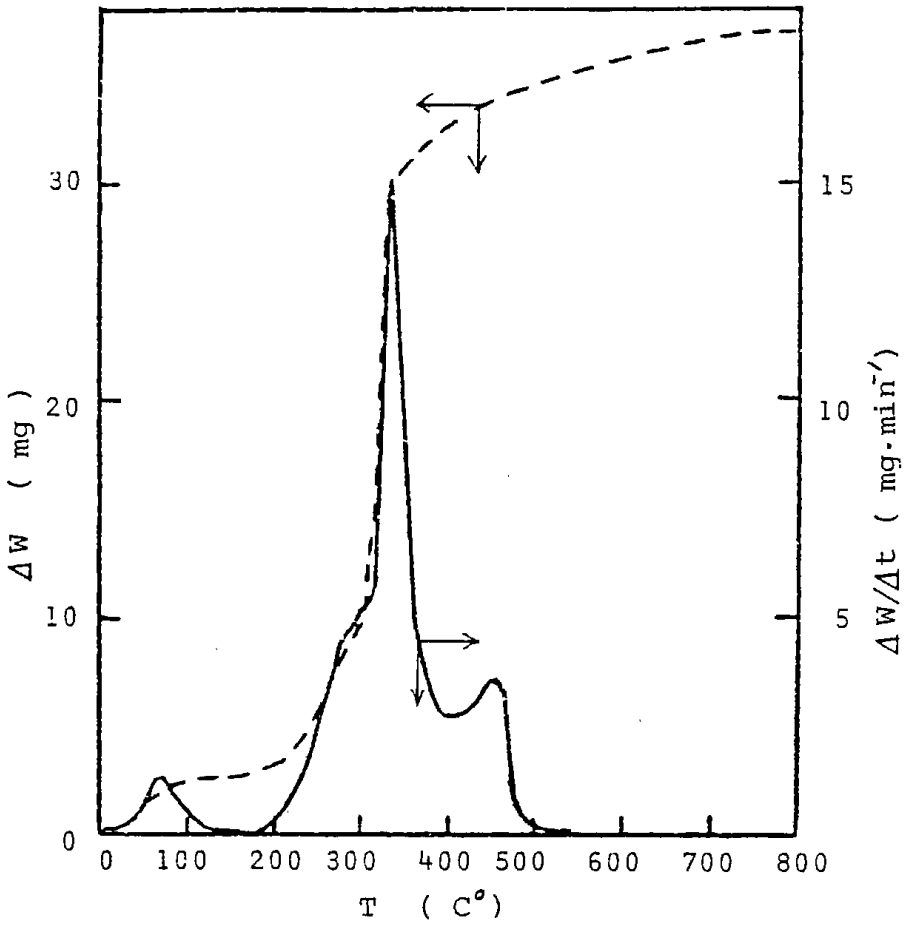

Fig. 2•4 T.G. Curve of Palosapis

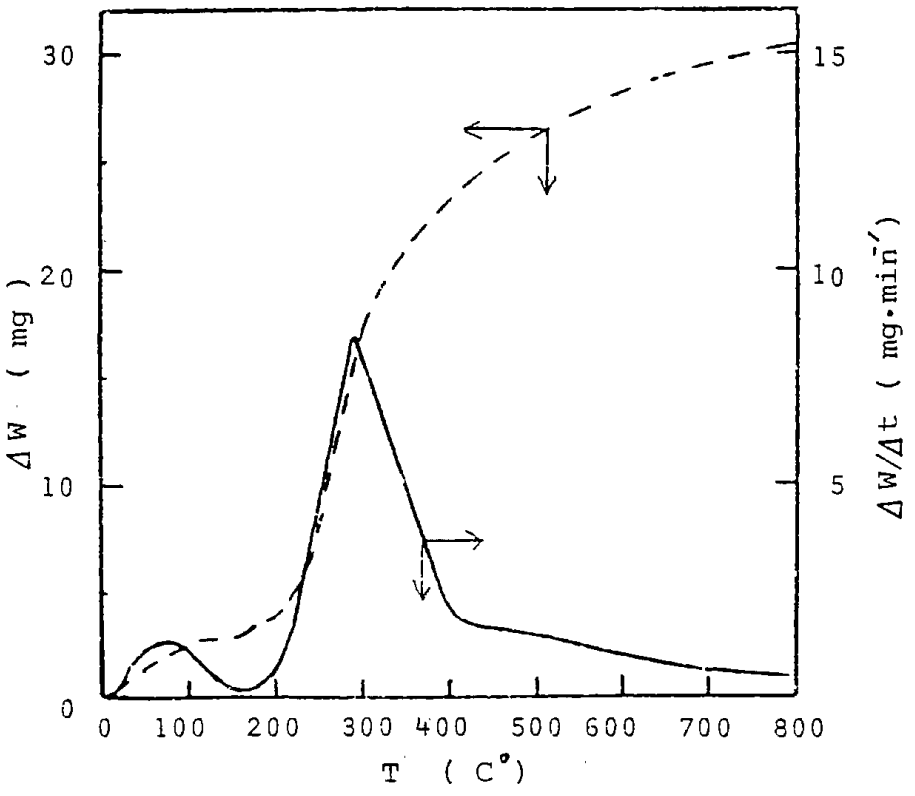

Fig. 2•5 T.G. Curve of Mayapis

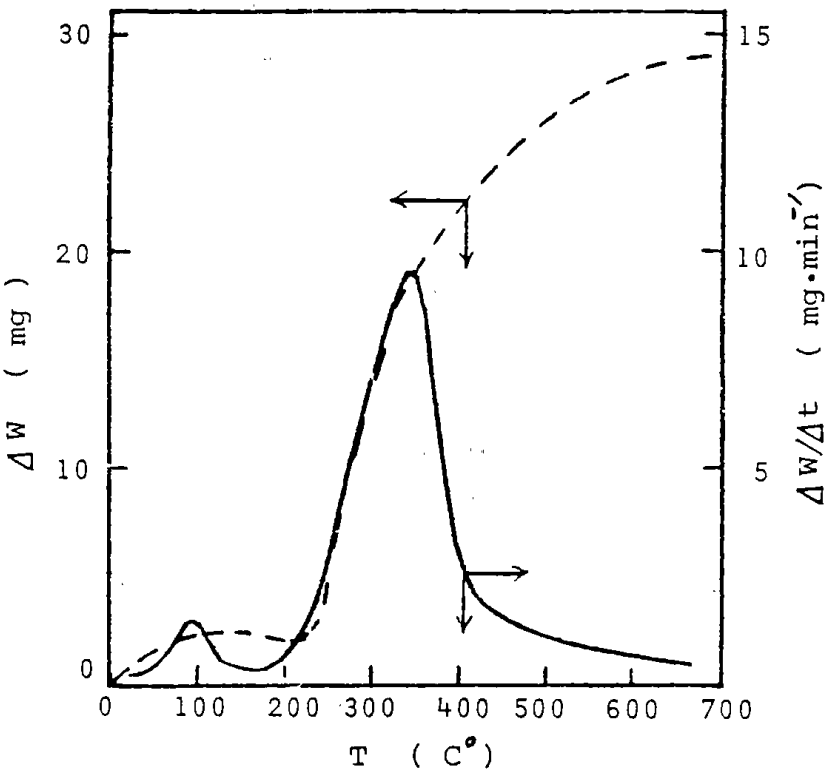

Fig. 2•6 T.G. Curve of Apitong

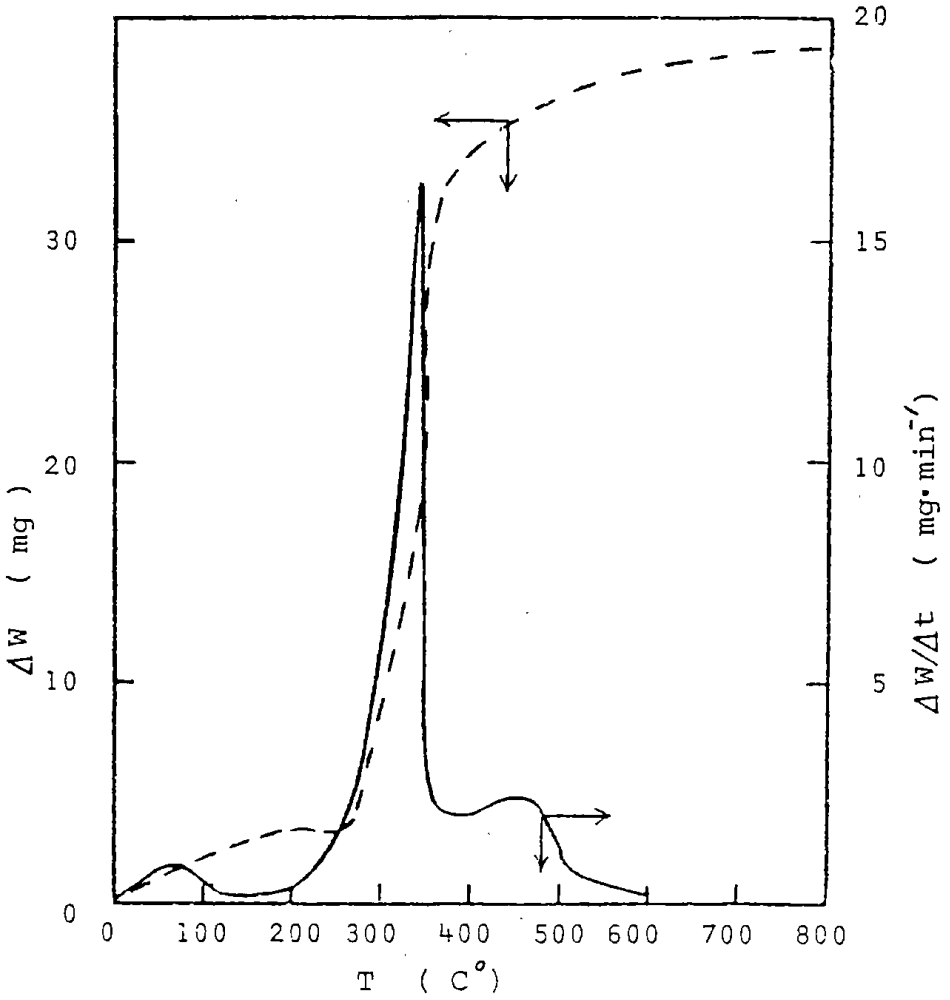

Fig. 2•7 T.G. Curve of Tangile

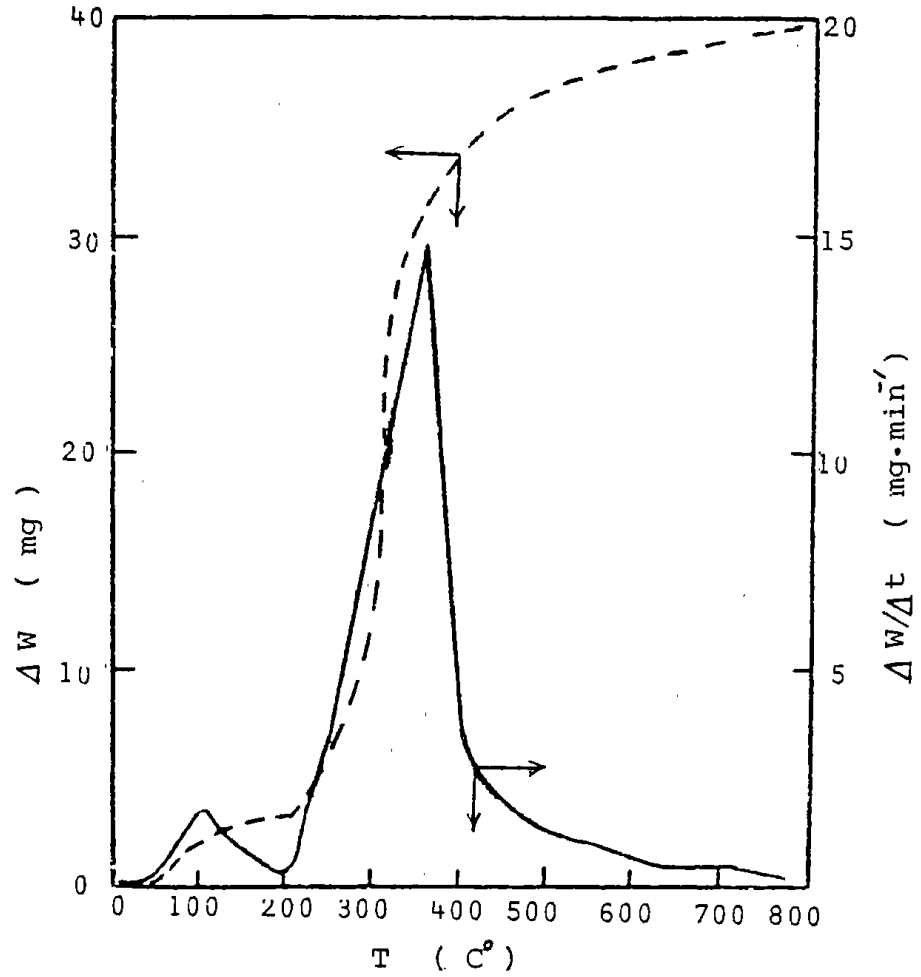

Fig. 2•8 T.G. Curve of Bakauan

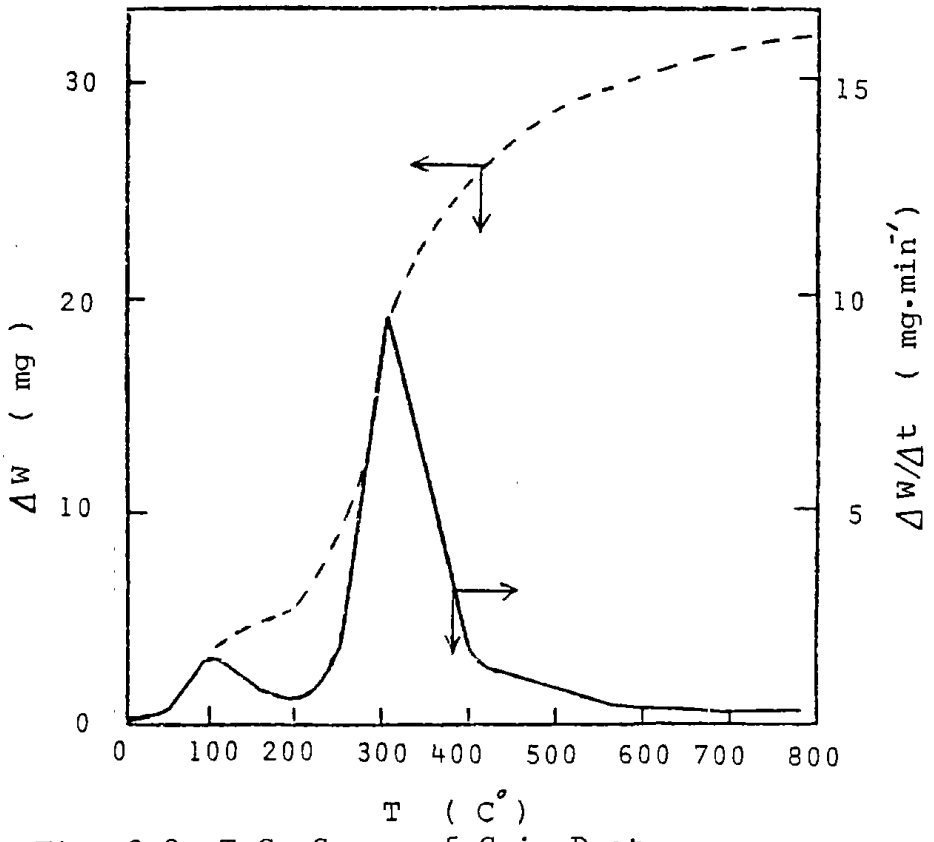

Fig. 2•9 T.G. Curve of Coir Dust

Table 3. Yield Rate and Bulk Density of Carbonized Woods under Various Carbonization Condition.

Sample Species	Tb (°C)	Uo (cm/sec)	F (kg/hr)	E (kg/hr)	Y (%)	θ (min)	Bd (g/cc)
Palosapis	430	14	17.8	1.86	10.4	12	0.08
Tangile	430	5	4.36	0.62	34.2	16	0.01
Apitong	430	6	7.7	0.68	27.8	24	0.12
Kakauate	430	8	12.13	1.48	25.0	18	0.17
Malabayabas	430	8	10.8	1.50	20.9	26	0.12
Bakauan	430	8	10.8	1.50	14.0	26	0.12
Coir-Dust	420	6	5.2	1.70	35.6	7	0.07
Ipil-ipil	430	-	-	-	25.9	-	0.18
Mayapis	430	-	-	-	23.3	-	0.16
K. Bangkal	430	-	-	-	10.0	-	0.11

Nomenclature

Tb : Temperature of carbonization.

Uo : Average gas velocity based on empty bed.

F : Feed flow rate of sample.

E : Weight of discharge.

Y : Yield rate of char.

θ : Reaction time.

Bd : Bulk density.

Table 4 shows results of proximate analysis of the chars: all the chars have low volatile matter content, higher ash and fixed carbon compared with that of the raw materials.

In the previous work, we found an experimental rule that feed ratio of raw material and air was constant at constant temperature in the inner heat type reactor as shown in Fig. 3. According to this, the carbonization temperatuer could be kept at almost constant by adjusting the feed rate of raw material under constant flow rate of air fed.

Table 4. Proximate Analysis of Chars

Sample Species	Moistuer (wt.%)	Ash (wt.%)	VCM (wt.%)	FC (wt.%)
Ipil-ipil	2.26	3.78	17.16	76.78
Mayapis	1.18	1.56	16.01	81.25
K. Bangkal	1.07	6.6	19.18	73.15
Coir-Dust				
Tb. 420°C	6.6	9.6	31.0	52.8
Malabayabas				
Tb. 420°C	7.3	3.7	14.9	74.1
Tb. 430°C	5.0	2.4	10.2	82.4
Bakauan				
Tb. 430°C	2.2	5.1	20.3	72.4
Kakauate				
Tb. 430°C	3.3	3.8	14.4	78.5
Apitong	7.41	3.69	23.94	
Palosapis	7.28	6.08	18.75	
Tangile	9.42	1.46	24.90	

VCM : Volatile Matter
FC : Fexed carbon

It was proved from the results that carbonization by fluidized bed method had the following advantages compared with other existent method:

1) Consumption of heat energy can be minimized by utilization of heat produced by the reaction between raw material and oxygen in feed air.

2) Temperature of the fluidizing bed can be controlled more easily and more steadily.

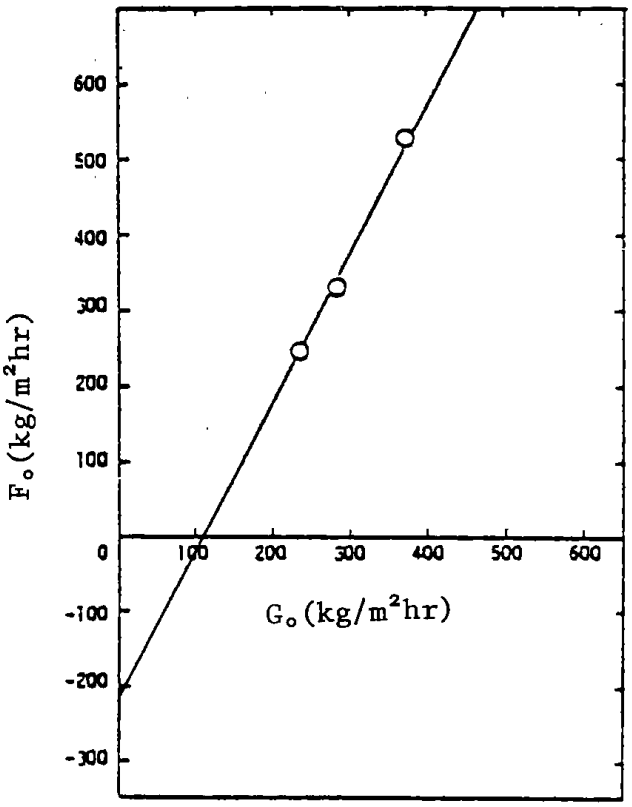

Fig. 3. Correlation between flow rate of feed sample(F_o) and feed air(G_o).

Part 2. Activation Step

K.Ishibashi, Y.Noda

Apparatus

The reactor employed is called external heat type batch reactor of which schmatic diagram is showen in Fig 1

Analytical procedure

1) Methylene blue value [MB]

The methylene blue value was measured by spectrpohtometry: 0.2g of sample was placed in a glass flask and 50ml of standard methylene blue apueous solution was added. The operation is repeated until the blue color of the solution persists. The concentration of the remaining methylene blue was measured.

The methylene blue balue is expressed as mg of methylene blue per gram of sample.

2) Iodine value [I] :

Iodine value was determined by volumetric titration with $Na_2S_2O_3$ solution. Iodine solution was prepared by dissolving 12.7g of I_2 and KI into 1 liter of biffer solution and was standardized against 0.1N $Na_2S_2O_3$ solution.

The value is expressed as mg I_2 per g AC.

3) Intermal surface area [S]

Internal surface area of activated carbon was measured by BET method, expressed as m^2/g.

4) Pore distribution analysis:

Pore distribution in unit weight of activated chars were analyzed (1) terms of the range of pore's radii from 5Å to 100Å, calculated by C.I. method from isothermal adsorption curve of liquid nitrogen.

Experimental Procedure

The obtained chars were activated in a batch type fluidized bed reactor under the atmosphere of super heated steam.

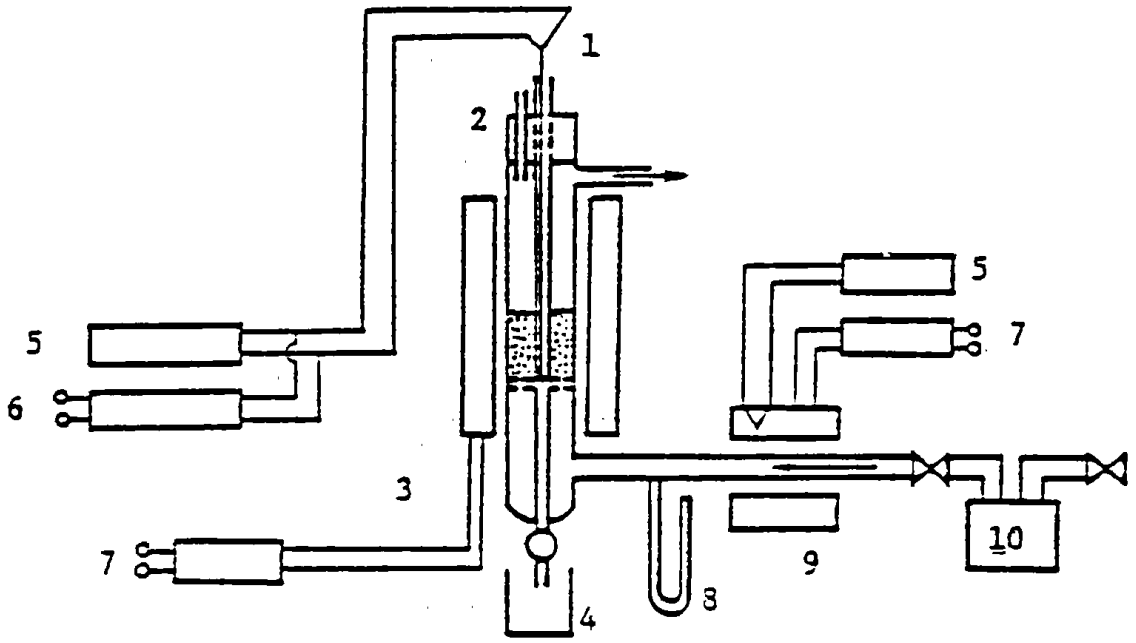

1. Thermocouple
2. Sample inlet
3. Electric furnace
4. Vessel
5. Temperature indicator
6. Temperature controller
7. Electric transformer
8. Manometer
9. Superheater
10. Boiler

Fig. 1 Schematic Diagram of Activation Apparatus with Batchwise Ftuidized Bed.

A 100ml portion of char was taken for every experinental run. The reactor was heated up to operating temperature and nitrogen was brown into it before charging of char.

Nitrogen was switched to steam immediately after charging so that activation could be proceeded in the atmosphere of complete steam.

The activated carbon products were taken out at various reaction time to examine yields and adsorptive capacities.

Results and Discussion

The chars decreased in weight as time proceeded with respective velocity which followed first order kintics: a semi-logarithmic plotting of weight decrease ratio $(\frac{y_o-y}{y_o})$ against reaction time [θ] gave a linear curve as shown in Figure 2, so that the velocity could be formulated as;

$$\frac{y_o-y}{y_o} = Ae^{-K\theta} \quad - - - \quad (1)$$

Where y_o : initial weight of char
y : remaining weight of char ar reaction time [θ]
k : apparent rate constant
A : constant

The weight loss velocity is roughly inversely proportional to the formation valoxity of the activated products, therefore, it can be said that chars having higher value of K are activated faster than that of lower value.

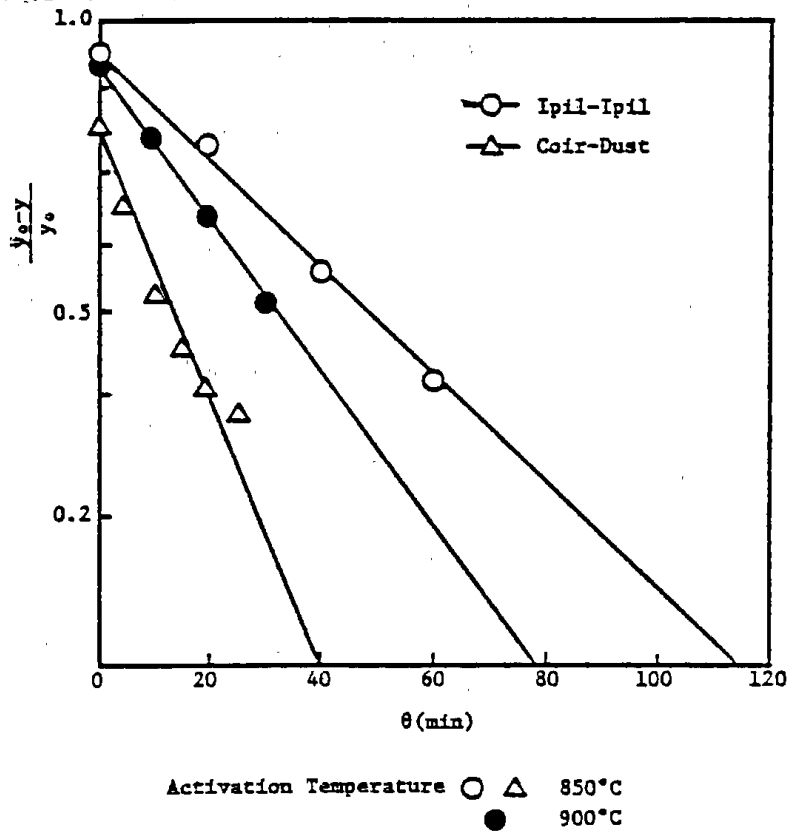

Fig. 2 Weight decreasing velocity of chars during activation reaction.

Table 1 shows values of K obtained at 850°C and bulk density of respective chars. The value of the chars having relatively high bulk density was approximetely a half less than that of lower bulk density.

It is considered from the results that the so called soft woods are activated in relatively short time but with low yield rate, while hard woods take longer to activate but yield rate are higher.

In order to evaluate the activated products, methylene blue value [MB], iodine value [I], internal surface area [S], and pore distribution were measured,

Table 1. Apparent Rate Constant, K, of the Char

Sample Species	k	Bd (g/cc)
Ipil-Ipil	19.57×10^{-3} min^{-1}	0.18
Mayapis	19.32×10^{-3} min^{-1}	0.16
Kakauate	16.55×10^{-3} min^{-1}	0.17
Kaataoan Bangkal	42.99×10^{-3} min^{-1}	0.11
Bakauan	34.85×10^{-3} min^{-1}	0.12
Coir-Dust	54.76×10^{-3} min^{-1}	0.07
Tangile	67.64×10^{-3} min^{-1}	0.01
Malabayabas	29.48×10^{-3} min^{-1}	0.12
Apitong	41.07×10^{-3} min^{-1}	0.12
Coconut shell	15.97×10^{-3} min^{-1}	

Activation temperature : 850°C

Bd : Bulk density

Figure 3 shows the curve plotting [MB] of Ipil- Ipil and Coir-Dust under activation temperatures of 850°C and 900°C, against time [θ]. The other activated products also showed curves similar to Ipil-Ipil or Coir-Dust: [MB] increased up to their maximum value, then decreased slowly as time proceeded.

The activation time required to reach maximum[MB], which varied with the species, was from 15 minutes to 60 minutes: Coir-Dust and other three species such as polosapis Kaatoan-Bangkal, and Tangile were within 15-25 minutes, while Ipil-Ipil and other 6 species were 45-60 minutes. However, the yield rate of the activated products having maximum [MB] value was approximetely 30% regardless of the species.

[S] also showed similar relation to [MB] as in Figure 4. It was found from the results that all activated products produced at the yield rate of 30% had high adsorptive capacity, almost equivalent to commercialized activated carbons.

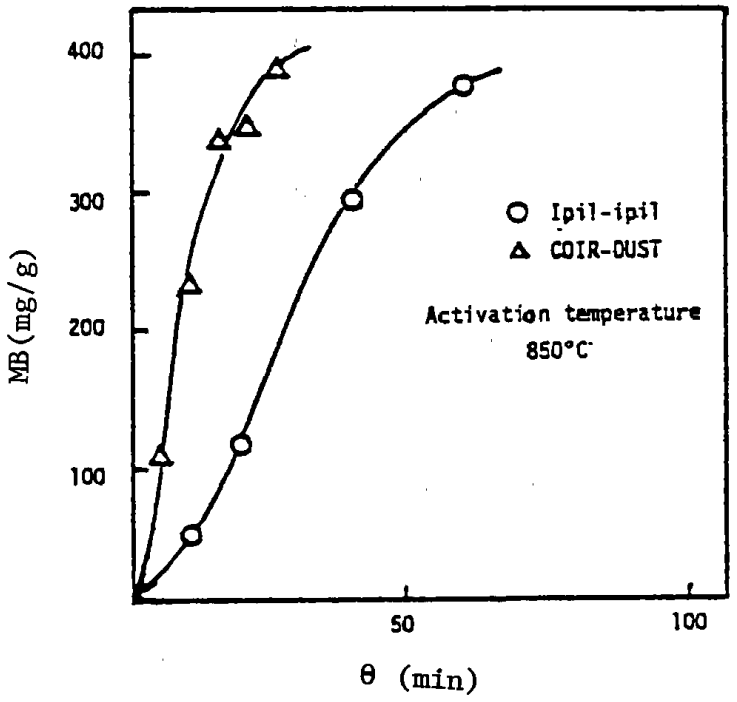

MB : Methylene Blue Value

θ : Activation time

Fig. 3. Effect of activation time on methylene blue value of the activated products.

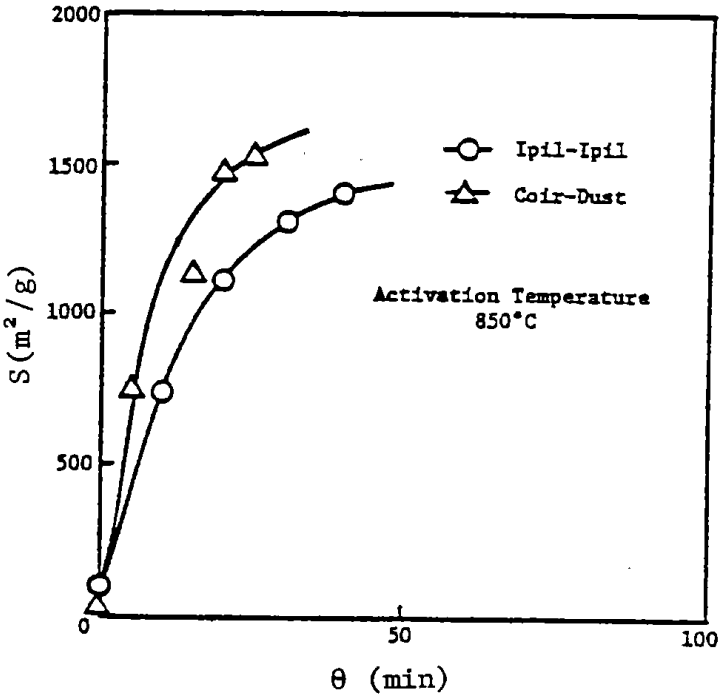

Fig. 4. Effect of activation time on internal surface area of activated products.

Figure 5 shows correlations between [MB] and [S], [I] and [S]: both [MB] and [I] are proportional to [S] but their linear curves have different gradient and intercepting point on horizontal axe.

The proportion coefficients obtained are 0.43 for [MB], 1 for [I], and the intercepting points are at 500m² for [MB], almost zero m² for [I] respectively.

It is assumed that molecular size of methylene blue and iodine are approximetely 14Å and 11Å respectively, so that methylene blue molecule can not pass through pore of less than 14Å in diameter where iodine molecule can pass, therefore, the difference of the intercepting points between the linear curves of [MB] and [I] are caused by those pores.

Figure 6 shows a typical pore distribution curve of the activated products: the pore's volume observed are mainly distributed in the pore's radii ranging from 8Å to 10Å, therefore, the activated products seem to have ability for adsorption of small molecules like gases.

From the results presented here, following conclusion is obtained: activated carbons produced from the tropical plants tested with steam

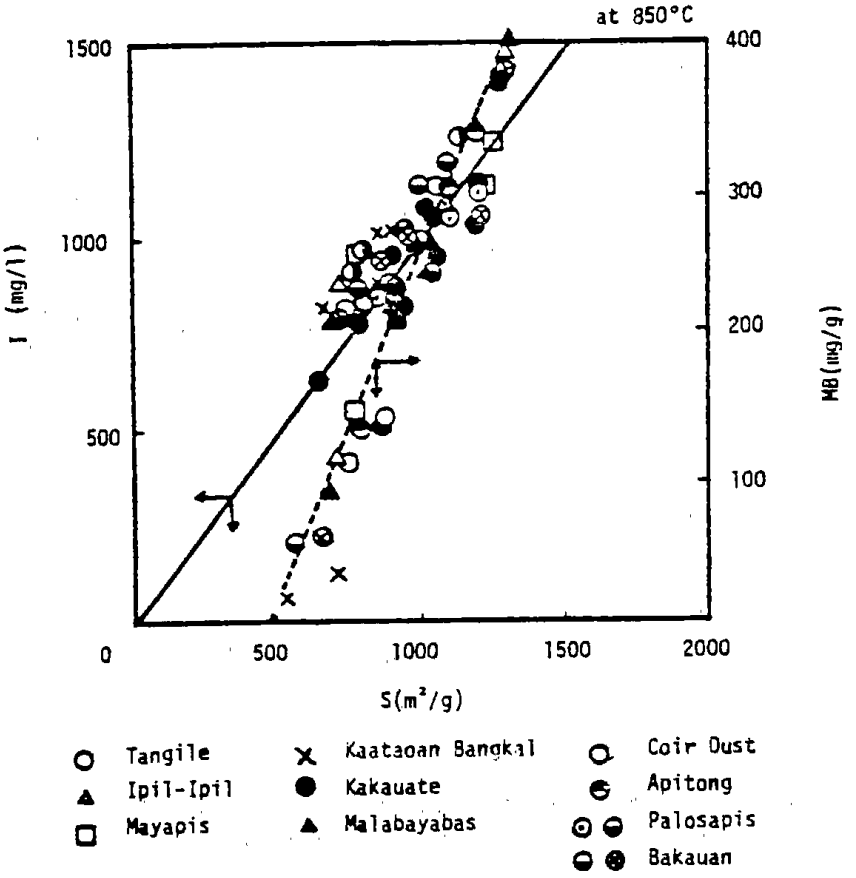

Fig.5. Relation between [I] and [S], [MB] and [S].

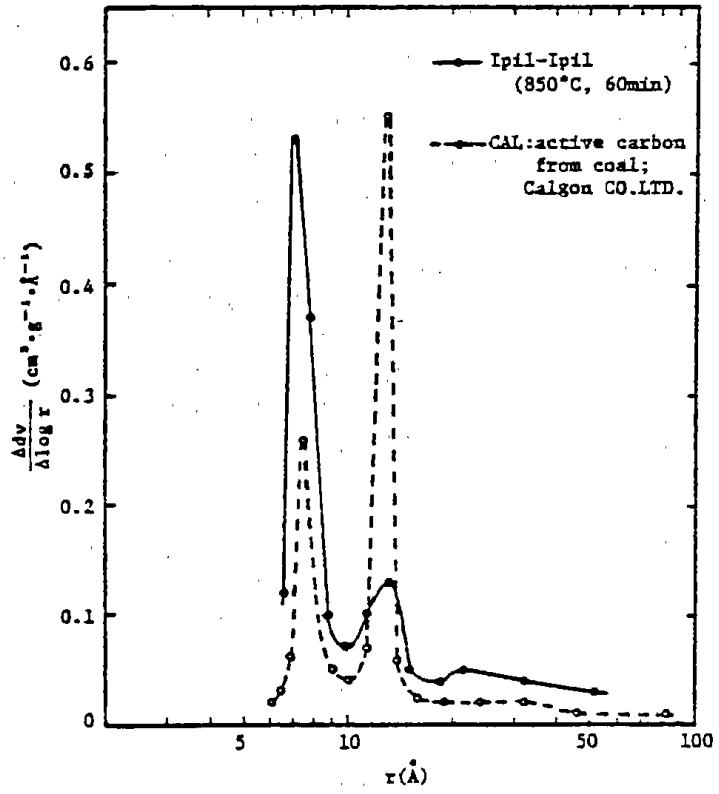

Fig.6. Differential curve of pore size distribution of Activated products.

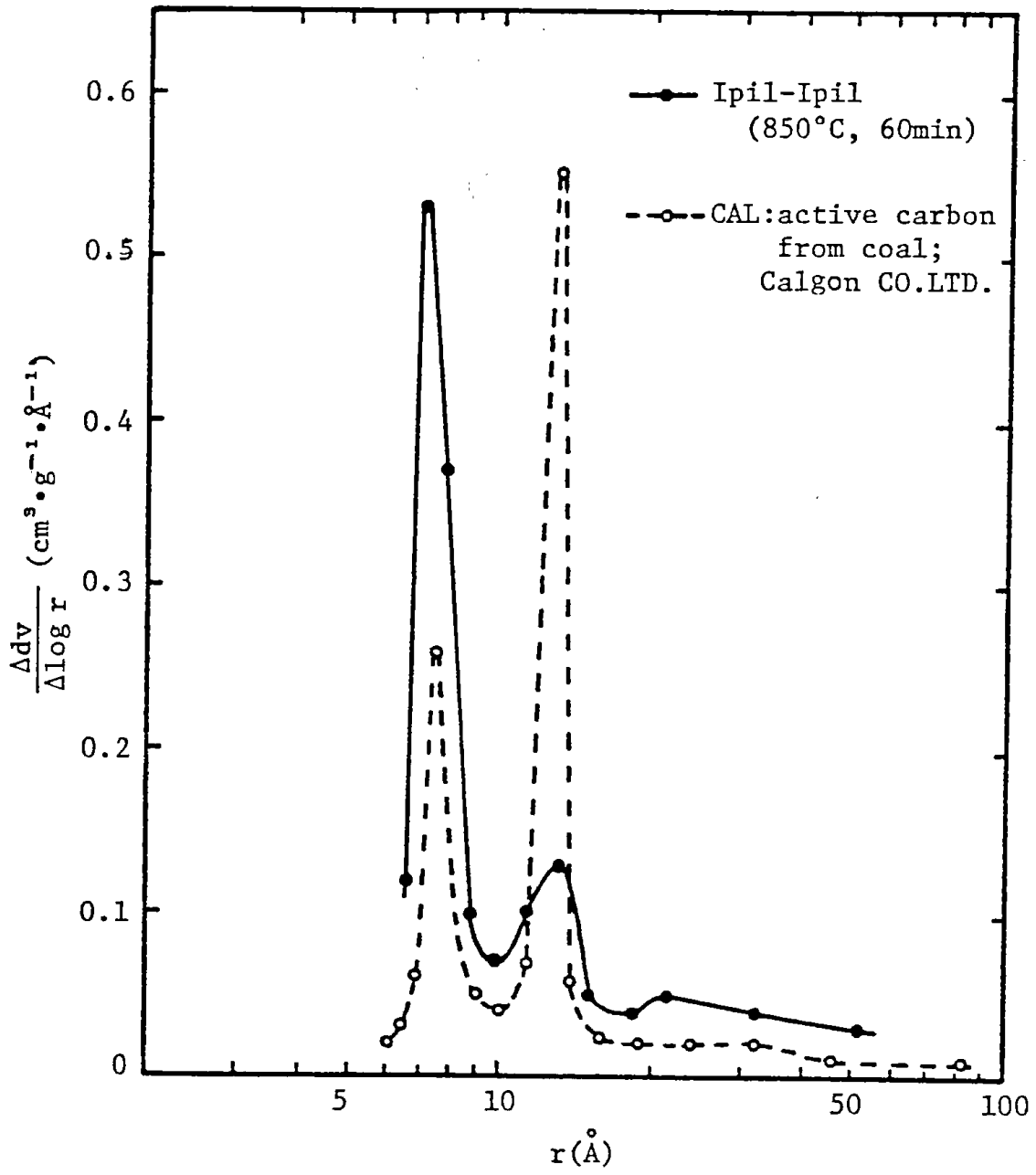

Fig. 10 Differential volume-distribution curve for micro pore of the activated carbon according to size. (v:cm^3/g, r:Å)

activation in the fluidizcd bed reactor commonly have characteristics of (1) high adsorptive abilities equal to commercialized carbons. (2) rich in micro pores having below 10Å in radius. (3) low ash contents. Therefore, the activation carbons would be able to be applied for gas adsorbents and mediciaments.

Fnrther work should be carried out in this area.

PRODUCTION OF HIGH QUALITY ADSORBENTS FROM TROPICAL PLANTS: II. Production of Granulated Activated Carbon

Part 1. Granulation of chars using molasses as binder.

by

K. Ishibashi. Y. Noda.

K. Niikawa. H. Hosoda.

From a total of 12 Philippine wood species, two were selected for the production of good quality granulated activated carbon, namely ipil-ipil and coconut coir dust. Fluidization method was used in the study. The conditions for the granulation of the carbonized chars using molasses as binder was studied. An optimum ratio of 1:0.5 and 1:0.8 (char: binder) was used in the granulation process for ipil-ipil and coir dust, respectively. The carbonization was done at a gradually increasing temperature of 3°C/min at 600°C. Carbonized granules with particle size ranging from 0.5 - 2.0 mm were used for the activation study. The produced granules were activated using an external heat type stainless steel reactor according to the procedure discussed in the previous report. Steam was used as the activating agent at the rate of 2.5 mlH_2O per minute at an activation temperature of 850°C and 900°C, respectively. Maximum value for methylene blue adsorption and internal surface area obtained for ipil-ipil are 290 mg/gAC and 1200 m^2/gAC at 900°C; for coir dust, 390 mg/gAC and 1000 m^2/gAC at 850°C. The gas adsorption test done for both ipil-ipil and coir dust showed that both exhibited maximum adsorbability at 900°C. Maximum value of 40-50% (by wt.) was observed for both benzene and acetone; while 70-90 % (by wt.) was obtained for carbon tetrachloride. Results of the study indicated that the activated granular char products obtained from both ipil-ipil and coir dust would possibly be suited for adsorption of organic solvents, gas adsorption processes and water treatment, among others.

INTRODUCTION

The Philippines is one of the countries endowed with rich natural resources. Its tropical forests have been acclaimed as one of the most valuable in the world. Its wood industry is a big dollar earner. During the logging operation, forest residues and wastes are unavoidable, such that for every 100 cu. m. of log harvested, approximately 51 cu. m. are formed. Wood materials are valued as potential sources of quality activated carbon.

A total of 12 Philippine wood species including coconut waste (coir dust) were studied to determine their potentiality as sources of activated carbon. This paper presents the results of the study on the granulation of powdered charcoals from two of the most promising ones, namely ipil-ipil and coir dust, for the production of good quality activated char granules using molasses as binder.

Granular activated carbons are generally used for adsorption of gases and vapors while powder activated carbons are used in the purification of liquids. There is an increasing trend in the application of granulated activated carbon for liquid phase adsorption process (among which are in water purification and in the sugar and oil refining industries) because it is easy to handle and can be regenerated for reuse.

Wood cellulosic sources particularly woods, yield low density products when carbonized and activated. To convert such products into mechanically strong dense carbons, granulation using a binder was employed.

This study is in consonance with our desire to expand the application of granulated activated carbons from woods and wood wastes for such purposes as water purification, vapor and gas adsorption in addition to finding use for molasses which is a by-product of many sugar refining industries in the Philippines. Its immediate objective is to determine the optimum conditions for the production of granulated activated carbon from wood materials and the realization of high product yield using the fluidized bed method.

EXPERIMENTAL PROCEDURE

Raw Materials and Sample Preparation

Two of the most promising wood sources were selected in the study namely: Ipil-ipil - the wood samples were procured from NSDB compound in Bicutan, Metro Manila, Philippines. Size reduction of sun dried wood

chips to 0.2 - 2.0 mm was done using a crushing machine.

Coir dust - this comprises 65% of the husk. It was procured from Coirflex Decorticator Co., San Pablo City, Philippines. The sample was allowed to pass through a mechanical shaker to separate pure coir dust with an average particle size of 0.56 mm. Moisture content was reduced from 70% to 18% by sun drying.

The prepared samples were carbonized at 430°C using a fluidized bed reactor as discussed in the previous paper. Table 1 shows the results of the proximate analysis and physical properties of the above raw materials and products.

Table 1. Proximate Analysis and Phyical Properties of Raw Materials and Chars

Sample	M (Wt.%)	Ash (Wt.%)	VCM (Wt.%)	FC (Wt.%)	S (m^2/g)	B_b (g/cc)	D_p (mm)
Ipil-ipil Wood	11.67	1.10	74.18	13.04	-	0.17	0.25-2.0
Ipil-ipil Char	7.75	4.30	15.98	71.94	12	0.28	-200mesh
Coir dust	19.14	3.50	68.40	8.90	-	0.08	0.25-2.0
Coir dust Char	9.07	8.60	18.54	63.76	5	0.17	-200mesh

Where: M = moisture
VCM = volatile combustible matter
FC = fixed carbon
B_b = bulk density
D_p = particle size
S = Internal surface area

Methods of Analysis

Most of the methods employed were in accordance with the Japan Industrial Standard (JIS) procedure or with slight modification there of as mentioned in the previous paper.

Proximate analysis and physical properties of the raw materials, charcoals and activated carbons were determined.

Adsorptive Properties - methylene blue test was done on the activated granulated products.

Production of High Quality Adsorbents from Tropical Plants, Part I (ITIT Symposium 1980).

Granulation Process

The various stages involved in the granulation process are shown in Fig. 1. The charcoals were each pulverized to 200 mesh under(Tyler). Molasses (obtained from a Philippine sugar refining company) was used at a ratio of 1:0.5 and 1:0.8 for ipil-ipil and coir dust, respectively.

Molasses diluted with water to 50% was mixed with the pulverized charcoal. The mixture was passed through an extruder and the extrudates (1 mmØ) were subsequently passed through a disk type pelletizer at 450 rpm. The granules obtained were dried at 110°C for 5 hours, the granules (0.5 -2.0 mm) were then carbonized in a covered stainless steel box using a muffle furnace at a heating rate of 3°C/min. until the temperature of 600°C was attained.

Data obtained on the granulation of ipil-ipil and coir dust chars including the yield and density are shown in Table 2. The thermal balance analysis of the molasses obtained from the Philippines* and Japan** were determined and compared as shown in Fig. 2.

Table 2. Data on the Granulation of Powdered Char at Optimum Conditions.

Sample	Coir dust	Ipil-ipil
Ratio (Char:Binder)	1:0.8	1:0.5
Bulk Density of Char (g/cc)	0.17	0.28
Weight of Char (g)	200	300
Weight of Molasses (g)	160	150
% Dilution	50	50
Weight of Water (g)	80	75
% Yield (Carbonized granules)	75	73
Bulk Density of Granules (g/cc)	0.51	0.56

Activation Process

The granulated chars produced from ipil-ipil and coir dust were each subsequently activated using an external heat type activating apparatus. It consists of a stainless steel reactor (2 in. Ø) equipped with an external heater. Steam (2.5 ml H_2O/min) was allowed to pass through a high temperature oil bath to generate steam which was subsequently charged at the lower part of the reactor, then through the bed of char-

Analysis of Molasses: * Total solids, 64.6%; sugar content, 18.6%; ash, 5.0%
** Total solids, 86%; sugar content, 16.3%; ash, 7.23%.

coal at the desired temperature and reaction time.

Activation of the granulated chars were done at 850°C and 900°C, respectively with varying reaction time from 10 to 60 minutes.

Determination and Evaluation of Adsorptive Properties of Activated Carbon

The bulk density, internal surface area and pore destribution of the activated carbon products obtained at various reaction time were measured by the respective methods described in the previous report.

The adsorptive capacity of the obtained products were evaluated by methylene blue adsorption [MB] test as discussed in the previous report.

RESULTS AND DISCUSSION

Effect of activation time on product yield

Correlation of the yield of activated char granules with activation time shows that there was significant loss in weight of product as activation time proceeded. More pronounced decrease in yield was noted with increasing temperature as shown in Fig. 3. Higher weight loss which resulted to lower yield was observed in coir dust as compared to that of ipil-ipil.

In the activation process, the reaction rate of charcoal with steam in terms of weight loss was calculated as discussed in the previous report. The value of k (apparent constant) for coir dust was twice the k obtained for ipil-ipil as shown below:

Activation Temp. t (°C)	k	
	Coir dust	Ipil-ipil
850	57.5×10^{-3} min^{-1}	$29.48 \times 10^{-3} min^{-1}$
900	92.0×10^{-3} min^{-1}	$35.93 \times 10^{-3} min^{-1}$

The above data show that coir dust can be activated faster than ipil-ipil, thus the former required shorter time for activation.

Correlation of Methylene blue [MB] Adsorptive Capacity and Internal Surface Area [S] with Reaction Time (θ)

Figures 4 & 5 show the correlation of reaction time with [MB] and [S] respectively. A gradual increase in [MB] adsorbability was noted with increasing reaction time. For coir dust, activation was more effective at lower temperature. Maximum value of 390 mg/g AC was obtained at 850°C and 30 minutes. Beyond this point, [MB] value tended to decrease. For ipil-ipil, longer reaction time (60 min.) was needed to attain the maximum value of 300 mg/g AC at 850°C.

The results of the internal surface area [S] determination also gave the same increasing trend of results with reaction time until a saturation point was reached. Beyond this point, an abrupt decrease in the surface area was noted. Development of internal surface area for ipil-ipil was more effective at higher temperature. Thus higher [S] of 1,200 m^2/g AC was obtained at 900°C for ipil-ipil while 1,000 m^2/g AC at 850°C was obtained for coir dust.

Correlation of [MB] Value and [S]

Fig. 6 indicates that the [MB] value is directly proportional to the [S] for both coir dust and ipil-ipil. Linear lines with the same slopes which indicate good inference was obtained. At [MB] = 0, the intercept gave values of 380m^2/g AC and 450 m^2/g AC. From the slope, the area occupied by individual molecule on the activated products was determined at a value of 150$Å^2$ for both samples. An accessible area of 192$Å^2$ was obtained for Graphon (a non porous carbon)[3]. This nearly similar values is an indication that adsorption of MB on the obtained products is physical adsorption.

Correlation Between Bulk Density and Reaction Time

Finally, the bulk density of each of the activated products obtained with particle sizes ranging between 0.5 - 2.0 mm were compared with the commercial activated carbon of the same particle size range. Comparative results as shown in Fig. 7 indicates that the bulk density of the activated granular char products compare favorably or is even higher than that of the commercial product.

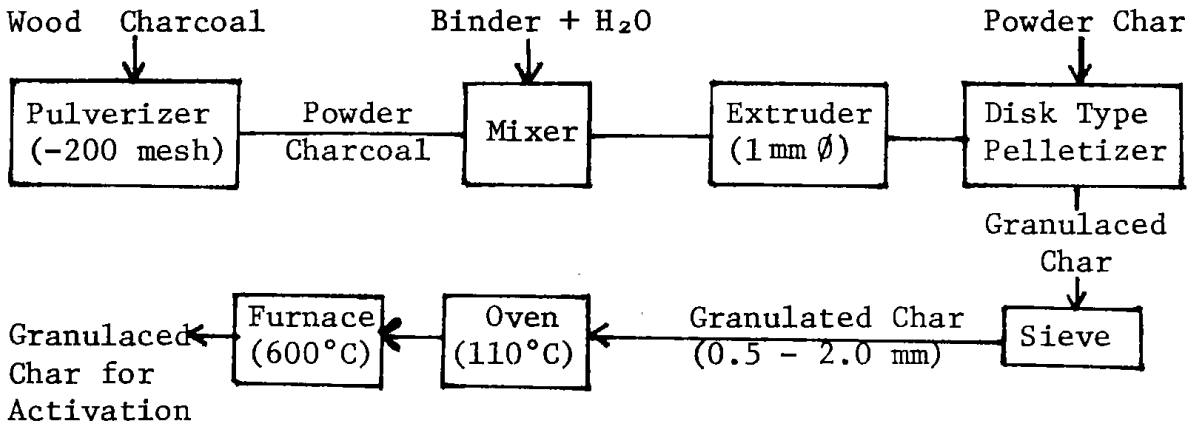

Fig. 1. Schematic Diagram of Granulation Process for Powder Char

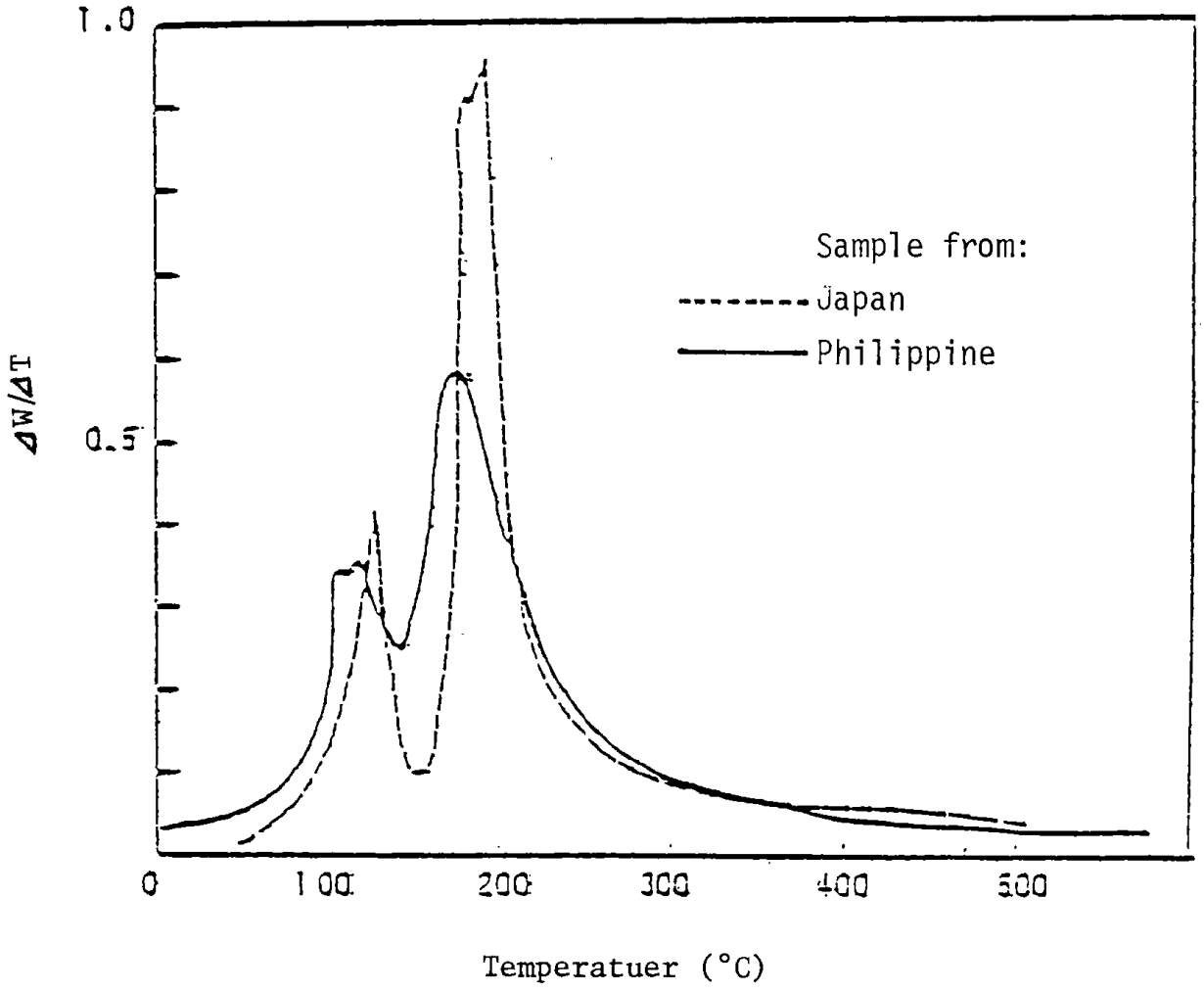

Fig. 2. Thermogravimetric Curve of Molasses.

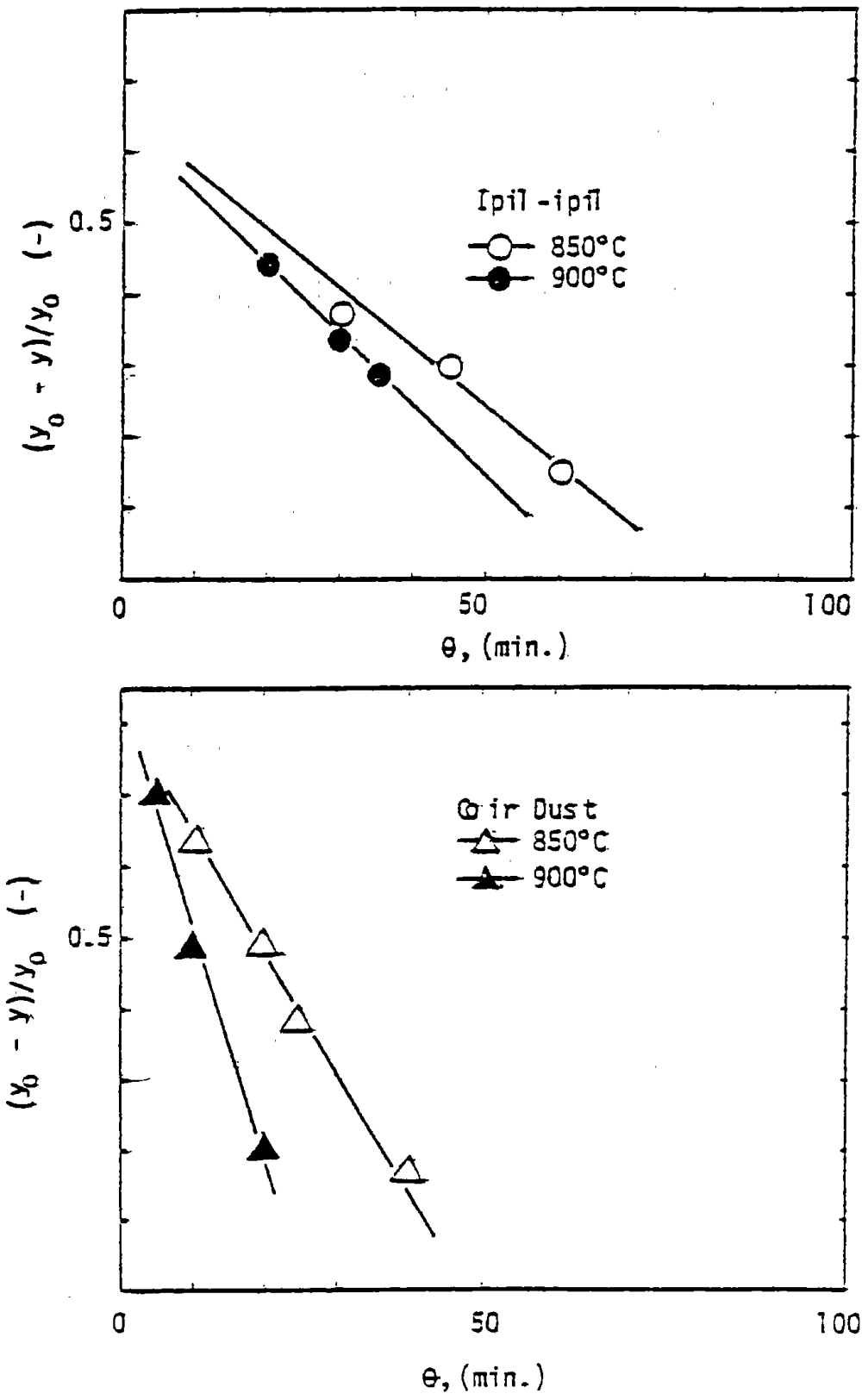

Fig. 3. Correlation between change in weight and reaction time.

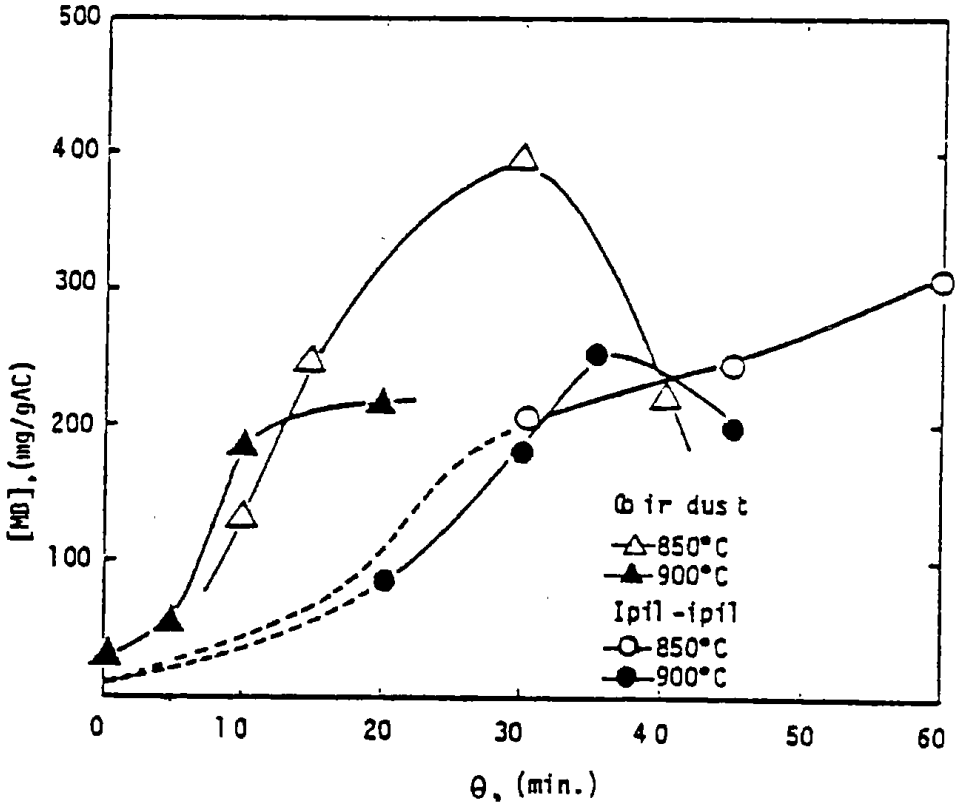

Fig. 4. Effect of reaction time on methylene blue value of the products.

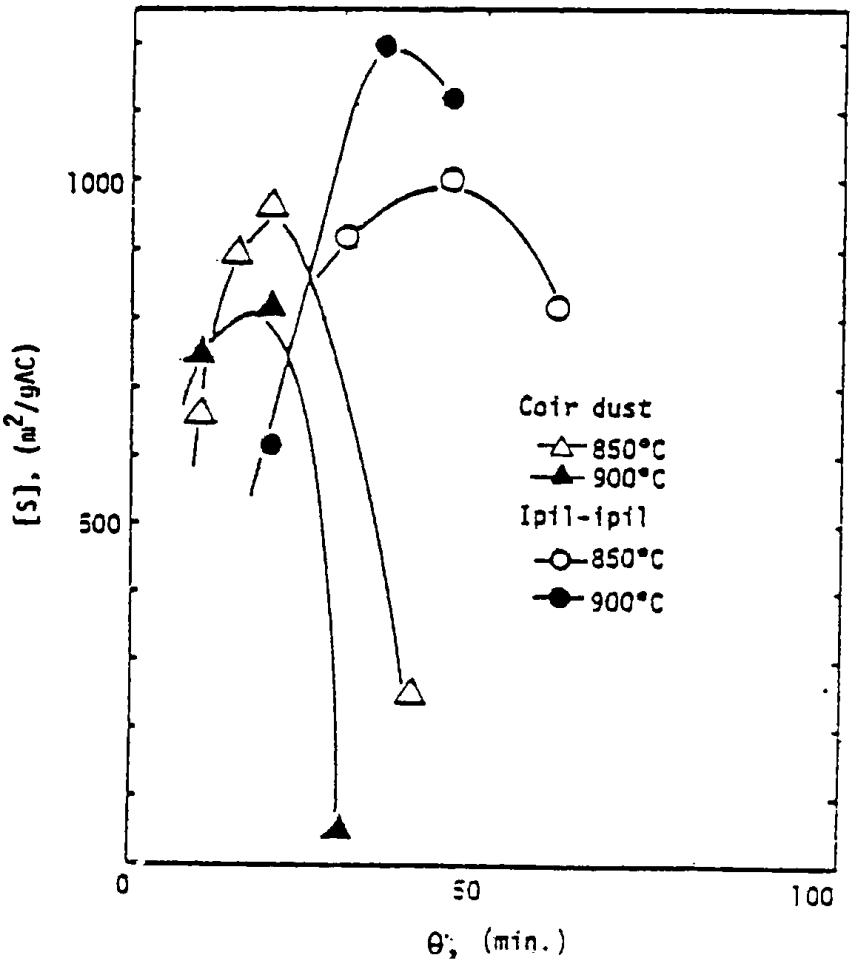

Fig. 5. Effect of reaction time on internal surface area.

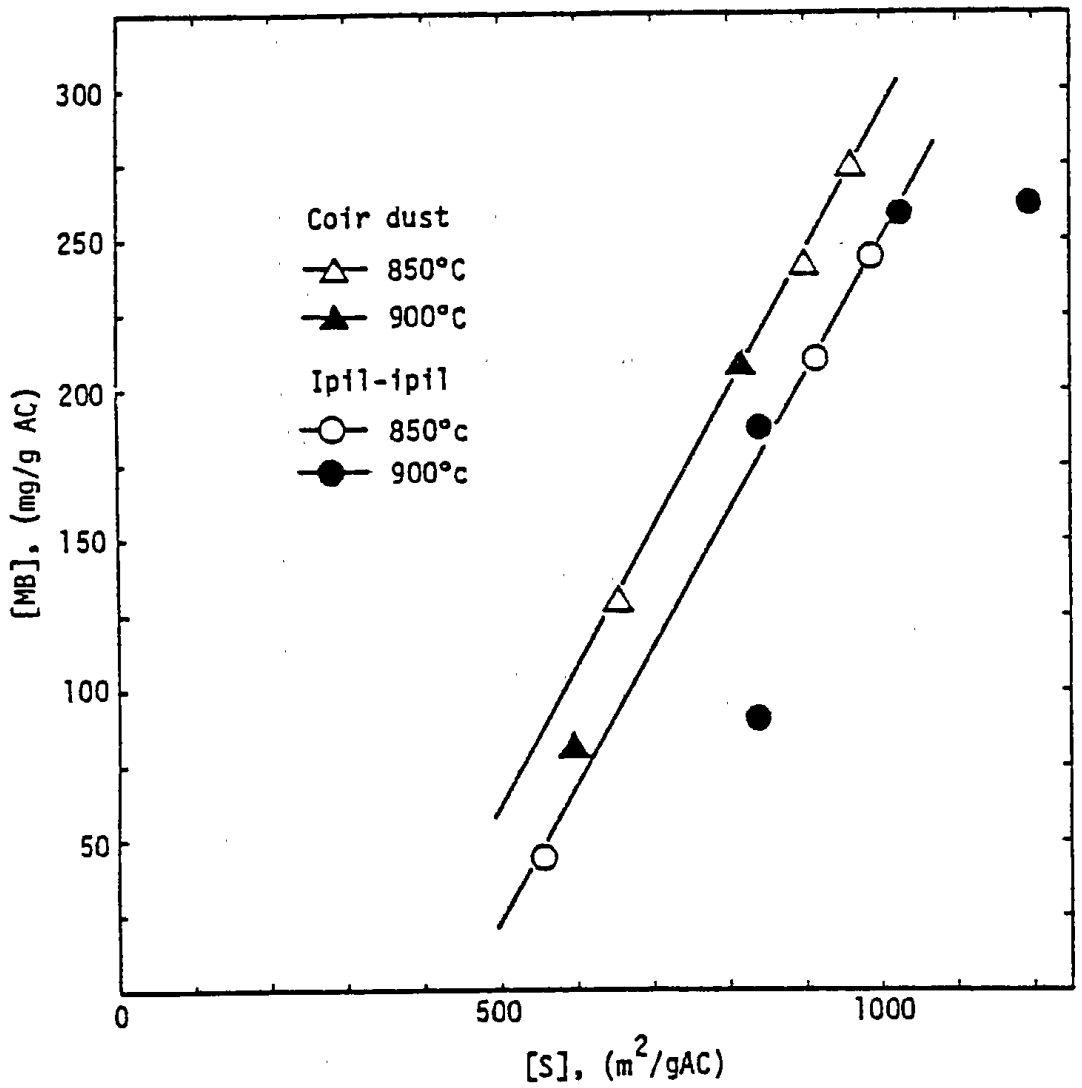

Fig. 6. Correlation between methylene blue value and internal surface area.

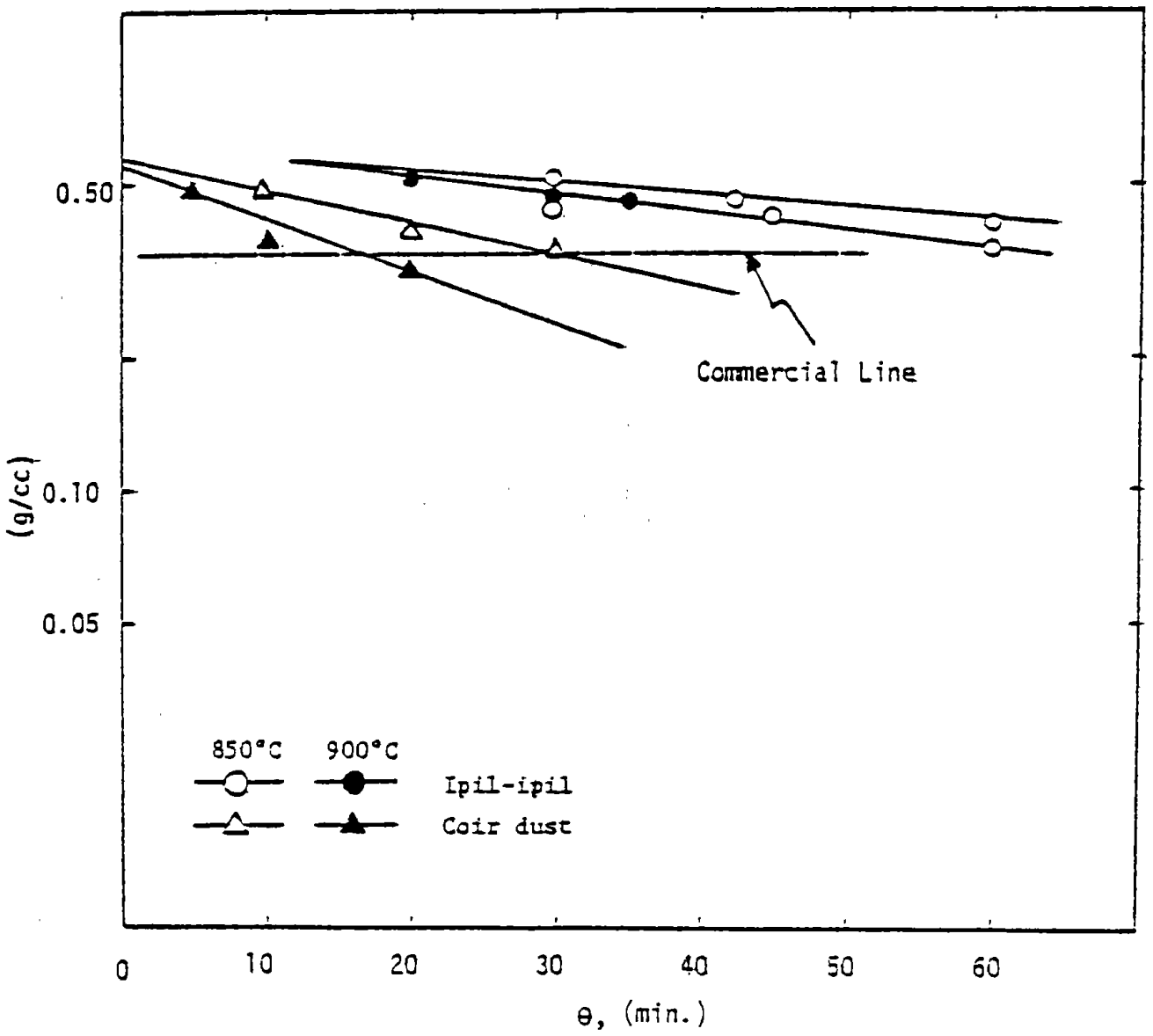

Fig. 7. Correlation between bulk density and reaction time.

Part 2.

Adsorption of organic Solvents in gas phase on the granulated activated carbon.

Y. Noda, K.Ishibashi

This paper describes experiment about adsorption of some organic solvents in gas phase on the granulated activated carbon prepared by the method described in previous paper.

Experimental procedure

Determination of gas adsorbability was done according to the procedure of Hirata[1] as follows: weighed quantity of sample (0.2g) is placed in one vessel and the solvent (2ml) is placed in the other vessel. The two glass vessels are joined together to make a closed system. It is then placed at controlled temperature in an air-bath oven for one week each at 15°, 20°, 25° and 30°C. The quantity of the solvent adsorbed is calculated from the increase in weight of the char granules.

The organic solvents used are as follows: Benzene, Acetone, and Carbon tetrachoride were used for the test.

Experimental results and discussion

Table 1 shows the data on the gas adsorption test that was done on the activated carbon products using three gases namely C_6H_6, CCl_4 and CH_3COCH_3 at temperature of 15°,20°,25° and 30°C, respectively.

At 25°C, correlation of each of the gases adsorbed by the activated carbon products obtained at 850°C and 900°C in terms of weight % and reaction time are shown in Figures 1,2 and 3.

Comparing the adsorptive capacity of the activated granule char products for each gram mole of gas adsorbed at 25°C, Ipil-Ipil was 1.1-1.2 times more adsorptive than coir dust for acetone, 1.1-1.6 times and 1.6 times more adsorptive, respectively, for CCl_4 and C_6H_6.

Table 1. Data on the Gas Adsorptive Capacity of products Obtained at Varying Temperature Using Various Solvents

Sample	C_6H_6(g/gAC)			CCl_4(g/gAC)			CH_3COCH_3(g/gAC)		
	15°C	25°C	30°C	15°C	25°C	30°C	15°C	25°C	30°C
I-850-30	0.30	0.35	0.35	0.61	0.65	0.71	0.34	0.34	0.34
I-850-45	0.29	0.37	0.38	0.66	0.70	0.71	0.34	0.37	0.37
I-850-60	0.33	0.43	0.44	0.75	0.82	0.82	0.43	0.45	0.45
I-900-20	0.23	0.24	0.24	0.39	0.42	0.43	0.24	0.26	0.27
I-900-35	0.30	0.43	0.45	0.75	0.89	0.89	0.44	0.48	0.48
I-900-40	0.32	0.42	0.43	0.72	0.81	0.81	0.41	0.43	0.44
CD-850-10	0.26	0.27	0.28	0.40	0.43	0.41	0.29	0.30	0.27
CD-850-15	0.31	0.32	0.30	0.51	0.61	0.54	0.37	0.34	0.32
CD-850-20	0.35	0.38	0.34	0.57	0.71	0.67	0.42	0.38	0.36
CD-850-30	0.38	0.43	0.37	0.69	0.79	0.71	0.43	0.39	0.40
CD-850-40	0.11	0.11	0.28	0.11	0.44	0.22	0.27	0.21	0.22
CD-900- 5	0.22	0.21	0.34	0.24	0.52	0.55	0.25	0.26	0.22
CD-900-10	0.30	0.31	0.34	0.31	0.60	0.54	0.30	0.34	0.27
CD-900-20	0.38	0.42	0.37	0.37	0.79	0.77	0.46	0.42	0.39
Commercial AC	0.41	0.42	0.44	0.85	0.85	0.78	-	-	-

where: I = ipil-ipil CD = coir dust

Correlation Between Gas Adsorbed and Internal Surface Area

As noted on Figures 4,5 and 6 for Ipil-Ipil and coir dust, % gas adsorbed was found to be directly proportional to the surface area. The linear lines obtained passed through the zero point in the axes. From the slope obtained, one molecular area ($Å^2$) as calculated revealed that Ipil-Ipil and coir dust exhibited almost the same adsorbability value as follows:

Sample	Solvent		
	C_6H_6 ($Å^2$)	CCl_4 ($Å^2$)	CH_3COCH_3 ($Å^2$)
Ipil-Ipil	55.0	30	138
Coir Dust	65	30	131

Correlation between Pore Distribution and Pore Volume

Plotting the derivative of volume with respect to pore radius as shown on Fig. 7, the pore size distribution of the activated products from Ipil-Ipil and coir dust ranges between 5Å and 15Å. The ability of activated carbon to adsorb takes place within the pore size distribution. usually ranging between 5Å and 30Å (micropore). Results obtained show that the pore size distribution is within the range of the active pore sites of activated carbon.

Based on the results of the study, activated granule chars obtained from Ipil-Ipil and coir dust find suitable application for the adsorption of organic solvents, for gas adsorption processes and for water treatment, among others.

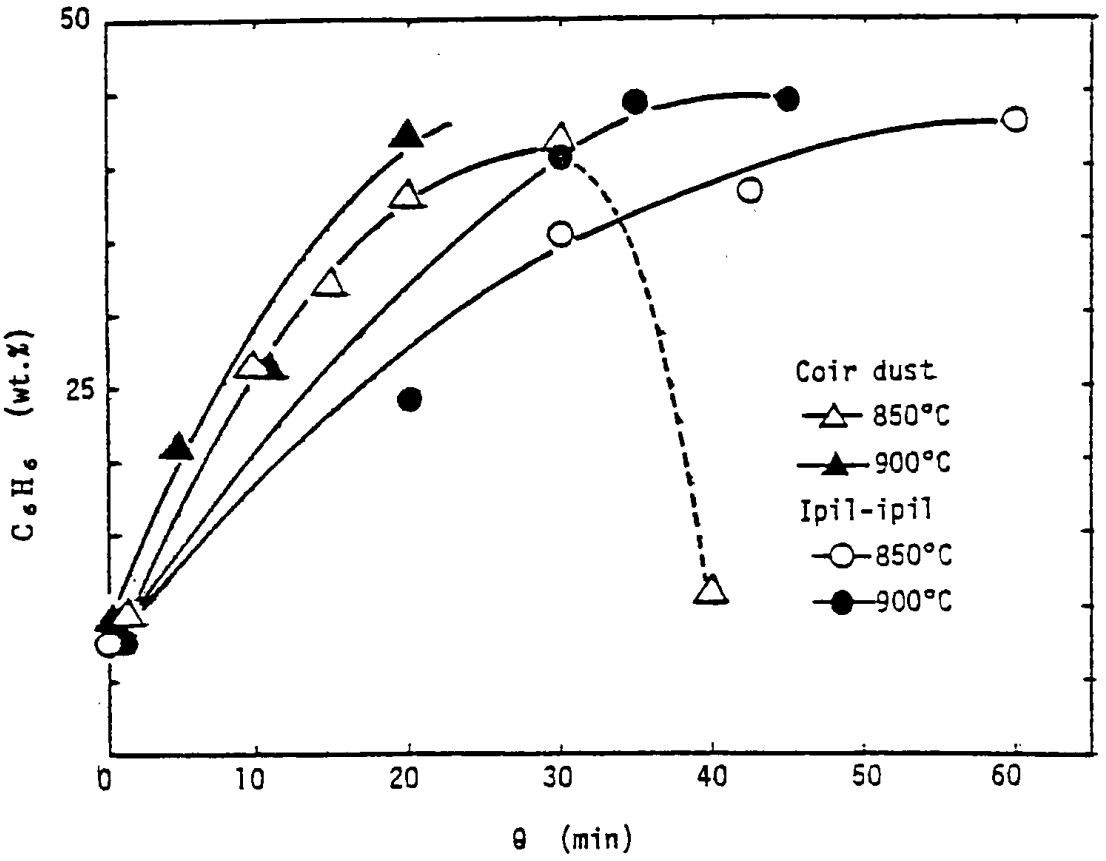

Fig. 1.Effect of reaction time on benzene adsorbability at 25°C.

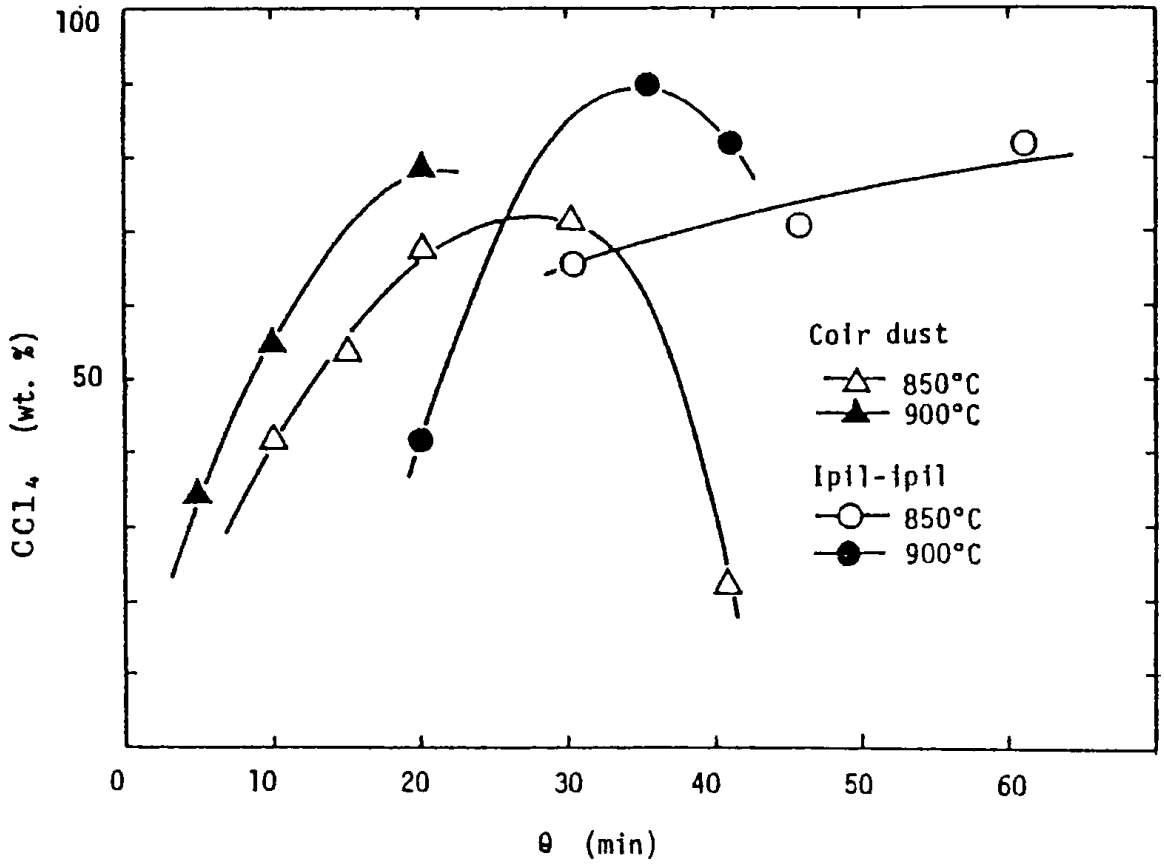

Fig. 2. Effect of reaction time on carbon tetrachloride adsorbability at 25°C

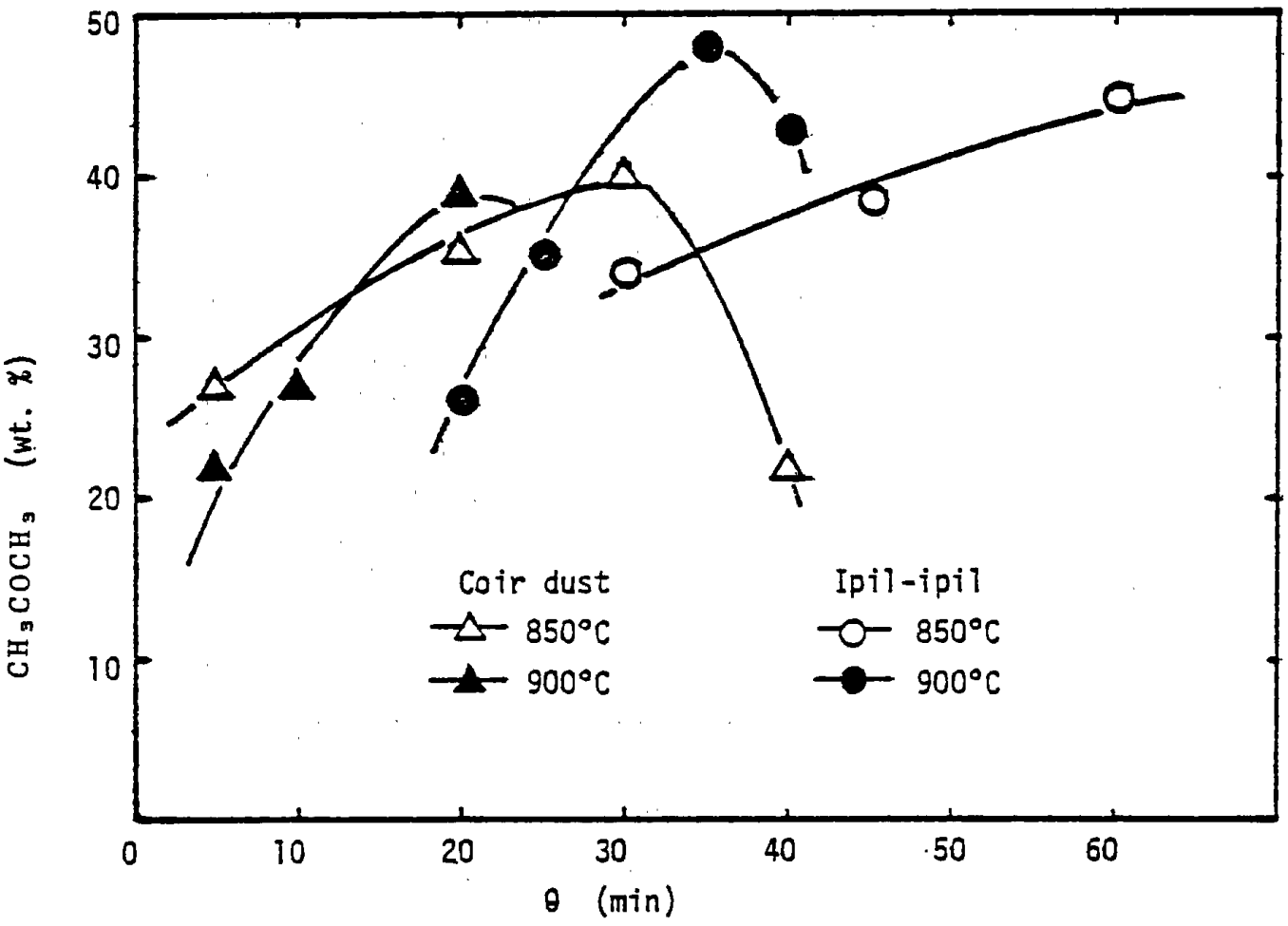

Fig.3. Effect of activation time on acetone adsorbability at 25°C

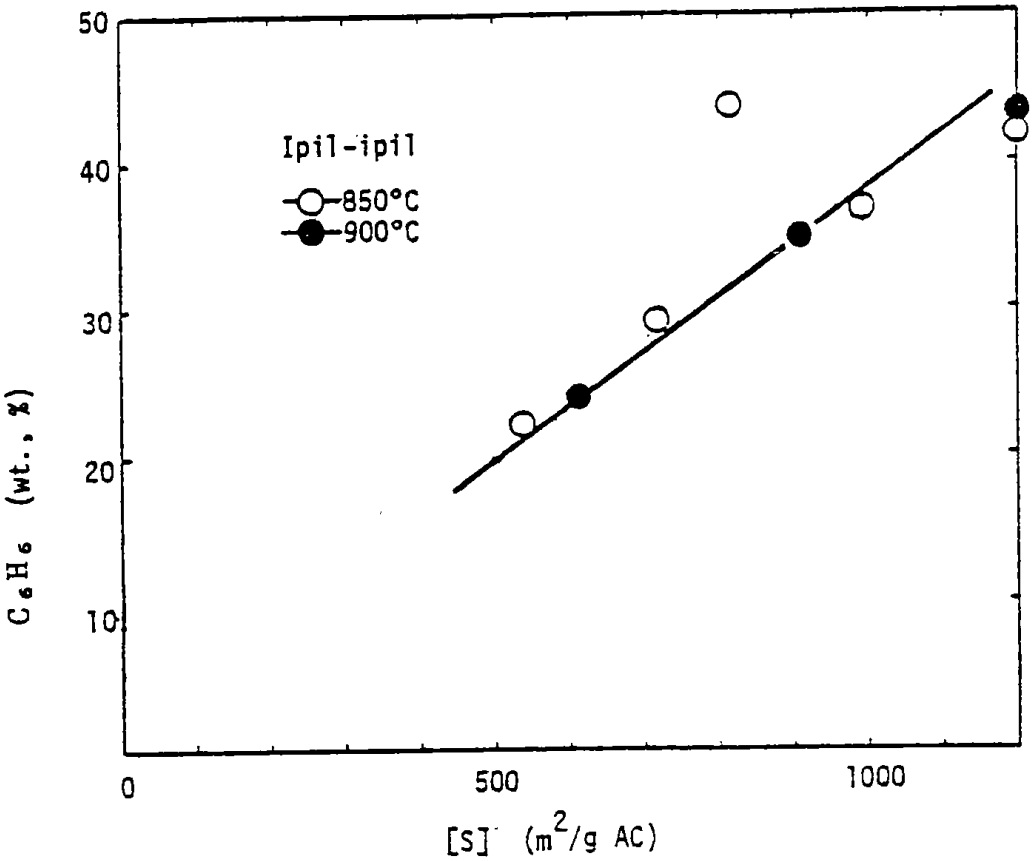

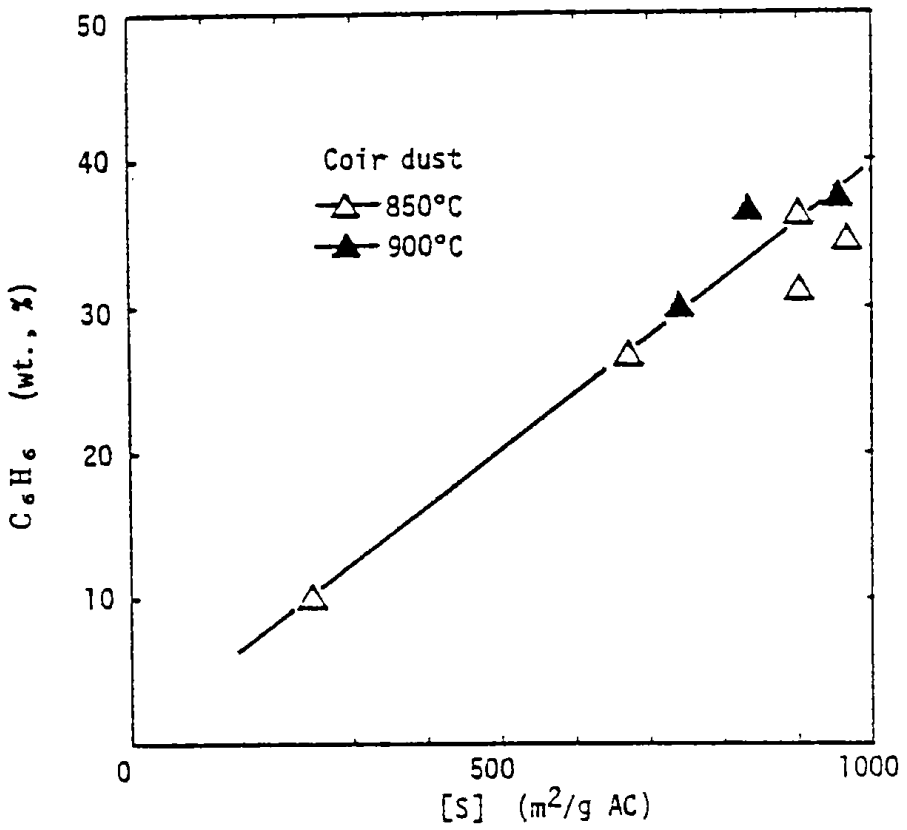

Fig. 4. Correlation between benzene adsorbability and internal surface area.

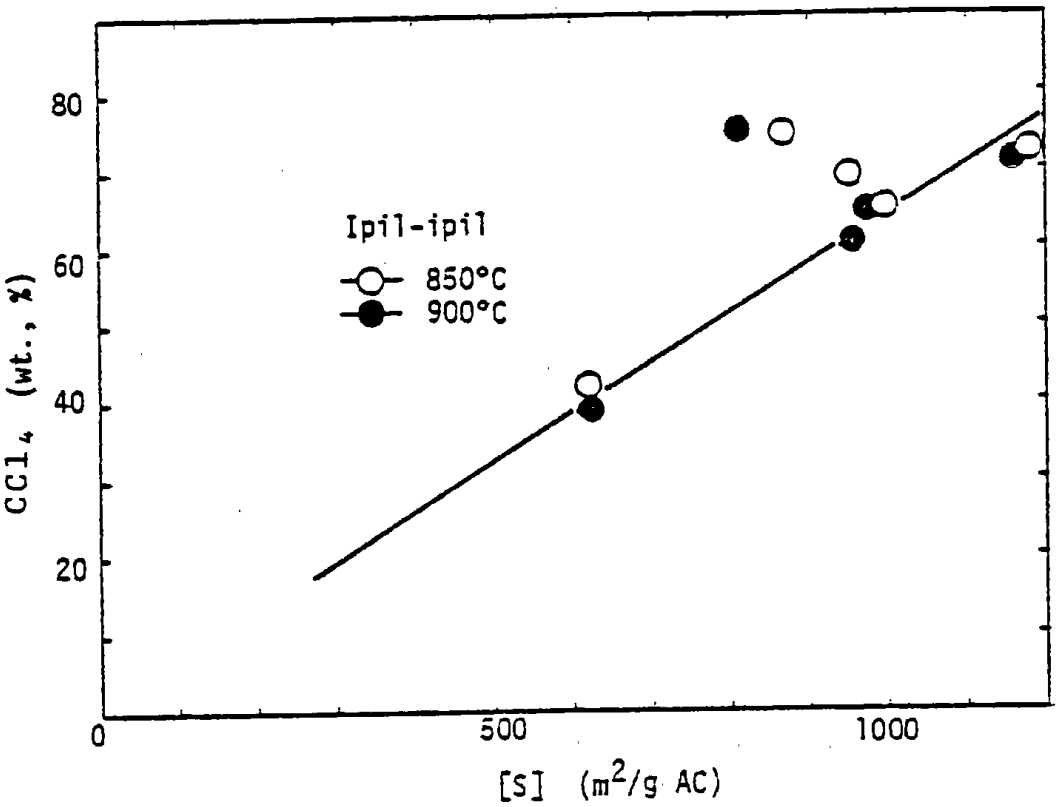

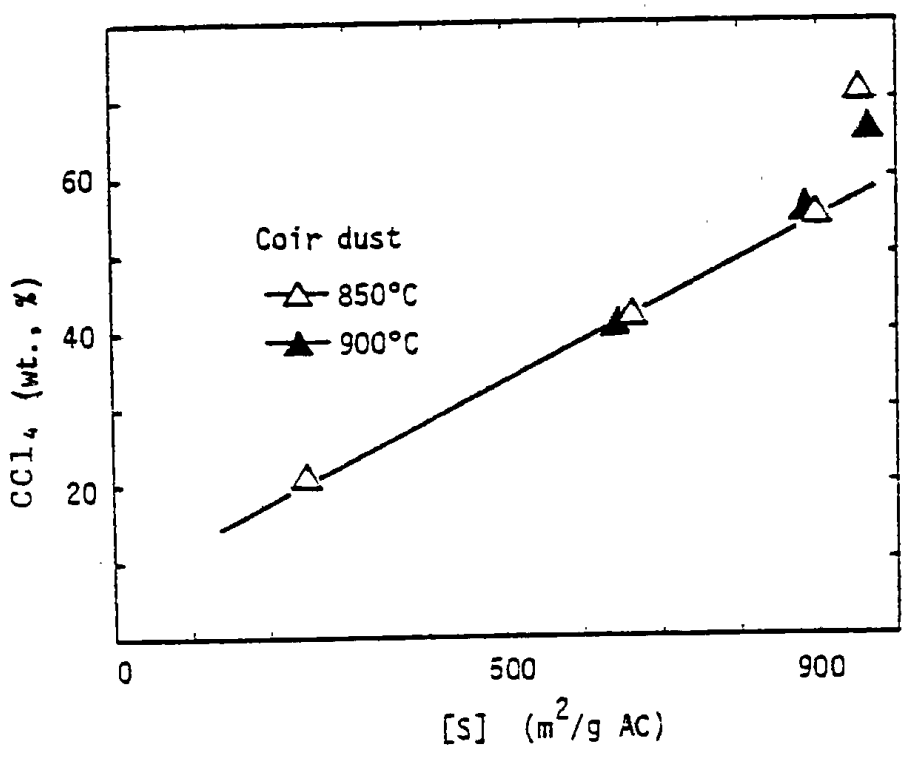

Fig. 5. Correlation between carbon tetrachloride adsorbability and internal surface area.

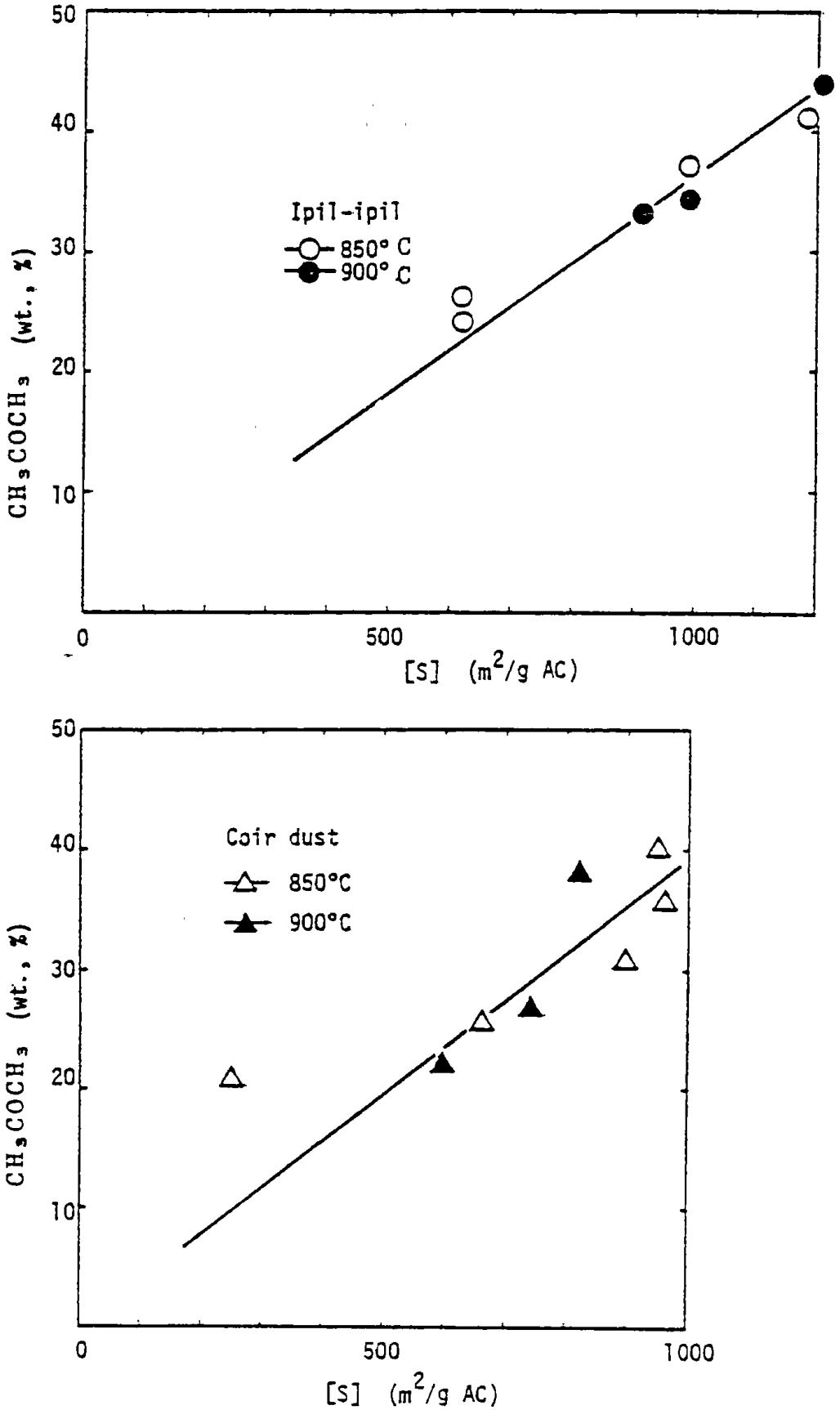

Fig. 6. Correlation between acetone adsorbability and internal surface area.

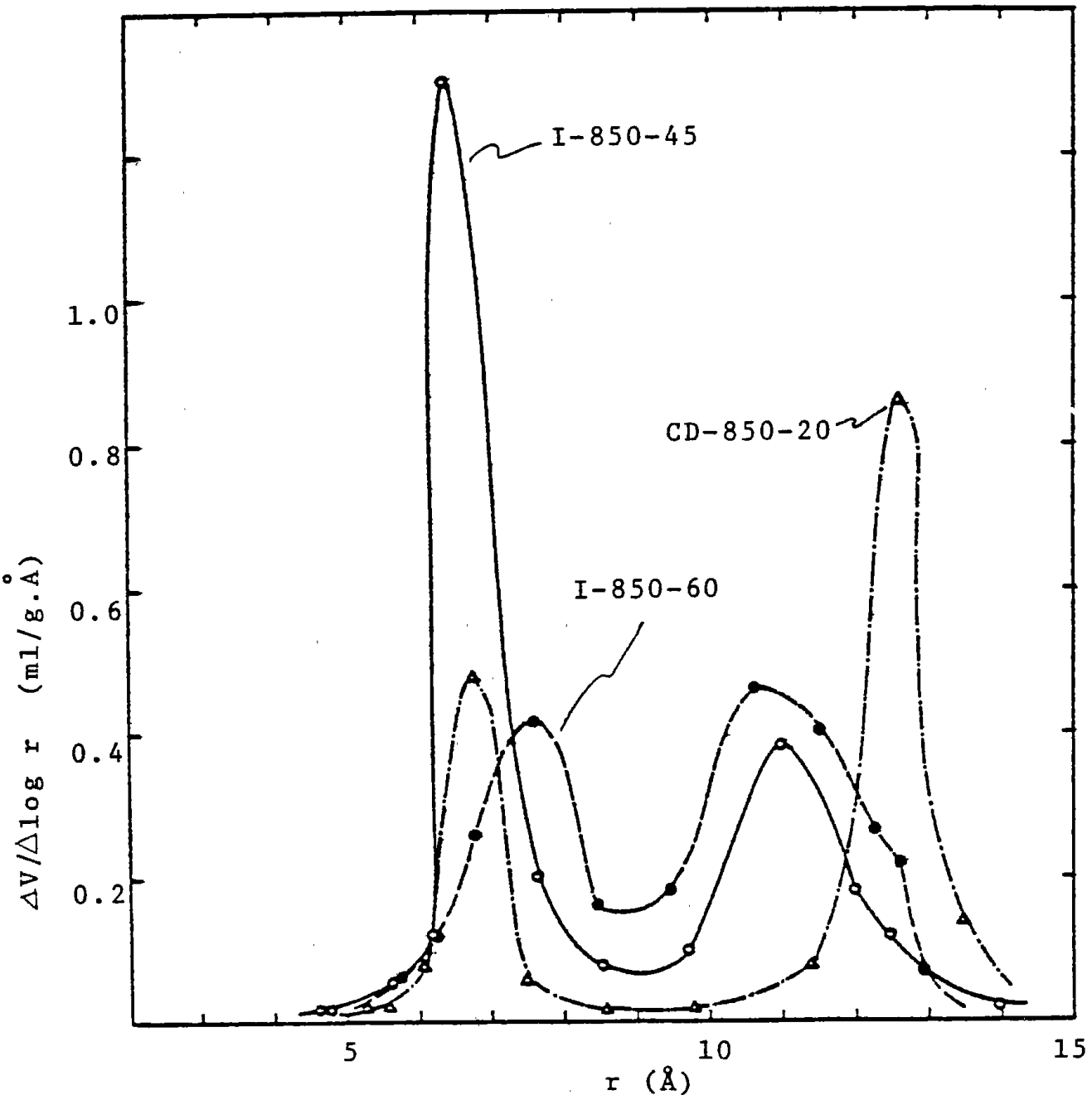

Fig. 7. Pore size distribution curve of activated carbon products.

III Steam activation of chars by the use of an inner heat type fluidized bed reactor.

by
Hideo Hosoda, Kazuhiko Niikawa,
Katsuji Ishibasi, Yoshio Noda

In the previour works, as described in part I and 2 in this report, we obtained basic data and parameters about production of activated carbon from tropical plants using an external heat type batch reactor.

It is known, however, that the reactor is not beneficial for practical use because of it's high energy consumption.

The present work was done to evaluate activation of chars using an inner heat type fluidized bed reactor to explore practical process for the production of activated carbon from tropical plants.

Experimental

Sample preparation

IPIL-IPIL and Coir-Dust were selcted as raw materials, and were carbonized using the procedures described before. The powder and the granulated chars prepared by the previous method were used as sample.

Apparatus

A flow sheet of the inner heat type fluidized bed reactor is shown in Fig.1.

The reactor, 160cm long, made of stain-less steel was shaped as seen in the figure: upper part was step wise expanded by two different sizes of diameter so that the small particles of sample could be retained longer in the reactor.

Sample was fed into the reactor by a screw feeder fixed at just above level of a perforated plate. The activated carbon products were taken out from a take off pipe by opening a valve fixed at it's inlet located at the opposite side of the screw feeder.

A propane gas burner connected with an air pipe was located at just below the perforated plate. Steam was fed into the bottom side of the reactor from a water boiler through a steam heater with which steam was heated to 650°C. The feed rates of the fuel gas, air and steam were measured by gas flow meters, weighing loss of water in the boiler respectively. Temperatures in the reactor were measured, recorded by thermometers located at six point of it.

The exhausted gas possed through a dust collector box was led into a condender in which steam was condensed and removed, then purged from an outlet of the water collector box.

Analytical procedure

Gas analysis was done in terms of O_2, CO_2, CO, H_2, and CH_4, in the exhasted gas by gas chromatography.

The methelene blue adsorptive valve, iodine number, internal surface areas and pored distribution of the activated carbon products were measured by the methods described in previous paper.

Experimental procedure

All experiments were carried out by batch method.

The amount of sample taken for each experimental test were 100grs. for powders, 200grs. for granules respectively. Table 1 shows proximate analysis of samples used.

The reactor was heated previously up to 900°C in it's temperature under a certain feed rates of gases before sample feeding. The feed rates of fuel gas, air and steam are listed in table 2.

The activated carbon products were taken out at various reaction time and calculation of the yields expressed as percent weight of chars fed, adsorptive ability tests were performed.

Resrlts and discussion

Fig.2 shows temperature change at the center of the fluidized bed about 200mm above the burner nozzle during activation reaction; the temperature droped rapidly from 900°C to near 800°C immediately after sample feeding, then went down slowly to it's minimum point, 720°C for powders, 760°C for granules, and then raised up as time procceded.

The yields of carbon decreased with procceding of the time as shown in Fig.2 expressed the relation between them as inverse proportional.

The activation of granules completed in relatively short time than that of powders: yields of the former became almost zero percent within 20 minutes, while the latter 40 minutes.

The difference may be caused by the following reason. The bulk density of the granules is about 4 times larger than that of the powders as seen in Table 1 besides sharp factor of the latter is considered to be smaller than the former, therefore the incipient fluidization velocity (Umf) of the former become larger than the latter as listed in below:

	Umf (cm/sec)			
IPIL-IPIL	P	7.5	G	18
Coir-Dust		2.5		15

This indicates that the granules are fluidized in the reactor at relatively lower part in which temperature is higher than the upper part where the powders tend to be fluidized, so that the activation reaction of the former can be promoted than the latter.

The adsorptive capacities of the activated carbon products such as methylene blue value and internal surface areas varied with activation time as seen in Fig. 4 and 5 .

Both values increased to their maximum then decreased with proceeding of time.

The yields of the products having the maximum values were between 10 to 20 percent regardless of the form of samples.

Those maximum values and the yields are listed in Table 3 compared with the results obtained with the external heat type reactor.

The fact that the adsorptive capacities of the carbons produced from the inner heat reactor are not so inferior to those from the outer heat reactor, even though the activation time was short and that the temperature is lower, is noticed. This may be difficult to rationalize, however it is assumed that some gases in atomosphere in the inner heat reactor such as oxygen, CO_2, and others seen in Table 2 contribute to the activation reaction of which main activating gas is steam, on the other hands, only steam is used in outer heat reactor.

The adsorptive capacities such as methylene blue value or iodine number were roughly proportional to the surface area as seen in Fig. 6, more over, shape of the linear curves, either the gradient or the intercepting point on the horizontal axis, was similar to the result from the outer heat type reactor. Pore destribution in the carbons was also similar.

Fig. 7 shows pores destribution curves of granulated carbons from coir-dust at various activation time. The pore radii of all samples were observed mainly in the range from 5°A to 15°A and total volume of the pores having those radii decreased with proceeding of reaction time.

The result suggests that the optimum activation time is around 15 minutes.

Table 4 shows methyelne blue value in the IPIL-IPIL powdered carbon of different particle size group.

The fact that the value for both group is nearly same except for those obtained in short activation time like 10 minutes suggests an advantage of a fluidized bed to get products of homogeneous quality due to violent agitation in it.

Conclusion

From the results obtained by the current experiments, it was cleared that the inner heat reactor had following advantages and disadvantages for the activation of chars from tropical plants compared with the outer heat reactor :

Advantages.

1. considerable saving in energy consumption.
   Although quantitative comparison for the energy consumption in the both reactor was not done, it is obvious, from the view point of the heating system and energy efficiency, that the inner heat reactor will be able to save considerable energy consumption.
   However, further research would have be carried out in this area.
2. Time reduction for activation.
   As descrived before, the optimum activation time for the samples tested was within 15 minutes in the inner heat reactor while the outer heat reactor required 30 minutes or more to get carbon of same quality and yield.
   However, quantitative explanation for the fact could not obtain from both view point of chemical reaction and of chemical engineering.
   Further research is required in this area.

Disadvantages

As gaseous or liquid fuels are used for the heat sources in inner heat reactors, it is difficult to control the temperatures in the reactors without any disturbance to the fluidizing conditions for solids: If a certain amount of solids requires higher temperature, the only way is to increase the feed rate of the fuel gas (liquids) but it brings change in verocity of fluid in the reactor like Umf and, in the extreme case, solids are blown out of the reactor.
Further research including design of reactors and burning system of fuels would be carried out in this area.

Table 1. Proximate Analysis of samples

Sample	W [%]	V M [%]	Ash [%]	F C [%]	ρ_b [g/cc]	$\bar{D}p$ [mm]
Ipil-ipil raw material	10.25	72.94	1.52	15.29	0.31	1.15
(P) Ipil-ipil char 430	2.26	17.16	3.78	76.16	0.15	0.74
(G) Ipil-ipil char 430	7.11	29.78	7.28	55.83	0.63	1.10
(G) Coir dust char 430	7.08	28.43	11.01	54.48	0.44	1.00

(P) : Powderd char produced at 430°C
(G) : Granulated char produced at 430°C
V M : Volatile Combustible Matter
F C : Fixed Carbon
ρ_b : Bulk density
$\bar{D}p$: Average perticle diameter

Table 2. Gas component of atomosphere in the reactor before and after sample feeding

feed gases: (l/min)	fuel gas (from LPG); 2, air; 4, steam; 0.11					
	Gas component %					
	H_2	O_2	N_2	CO	CO_2	CH_4
before sample feeding (fuel combustion gas)	4-7	1.5-1.6	74-78	3.2-3.5	12-14	—
after sample feeding	18-21	0.5-0.7	49-55	9-13	14-20	0.2-0.5

Table 3. Comparison of adsorptive capacities of activated carbons obtained with different reactors

Reactor Type	Sample	θ(min)	t(°C)	MB(mg/g)	S(m^2/g)	Y(%)
OHA	IPIL-IPIL P	60	850	370	1520	30
IHA	IPIL-IPIL P	30	750-800	262	1024	27
OHA	IPIL-IPIL G	45	850	285	1000	20
IHA	IPIL-IPIL G	15	710-750	230	850	27
OHA	Coir-Dust G	20	850	320	950	47
IMA	Coir-Dust G	10	710-750	269	965	27

OHA : Outer heat type reactor

IHA : Inner heat type reactor

Table 4. Methylene blue value of activated products produced with the inner heat reactor from different particle size of chars.

θ (min.)	Y (%)	MB (mg/gAC)	Dp (mm)
10	50.3	83.5	A
	49.8	108.5	B
15	37.5	141.0	A
	39.2	130.0	B
20	36.9	183.5	A
	40.0	185.5	B
30	30.0	262.0	A
	11.8	204.0	B
35	9.3	170.0	A
	2.5	178.0	B

Dp : Average particle size

A : 1.19 mm under

B : 1.19 - 2.83 mm

Fig. 1. Schematic flow diagram of the experimental apparatus

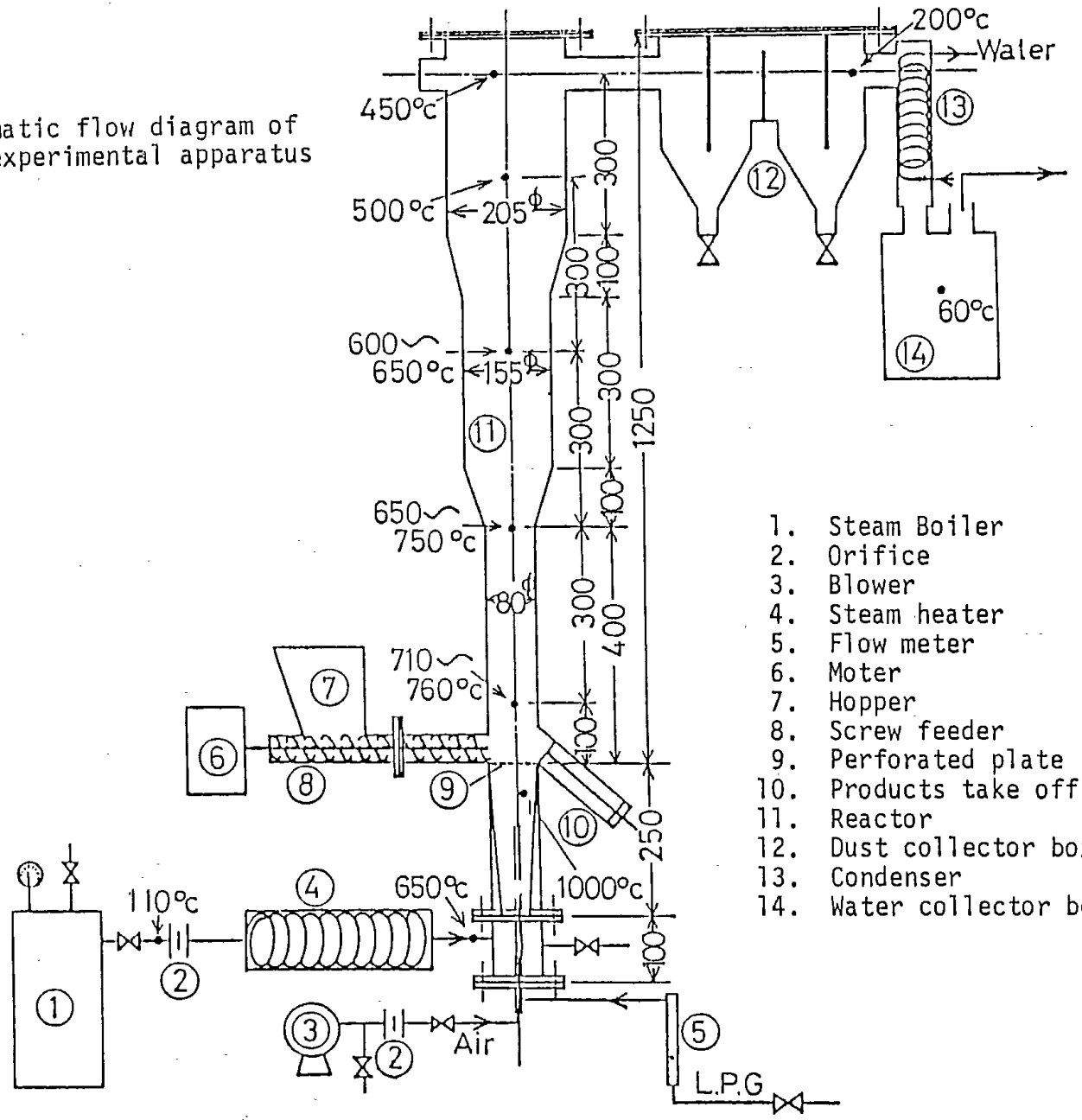

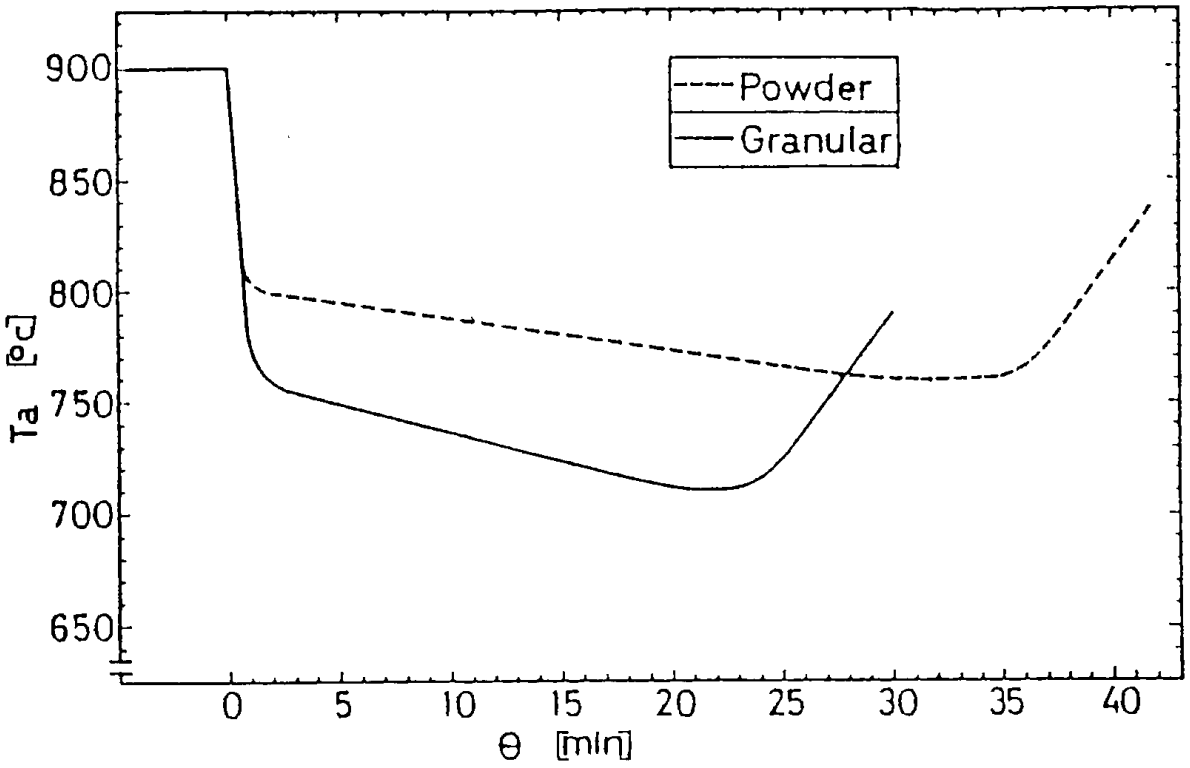

Fig. 2. Changes in the bed temperature during activation reaction

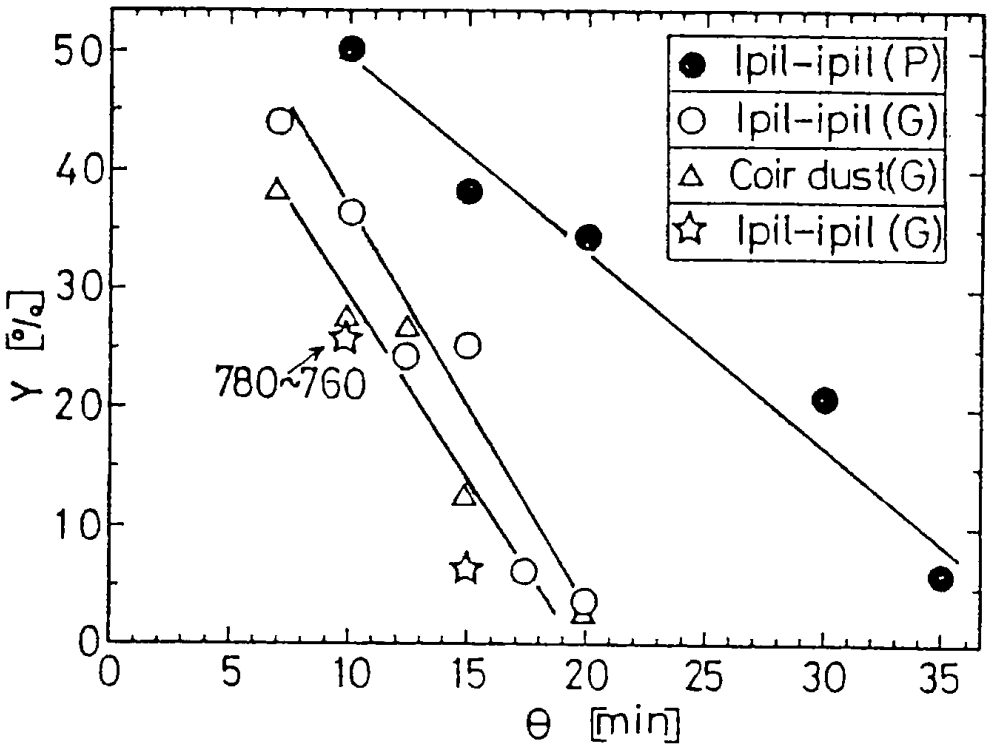

Fig. 3. Correlation between yield and reaction time

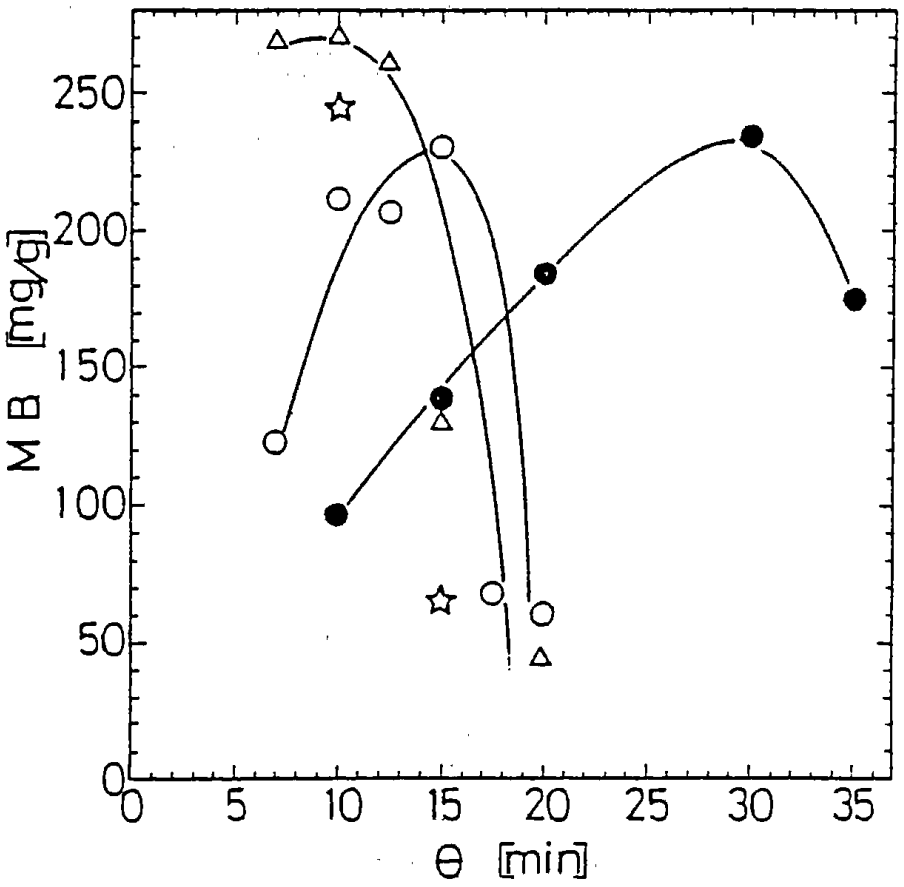

Fig. 4. Effect of activation time (θ) on MB value of activated carbon products.

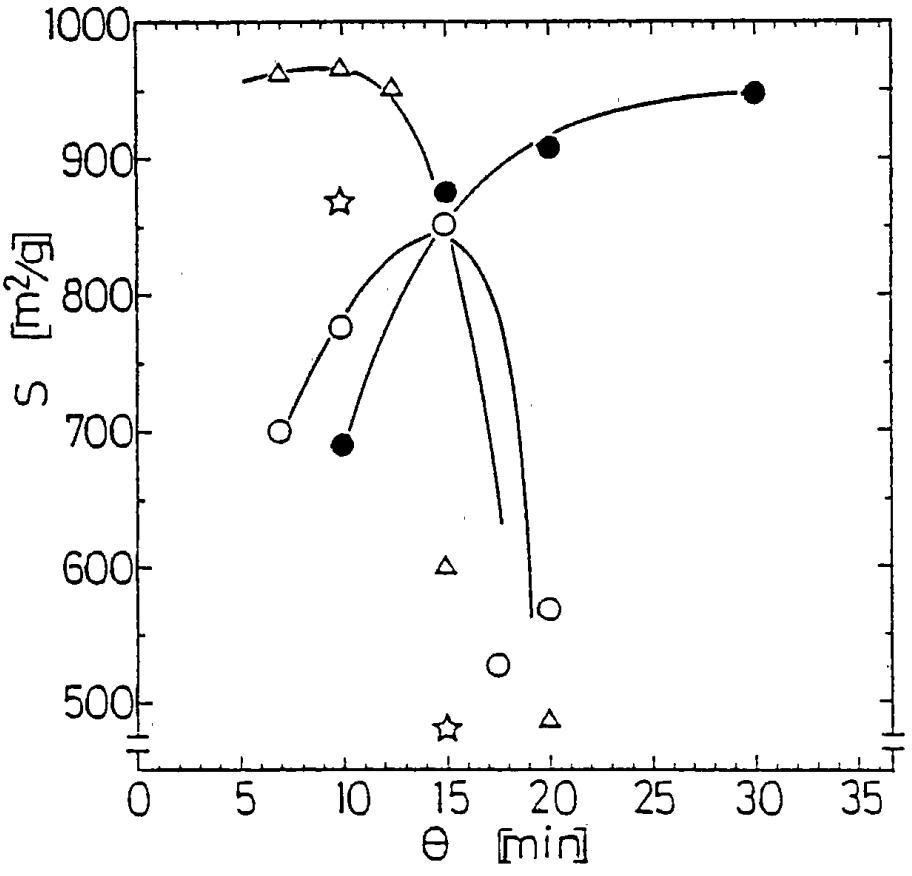

Fig. 5. Effect of reaction time (θ) on surface area (S) of activated carbon products.

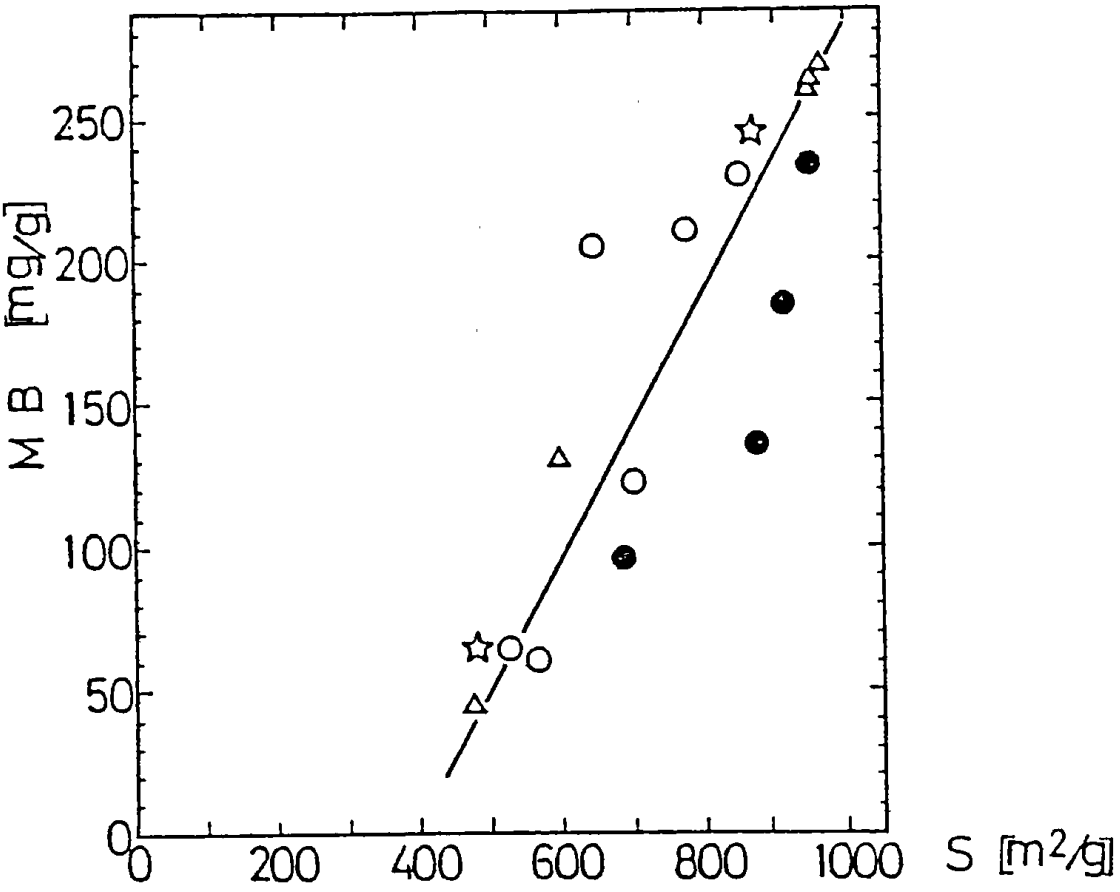

Fig. 6. Correlation between MB value and surface area (S).

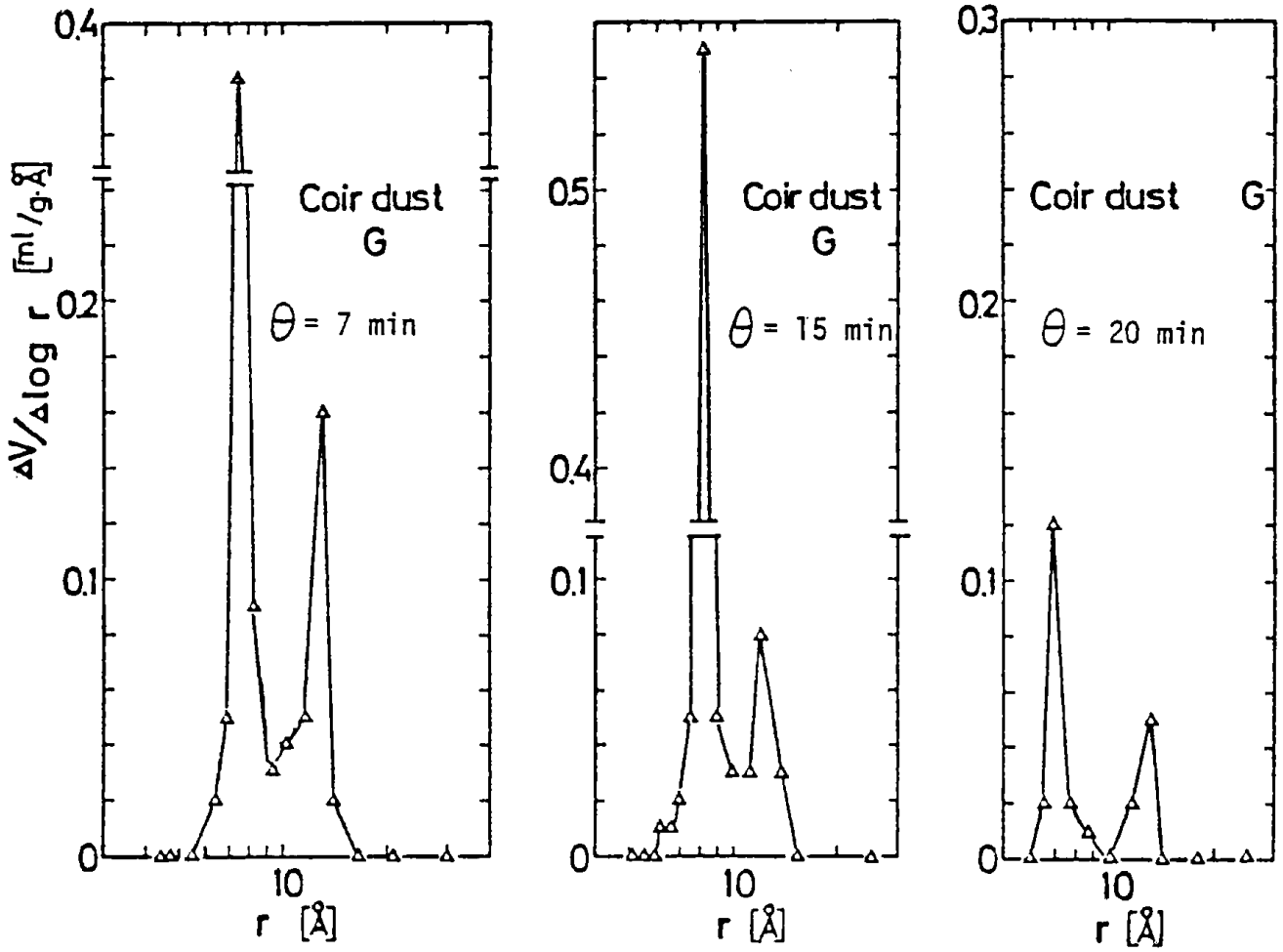

Fig. 7. Pores destribution curves of activated carbons obtained at various activation time

Infrared Studies on Water Adsorption Systems with the Use of HDO. II. Na-Y Zeolite

Masao HINO* and Yasuko MIKAMI

Government Industrial Development Laboratory, Hokkaido, Higashi-tsukisamu, Toyohira-ku, Sapporo 061-01

(Received July 5, 1978)

Infrared spectra of the systems of Na-Y zeolite–H_2O, D_2O, and HDO were measured. It was shown that there are three types of adsorbed water in the zeolite–water system. Type I: adsorbed in a state in which two hydroxyl bonds are highly non-equivalent; it gives absorptions at 3695, 3400, and 1645 cm^{-1}, and is the same type as that on the Molecular sieve 13X.[1] Type II: adsorbed in another state in which the bonds are nearly equivalent; it gives bands at 3610, 3540, and 1645 cm^{-1}. Type II was more resistant to dehydration than Type I, and was irreversible for the back-adsorption of a small amount of water at room temperature, whereas Type I was almost completely reversible. Type III was observed for back-adsorption under this condition; it gives bands at 3635, 3500, and 1655 cm^{-1}. Type III can be transformed into Type II by heat treatment at a temperature which varies depending on the amount of adsorbed water. The other bands were assigned as follows: Bands at 3750 and 3645 cm^{-1} correspond to stretching of surface structural OH, and that at 3240 cm^{-1} to overtone deformation of adsorbed water. The sites of adsorbed water molecules of Types I and II were discussed.

In a previous paper[1] one of the authors showed that HDO could be effectively used for the IR analysis of water adsorption systems through the analysis of the system on Molecular sieves 13X and 4A. In the present paper, the water adsorption system on Na-Y zeolite will be analyzed by employing the same technique.

A number of IR studies have been published on the water adsorption system.[2–5] However, not all of the bands have been clarified, and there are some disagreements about the spectra observed and their assignments. The purpose of the present work is to analyze the spectra of the system on the basis of information obtained from a new technique employing HDO. The sites of the adsorbed water molecules will also be discussed.

Experimental

Linde Molecular sieve SK-40 (UNION SHOWA Co., Ltd.), which is a synthetic Na-Y zeolite, was used as the sample. Major components of the material were SiO_2 63.5, Al_2O_3 23.5, and Na_2O 13.0 in wt%. The crystallinity of the sample was confirmed to be sufficiently high by the measurements of X-ray diffraction and surface area (903 m^2/g, N_2).

Two IR spectrophotometers, a DIGILAB Model 15-B FTS and a JASCO Model 402-G, were used for recording the spectra. The latter instrument was calibrated against the former by use of ammonia, water vapor, and hydrogen bromide.

Other materials, apparatus, and procedures were the same as described before.[1]

Results

Spectra for the Desorption Process. The spectra of Na-Y zeolite–D_2O and H_2O systems after being evacuated at various temperatures are shown in Figs. 1 and 2. As seen in the Figs. various bands observed in the spectra of the two systems after the corresponding evacuation treatments can be easily matched with each other. These matching bands will be referred to using the same letters: a, b,···, and g for the spectra of both systems. Frequencies of these observed bands

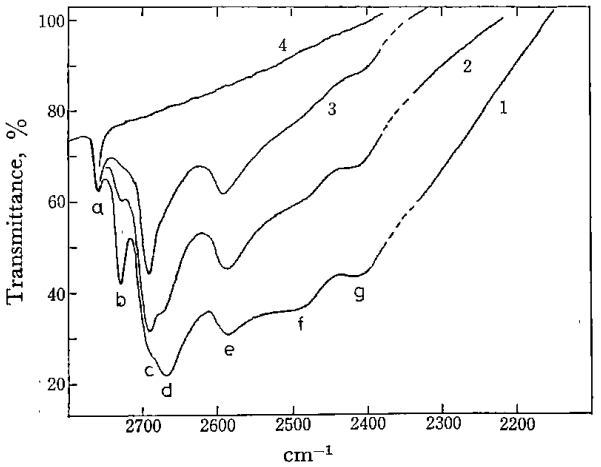

Fig. 1. Spectra of the Na-Y–D_2O system, on the desorption process.
Evacuated for (1) 1 h at 90 °C, (2) 1 h at 120 °C, (3) 30 min at 165 °C, (4) 3 h at 500 °C. "Thickness" of the sample piece was 18 mg/cm^2.

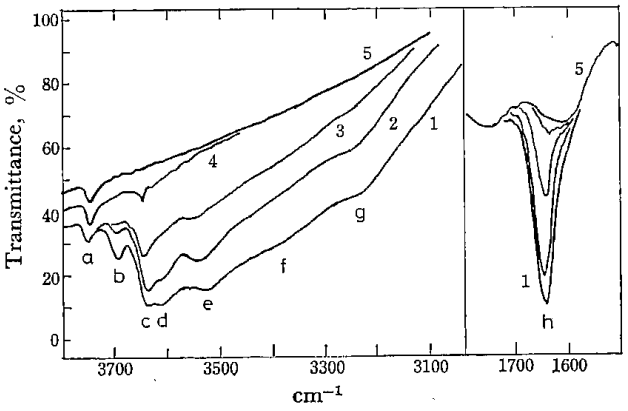

Fig. 2. Spectra of the Na-Y–H_2O system, on the desorption process.
Evacuated for (1) 1 h at 90 °C, (2) 1 h at 120 °C, (3) 30 min at 165 °C, (4) 45 min at 200 °C, (5) 3 h at 500 °C. Sample piece "thickness" 18 mg/cm^2.

TABLE 1. SUMMARY OF THE IR BANDS OF Na-Y ZEOLITE–WATER SYSTEM

Band symbol	D_2O system (cm^{-1})	H_2O system (cm^{-1})	HDO system (cm^{-1}) Stretching regions OD	OH	Deformation region	Assign
			(1) The desorption process			
a	2760	3750	2760	3750		1)
b	2730	3695	2714	3690		2)
c	2692	3645	2692	3645		3)
d	2668	3610	2647	3600		4)
e	2586	3540	2615	3540		5)
f	2490	3400	2490	3380		6)
g	2405	3240				7)
j				2940		8)
k					1460	9)
n					1422	
h		1645				
l					1450	10)
m					1440	
			(2730)			11)
			(2) The adsorption process			
a	2760	3750	2760	3750		12)
b	2730	3695	2717	3690		13)
o	2675	3635				
q			2580	3250		14)
p	2575	3500				
f	2480	3350	2465	3350		15)
g	2405	3240				16)
j				2960		17)
s		1655				18)
r					1495	
h		1640				
k					1460	19)
n					1422	

1,12), 3): OD(OH) stretching of structural deuteroxyl groups. 2,13), 6,15), 9,19): OD(OH) stretching and deformation of Type-I water. 4), 5), 10): OD(OH) stretching and deformation of Type-II water. 7,16): DOD(HOH) overtone deformation of adsorbed water. 8, 17): Overtone deformation of adsorbed HDO. 11): Arising from D_2O impurity. 14), 18): OD(OH) stretching and deformation of Type-III water.

are summarized in Table 1-(1) together with those of the corresponding bands observed for the HDO system and also with their assignments. The spectra observed for the H_2O system were similar to those reported by Ward,[2] with the exception that the band appearing at 3630 cm^{-1} in his spectra was observed to be clearly separated into two bands at 3645 (c) and 3610 cm^{-1} (d) in our spectra. Bands which were equivalent to these appeared at 2692 and 2668 cm^{-1} for the D_2O system.

Spectra observed for the HDO system in the OD, OH stretching and the HOD deformation regions are shown in Figs. 3 and 4. Those spectra shown in Figs. 3 and 4 were measured after the same evacuation treatments as those performed prior to the measurements of the spectra shown in Figs. 1 and 2, respectively, so that a comparison between the spectra of the D_2O or H_2O system and of the HDO system should be reasonable.

Correlations between the spectra in the OD stretching region of the HDO system and those of the D_2O system were analogous to those between the spectra in the OH stretching region of the HDO system and those of the H_2O system.

As in the case of the Molecular sieve 13X–water system,[1] bands a and c in the spectra of the D_2O or H_2O system appeared at just the same frequencies for the HDO system (bands a′ and c′ in Figs. 3 and 4). Band b shifted toward the lower frequency side by 16 cm^{-1} in the OD stretching region and by 5 cm^{-1} in the OH region for the HDO system. The weak absorption at 2730 cm^{-1} in Fig. 3 arises obviously from the D_2O present in the sample water mixture (about 6.3%). Band g disappeared from the spectra of the HDO system. A new band appeared for the HDO system at 2940 cm^{-1} in the OH stretching region; it can be attributed to an overtone deformation or a combination band of adsorbed HDO, like the band at 2945 or 2910 cm^{-1} which appeared in other zeolite–HDO systems.[1] Bands at 2668 (d) and at 2586 cm^{-1} (e) in the spectra of the D_2O system disappeared from the OD stretching region of the HDO system. Two

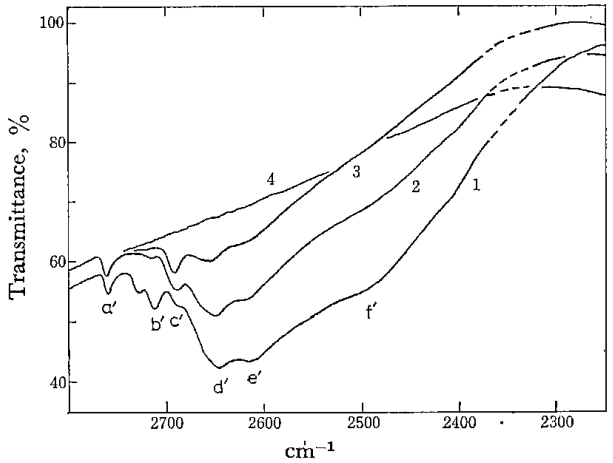

Fig. 3. Spectra of the Na-Y–HDO system in the OD stretching region, on the desorption process.
Evacuated for (1) 1 h at 90 °C, (2) 1 h at 120 °C, (3) 30 min at 165 °C, (4) 3 h at 500 °C after exposure to the vapor of H_2O–D_2O mixture of a molar ratio of 3 to 1. Sample piece "thickness" 40 mg/cm².

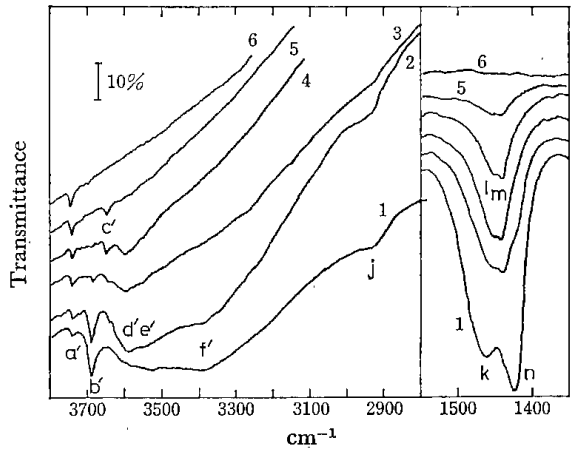

Fig. 4. Spectra of the Na-Y–HDO system in the OH stretching and deformation regions, on the desorption process.
Evacuated for (1) 10 min at 90 °C, (2) 1 h at 90 °C, (3) 1 h at 120 °C, (4) 30 min at 165 °C, (5) 45 min at 200 °C, (6) 3 h at 500 °C after exposure to the vapor of H_2O–D_2O 1 to 5 mixture. The spectra shown in the deformation region were obtained by rationing each observed spectrum against that after 500 °C evacuation of the Na-Y–H_2O system. Sample piece "thickness" was 26 mg/cm².

new bands, presumably corresponding to bands d and e, appeared at 2647 (d′) and 2615 cm^{-1} (e′) in the OD stretching region. In the OH region these bands d′ and e′ were detected in the spectra after evacuation at lower temperatures (curves 1 and 2 in Fig. 4) at 3600 and 3540 cm^{-1}, which were nearly the same frequencies as those of d and e in the spectra of the H_2O system. After the evacuation at higher temperatures, however, the band e′ could not be observed, probably because the absorption was weak and broad. In the deformation region four absorptions (k, l, m, and n) appeared at 1460, 1450, 1440, and 1422 cm^{-1} in the HOD deformation region for

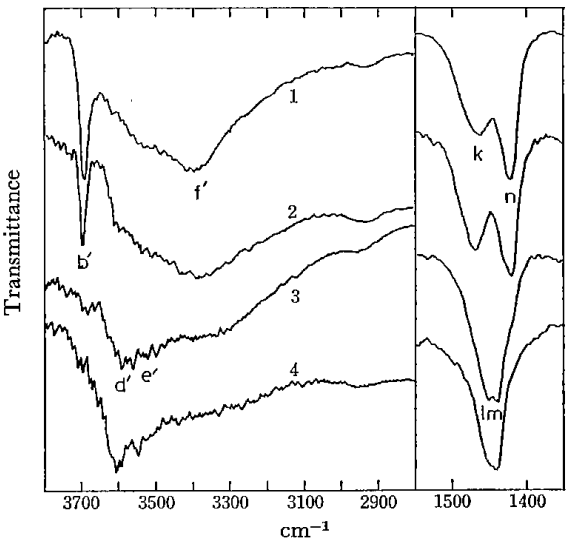

Fig. 5. Ratioed spectra of the Na-Y–HDO system in the OH stretching and deformation regions, on the desorption process. Obtained rationing (1) curves 1 and 2, (2) 2 and 3, (3) 3 and 4, (4) 4 and 5 of Fig. 4. The scale of the intensity is arbitrary as each curve is "auto expanded" into an identical hight in the frequency ranges indicated.

the HDO system, whereas only one at 1645 cm^{-1} (h) was found for the H_2O system.

On evacuation in a series where the evacuation temperature was elevated step by step, the intensity of the bands b and f for the D_2O (H_2O) system and also of the bands b′, f′, k, and n for the HDO system decreased preferentially in the initial steps, followed by the decrease of the bands d and e for the D_2O (H_2O) system and of d′, e′, l, and m for the HDO system. The intensity of band h decreased at a constant rate through the dehydration treatments. This can be seen directly in the ratioed spectra shown in Fig. 5. Those spectra were obtained for the HDO system by calculating the intensity differences between each curve shown in Fig. 4 by use of a computer system included in the FTS-15 spectrometer. Thus, it was suggested that bands b, f, and h for the H_2O (D_2O) system (corresponding bands b′, f′, k, and n for the HDO system) should have the same origin, while bands d, e, and the residual part of h (d′, e′, l, and m) came from another origin.

Spectra for the Adsorption Process. Spectral measurements on the adsorption process were also made for the systems of various kinds of water in the surface coverage of about 0—1.2 mmol/g. The general features of the spectra were almost identical irrespective of the degree of coverage in each of the systems, but were somewhat different from those of the spectra for the desorption process, as is seen in the typical examples shown in Figs. 6 and 7. Differences were found in two regions: one is the region where bands d and e appeared for the desorption process and the other is the deformation region. In the former, two relatively broad bands (o and p) appeared at 2675 and 2575 cm^{-1} for D_2O adsorption, and at 3635 and 3500 cm^{-1} for H_2O adsorption. Each of the former

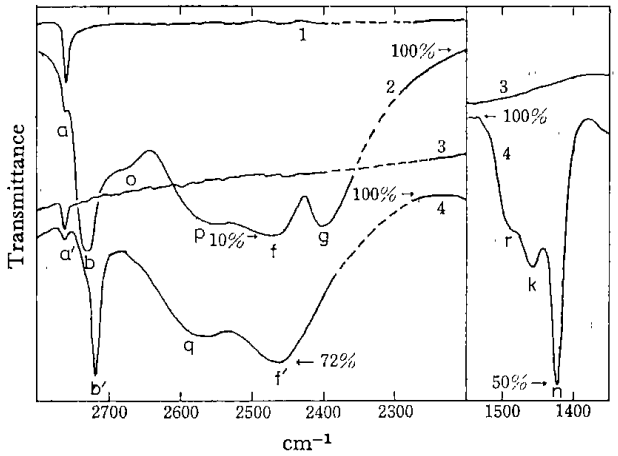

Fig. 6. Spectra of the Na-Y–D_2O and HDO systems in the OD stretching and the HOD deformation regions, on the adsorption process.
(1,3) Evacuated for 3 h at 500 °C, (2) 40 μmol of D_2O, (4) 40 μmol of H_2O–D_2O 7 to 1 mixture were readsorbed. All the curves were obtained by rationing the observed spectra against that after 500 °C evacuation of the Na-Y–H_2O system. Sample piece "thickness" 17 mg/cm².

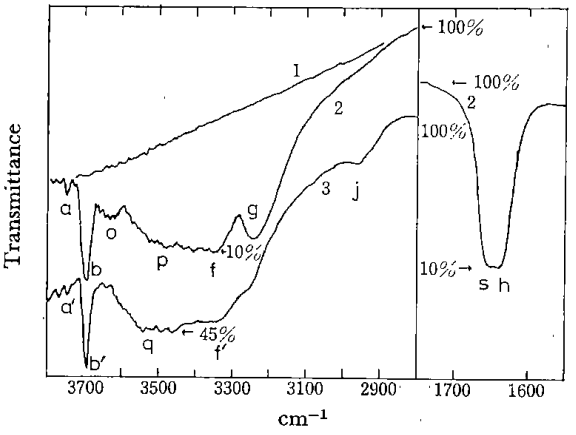

Fig. 7. Spectra of the Na-Y–H_2O and HDO systems in the OH stretching and the deformation regions, on the adsorption process. (1) Evacuated for 3h at 500 °C, (2) 24 μmol of H_2O, (3) 24 μmol of H_2O–D_2O 1 to 5 mixture were readsorbed. Curve 2 in the deformation region was obtained by rationing the observed spectra against that after 500 °C evacuation. Sample piece "thickness" was 17 mg/cm².

bands was very weak. For HDO only one broad band (q) was observed in the region around 2580 cm^{-1} for the OD region and around 3520 cm^{-1} for the OH region. Three deformation bands were observed for the HDO system, at 1495 (r), 1460 (k), and 1422 cm^{-1} (n), while two were found at 1655 (s) and 1640 cm^{-1} (h) for the H_2O system.

Observed frequencies of the various bands are summarized in Table 1-(2).

Discussion

Spectra for the Desorption Process. First, bands a and c can be assigned to the stretching vibrations of surface structural OH (OD) groups, while the remaining absorptions b, d, e, f, g, and h are attributable to some vibrations arising from adsorbed water molecules. This is because of the fact that each pair of corresponding bands, one appearing in the H_2O (D_2O) system and the other in the HDO system, of the former group appeared at the same frequency in the corresponding regions of the spectra of the H_2O, D_2O, and the HDO systems, while in the latter group the bands did not appear at the same frequency in at least one region of the spectra.

Thus there is just the same type of adsorbed water (Type I, adsorbed in a state in which its two hydroxyl bonds are highly non-equivalent) in the Na-Y zeolite–water system as the Type WX-I in the Molecular sieve 13X–water system which was reported in a previous paper.[1] That is, bands b, f, g, and h in the spectra of the present work are apparently attributed to the same vibrations as bands b, e, f, and at 1650 cm^{-1}, respectively, in the spectra of the 13X system. Each pair of these matching bands showed an almost identical behavior with the partial deuteration of the adsorption systems.

Absorptions d and e have been observed and reported only by Ward.[2] He assumed that they were due to some adsorbed water molecule, but no details were described. Our results in the present experiments support his assignment. Moreover, they give further information on the state of the adsorbed molecules as described below. When a water molecule is adsorbed in a state in which its two hydroxyl bonds are completely equivalent, the molecule is expected to give two stretching bands of ν_3 and ν_1 and one deformation band of ν_2 for H_2O (D_2O), as well as single OH and OD stretching bands which are located between the ν_3 and the ν_1 frequencies and one HOD deformation band for HDO. On the other hand, when the molecule is adsorbed in another state in which the hydroxyl bonds are not equivalent, H_A–O–H_B, it is expected that two OH stretching bands (one is rather characteristic of νOH_A and the other of νOH_B) and a single deformation band arise for H_2O and D-equivalent bands forD_2O. For HDO molecules in this state four stretching bands: νOH_A, νOH_B, νOD_A, and νOD_B and two deformation bands: $\delta H_A OD_B$ and $\delta H_B OD_A$ will occur. The degree of frequency difference between the vibrations νOH_A and νOH_B or between the two D-equivalent bands, as well as between the two deformation bands, will be larger, the larger the degree of the non-equivalency between the two hydroxyl (deuterioxyl) bonds. In the present results, bands d′ and e′, presumably corresponding to the $\nu OD_A(\nu OH_A)$ and the $\nu OD_B(\nu OH_B)$ of the HDO, appeared close to each other, being located between the frequencies of the corresponding bands d and e of the D_2O (H_2O). Thus, bands d and e can be assigned to the ν_3 and ν_1 vibrations of water molecules adsorbed in a state in which its two hydroxyl bonds are nearly equivalent (Type II). The result in the deformation region also supports this assignment. Two deformation bands (l and m) were observed to be very close to each other, with a difference of only

10 cm^{-1}, for the Type II adsorbed HDO. The corresponding difference was 38 cm^{-1} for the Type I water, in which the difference between the two OD stretching bands was 224 cm^{-1}. Hence, such a small difference of 10 cm^{-1} will be reasonable for the Type II water, in which the difference between the two OD stretching bands was 32 cm^{-1}.

In a previous paper[1] it was suggested that the weak absorption at 3590 cm^{-1} (D-equivalent band at 2645 cm^{-1}) in the spectra of the Molecular sieve 13X–water system was due to some type of adsorbed water molecule, but with no details. It is almost certain that the band arose from a similar type of adsorbed water to the present Type II water.

Spectra for the Adsorption Process. From a comparison with the spectra of the desorption process, the deformation band at 1640 cm^{-1} (h) in the H_2O system should correspond to those at 1460 (k) and 1422 cm^{-1} (n) of the HDO system, and the new band at 1655 (s) to that at 1495 cm^{-1} (r). This speculation is in harmony with the appearance of the bands in the stretching regions. Bands b, f, and g did appear at almost the same positions as those in the spectra of the desorption process; moreover, they showed similar behavior to those of the latter bands for the partial deuteration. On the other hand, bands o and p for the H_2O (D_2O) system and q for the HDO system are quite different in their spectral aspects from bands d, e, d′, and e′ of the desorption process. These facts indicate that the Type I water is almost reversible while the Type II is not, for readsorption of a small amount of water at room temperature.

The new bands o (3625, D-equivalent 2675 cm^{-1}), p (3500, D-2575 cm^{-1}), and s (1655 cm^{-1}) would be assigned to the ν_3, ν_1 and ν_2 vibrations of water adsorbed in some state with its hydroxyl groups equivalent (Type III), and bands q at 3520 and 2580 cm^{-1} and r (1495 cm^{-1}) to the OH stretching, OD stretching, and the deformation of the corresponding HDO molecules.

The state of these adsorbed molecules is obviously different from that of the Type II water, even if somewhat similar to it. In order to investigate this irreversibility a simple experiment was carried out. After 0.83 mmol/g of D_2O was back-adsorbed at room temperature, the sample piece, *in situ*, was heated up to 95 °C or 200 °C once, and then cooled slowly down to room temperature. It was found that the treatment at 200 °C gave rise to a great change in the spectrum, giving a similar spectrum to that on the desorption process with bands at 2694 (c), 2674 (d), and 2590 cm^{-1} (e). This indicates the rearrangement of the adsorbed water molecule, probably from the Type III to the Type II, and the formation of certain structural hydroxyl groups caused by dissociation of adsorbed water. And also it suggests that the Type II water is more stable than the Type III water. However, in the 95 °C treatment no spectral change occurred, whereas our spectra for the desorption process were obtained by 10 min of evacuation at 90 °C after the dried sample piece was saturated with water vapor. Thus, it is suggested that the occurrence of the rearrangement of adsorbed water and the formation of the hydroxyl groups depend on the degree of surface coverage as well as temperature. The details can not be known without further experiments.

Sites of Adsorbed Water Molecules. Mutual comparison of the results obtained for the present Na-Y zeolite and for the Molecular sieves 13-X (Na-X zeolite) and 4-A (Na-A zeolite)[1] makes it possible to discuss the sites of adsorbed water molecules.

Type I and Type II water existed on both the zeolites of Na-X and Na-Y, while on the Na-A zeolite Type I water could not be found. The single main type of adsorbed water observed on the Na-A is regarded to be similar to the Type II water in its symmetry.

Under such a condition of much lower surface coverage,[6] it is almost sure that the adsorption of water molecules occurred mainly on the zeolitic cations in such a manner that the lone pair electrons of the water oxygen atom are attracted to the positive charge of the cations, whether or not the hydrogen atoms are hydrogen bonded to the negatively charged oxygen of the zeolite lattice. Hence, it will be reasonable that the variety in the modes of adsorption should be discussed in connection with the kind of cation sites.

It is well known that the crystal structures of zeolites X and Y are essentially identical, but differ only in the number of their cations and the strength of the electrostatic force field around the cations. According to Rabo *et al.*,[7] there are three kinds of possible cation sites, S_I, S_{II}, S_{III}, in the zeolite structure. The number of each site is 16, 32, and 48, respectively, for a X type zeolite of which the ratio of Al and Si equals unity. These sites are occupied by exchangeable cations, fully or partially, depending on the type of the zeolite. On the other hand, Na-A zeolite[8] has another structure. But it includes sodalite cages similarly to the structure of the Na-X or Na-Y. There are two kinds of sites, S_1 and S_2, in the type A zeolite. For the Na-A, 12 Na cations are required per unit cell for electrical neutrality, of which 8 Na cations occupy the former site and the remaining 4 Na the other site.

Among those five kinds of sites, the site S_I can be ruled out of consideration because the cations positioned at that site will not be able to accept any adsorbate due to its small space. Site S_{II} is regarded to be similar to site S_1. Both are situated on the center of the six-membered rings of the sodalite cages facing toward the super cages of the zeolite structure, and have a C_{3v} symmetry in relation to the neighboring lattice oxygens. Site S_{III} is characteristic of zeolites X and Y, which is located on the center of four-membered rings of the sodalite cages and has a symmetry of C_{2v} in relation to the neighboring oxygens. Zeolite A has no such site.

From both the similarity and the differences among the three zeolites in the geometry around the possible cation sites and in the observed spectra, it is suggested that the Type I water is situated on the cations occupying the site S_{III}, whereas the Type II is on those of site S_{II}.

These attributions are supported by a comparison between the intensity of the spectra of each type of adsorbed water and the number of the cations occupying each site, as described below. The relative

amount of the Types I and II water on the Na-X and Na-Y zeolites can be estimated from the results shown in the present Fig. 1 or 2 and those shown in Fig. 1 or 2 of the previous report.[1] In that case, the intensity of the spectra of the 13-X water system must be compared with the other after being multiplied by a factor of 1.6, which appears from the differences in the sample thickness and the molecular weight per their unit cells.[9] Then, it can be seen that there is a much smaller amount of Type I adsorbed water on the Na-Y zeolite than on the Na-X. The Type II water is estimated to be present in much the same amount on both zeolites, or at least not so much less on the Na-X than on the Na-Y zeolite, though this is not very clear because of the overlapping of the spectra of the Types I and II water. On the other hand, according again to Rabo *et al.*,[7] the order of preference for cation occupation is $S_I > S_{II} > S_{III}$, which may lead to the conclusion that our Na-X sample (Si/Al=1.23) includes 16, 32, and 38 Na ions per unit cell for the respective sites, while the Na-Y sample (Si/Al=2.3) includes 16, 32, and 10, respectively. That is, the ratios of the cation number positioned on the same site in Na-X and Na-Y are 1:1 for the site S_{II} and 38:10 for the S_{III}. This may be comparable with the relative intensity of the spectral bands described above.

The molar absorptivity for the Type II water appears to be weaker than for the Type I water. This is probably due to the fact that the Type I water is more strongly polarized than the other. It has been shown by Dempsey[10] that the electrostatic force fields around the site S_{III} is some 50% stronger than that around site S_{II}.

It is obscure at present why and in what geometrical arrangements the Types I and II water are adsorbed on the sites, yielding such modes as described before. To answer this question, further experiments with the use of other techniques are necessary.

References

1) M. Hino, *Bull. Chem. Soc. Jpn.*, **50**, 574 (1977).
2) J. W. Ward, *J. Phys. Chem.*, **72**, 4211 (1968).
3) J. W. Ward, *J. Catal.*, **11**, 238 (1968).
4) C. L. Angell and P. C. Schaffer, *J. Phys. Chem.*, **69**, 3463 (1965).
5) G. Senkyr and H. Noller, *J. Chem. Soc., Faraday Trans. 1*, **71**, 997 (1975).
6) In the case shown in Fig. 7 the number of the adsorbed H_2O molecules corresponds to 0.05 in θ, provided that the cross section of the water molecule were 10.8 A^2, and to about one-sixth in number of the cations included to the sample.
7) J. A. Rabo, C. L. Angell, P. H. Kasai, and V. Schomaker, *Chem. Eng. Prog.*, **63**, *Sympo. Ser.*, No. **73**, 31 (1967).
8) P. A. Howell, *Acta Crystallogr.*, **13**, 737 (1960).
9) Thickness of the sample pieces were 12 mg/cm^2 and 18 mg/cm^2 respectively for the Na-X (Molecular sieve 13X) and Na-Y zeolites. Molecular weight of the zeolites per unit cells are 13423 g and 12809 g for Na-X and Na-Y, respectively.
10) Ref. 7, p. 33.

(Bulletin of the Chemical Society of Japan Vol. 52, No. 7, (1979) pages 2099~2104).

Fe(Ⅱ)-edta•$MgSO_3$水溶液によるNO吸収反応の赤外吸収スペクトル(Ⅰ)*

日野 雅夫，福田 隆至
新田 順子**，平間 康子

1. 緒　　言

燃焼排ガスに含まれる NO_x，SO_x の湿式同時除去の吸収剤として，エチレンジアミンテトラ酢酸と第一鉄〔Fe(Ⅱ)-edta〕，ならびに Fe(Ⅱ)-edta，Fe(Ⅲ)-edta にそれぞれ Na_2SO_3 あるいは $(NH_4)_2SO_3$ を加えた混合水溶液を用いる方法が多数報告されている[1~5]。

著者らは，既存の脱硫プロセスにおいてアルカリ土類化合物を用いる方法が数多く採用されていることから，それらのアルカリ土類化合物をNO吸収剤として用いる方法を検討し，Fe(Ⅱ)-edta に $MgSO_3$ を加えた混合水溶液が NO と SO_2 に対しすぐれた除去性能をもつことを見出している[6~7]。

本報では，NO と Fe(Ⅱ)-edta～$MgSO_3$ 吸収液との，反応の過程ならびに液相生成物に関する基礎的知見を得るために，これら反応系の FTIR による検討を行う。第Ⅰ報では，以後の研究に必要な基礎的知見となる NO～吸収液系の IR スペクトルの各吸収帯の帰属を行い，さらに反応過程の解析ならびに液中生成物の同定について若干の検討を行った。

2. 実　　験

2.1 試　薬

Na_2 edta，$FeSO_4$，$Fe_2(SO_4)_3$ は市販の特級試薬を用いた。$MgSO_3 \cdot 6H_2O$ は1級の酢酸マグネシウムと1級の亜硫酸ナトリウムから合成したものを用いた（キシダ化学製）。$N(SO_3K)_3 \cdot 2H_2O$ および $NH(SO_3K)_2$ は，Sisler ら[13]の方法で合成したものを用いた（キシダ化学製）。$N(SO_3K)_3 \cdot 2H_2O$ の組成分析値は，K：30.03，N：4.94，S：20.21重量%であり，また，$NH(SO_3K)_2$ では K：30.35，N：5.99，S：18.49重量%であった。いずれにおいても S 含量は理論値を下回っているが，これらの赤外吸収をKBr法で測定した結果そのスペクトルは服部ら[12]によって報告されているものと完全に一致した。

^{14}NO および N_2 は市販高純度ガスを用いた。^{14}NO 中の NO_2 含有率は約 500ppm であった。H_2O はイオン交換蒸留水，D_2O は MERK 製 99.75atom % のものを，それぞれ N_2 ガスを流通し脱酸素後用いた。

^{15}NO は British Oxygen Co., Ltd. 製 97.7atom %のものを用いた。

2.2 実験操作

標準的濃度の吸収液として，$FeSO_4$：0.1，Na_2edta：0.1 および $MgSO_3$：0.2mol/ℓ の混合水溶液または重水溶液を用いた。以後，これを標準吸収液と呼ぶ。

吸収管には，容積約 4 mℓ のガラスびんにゴム栓をしたものを用いた。NO，N_2 ガスの流通，吸収液の取出しなどは，すべてこのゴム栓に針付注射器を突き刺し，これを通して行った。

吸収液は，液量が約 2 mℓ になるように所要量の粉末試薬を吸収管に入れ，ゴム栓をした後，内部の空気を窒素で置換し，ついで所定量の水を注入して溶解して調製した。

NO ガスは，純 NO ガス，または窒素で 940ppm に稀釈したガスを用い，室温で流通法により吸収液に吸収させた。典型的な NO 導入量は，純 NO の場合は吸収液 2 mℓ にたいし 30mℓ/min の流速で10分間，稀釈ガスの場合は 400mℓ の吸収液を用い，同じ流速で3～5日間流通した。

^{15}NO に関する実験には真空装置を用いた。この場合の吸収管はバルブ，ジョイント付きガラス容器であり，^{15}NO はバッチ法で吸収させた。

赤外吸収スペクトルは DIGILAB，FTS-15B/D 型分光器を用いて KRS-5 によるサンドイッチ法で測定した。測定試料のサンプリングその他，吸収液が空気

＊ 本研究は，先に当所で実施された「固定燃焼装置からの窒素酸化物排出防止技術に関する研究」の一環として行われたものである。本報告を同研究の報告書「北海道工業開発試験所報告，第21号」の補遺とする。

**静修短期大学　札幌市豊平区清田153-799〒061-01

と接触する恐れのある操作は，すべて窒素ガス雰囲気中で行った。

pD 値は，pH メータで測定された値に0.40を加えて求めた[10]。

3. 実験結果

3.1 NO 吸収前および後の吸収液のスペクトル Fig. 1—(1)に標準重水吸収液のスペクトルを示した。(3)は同じ組成の軽水溶液のスペクトルである。これらの吸収液の pH(D) は5.2～5.8であった。

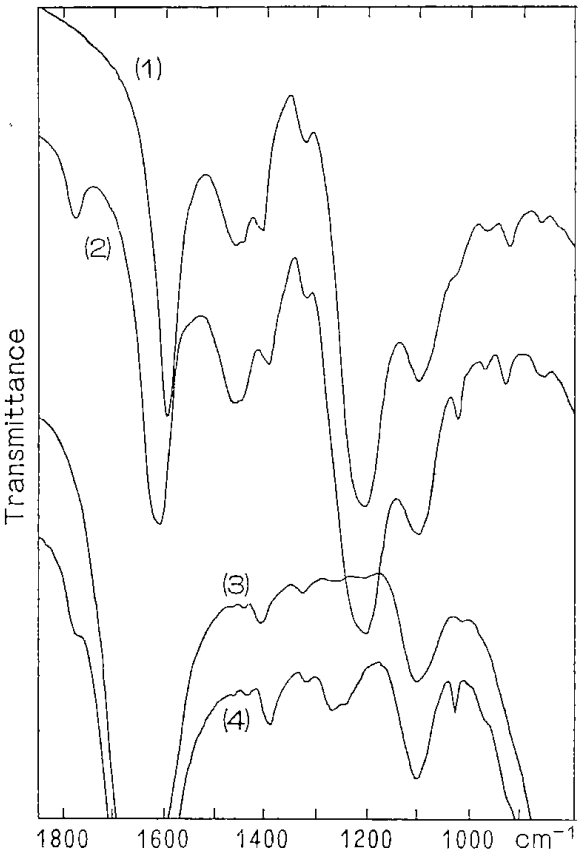

(1) (2) : $FeSO_4$ 0.1, Na_2edta 0.1, $MgSO_3$ 0.2 mol/ℓ D_2O solution before (1) and after (2) NO was absorbed. (3) (4) : corresponding H_2O solution before (3) and after (4) NO absorption.

Fig. 1. IR spectra of absorbing liquids before and after NO absorption.

1,597cm^{-1} および 1,405cm^{-1} の吸収帯は，edta 構造中の酢酸基のそれぞれ逆対称 (ν_aCOO) および対称伸縮振動 (ν_sCOO) によるものである。1,100cm^{-1} 吸収は SO_4^{--} の逆対称伸縮，また(3)に見られる1,630 cm^{-1} の強大な吸収および(1)の 1,210cm^{-1} はそれぞれ HOH，DOD 変角振動によるものである。(1)，(2)に現われている1,460cm^{-1} の吸収は HOD 変角振動に帰せられ，この HOD 分子は用いた試薬中の結晶水およびガラス器具の表面その他から溶液中に混入した H_2O によって生成したものである。935cm^{-1} に見られる微小な吸収は Na_2edta の重水溶液にも同程度の強度で現われているので edta によるものであり，恐らく edta 構造中の C–C 結合の伸縮によるものであろう。

Fig. 1—(2)および(4)は，それぞれ(1)および(3)に純 NO ガスを吸収させた後の吸収液のスペクトルである。この吸収液の pH (D) は7～8を示した。

NO の吸収によって 1,775cm^{-1} に新しい吸収帯が現われ，同時に 1,597cm^{-1} の ν_aCOO は約 13cm^{-1} 高波数側にシフトを示し(1,610cm^{-1}) かつ若干幅の広い吸収に変化した。また ν_sCOO は低波数シフトを示し 1,395cm^{-1} に移動した。1,260，1,230 近辺および 1,030cm^{-1} にも新しい吸収の出現が認められ，同時に

Table 1. IR bands of absorbing liquids before and after NO absorption. (cm^{-1}).

Absorbing liquids	After NO absorption	Assign
	1775	coordinated NO, νNO
1630	1630	H_2O, δHOH
	1620	$>\overset{+}{N}HCH_2COO$–Fe(Ⅱ) –NO and Fe(Ⅲ) edta, ν_aCOO
1597		$>NCH_2COO$ ＼ Fe(Ⅱ) ／ , ν_aCOO
	1610	$>NCH_2COO$ ＼ Fe(Ⅱ) ／ , ν_aCOO (NO)
1460		HDO, δHOD
1405		$>NCH_2COO$ ＼ Fe(Ⅱ) ／ , ν_sCOO
	1395	$>NCH_2COO$ ＼ Fe(Ⅱ) ／ , ν_sCOO (NO)
	1260, 1230	imido-di-sulfonate and or nitriro-tri-sulfonate, $-SO_3^-$, ν_aSO
1210	1210	D_2O, δDOD
1100	1100	SO_4^{--}, ν_aSO
	1030	imido-di-sulfonate and or nitriro-tri-sulfonate, $-SO_3^-$, ν_sSO
935	935	EDTA, νC–C

1,100cm^{-1} の吸収帯(SO_4^{--}) 強度が若干増加するのが認められた。1,260 および 1,230cm^{-1} の吸収に関しては再現性が必ずしも良くなく，実験のたびに波数および相対強度に多少の変動が認められた。窒素ガスで稀釈した NO の導入によって得られた結果は，純 NO によるものと一致した。各吸収帯の波数値をそれらの帰属とともに Table 1 に示した。

3.2 Fe(Ⅱ), Fe(Ⅲ), Mg(Ⅱ) および Na～edta 錯体重水溶液のスペクトル

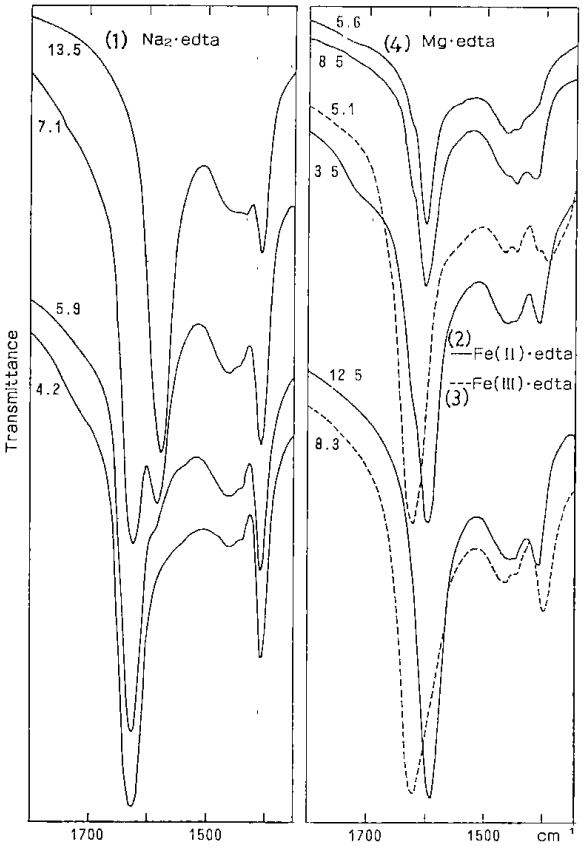

Fig. 2-a
Numbers by the curves represent the pD value of the solutions.

Fig. 2. IR spectra of EDTA complexes in D_2O solutions.

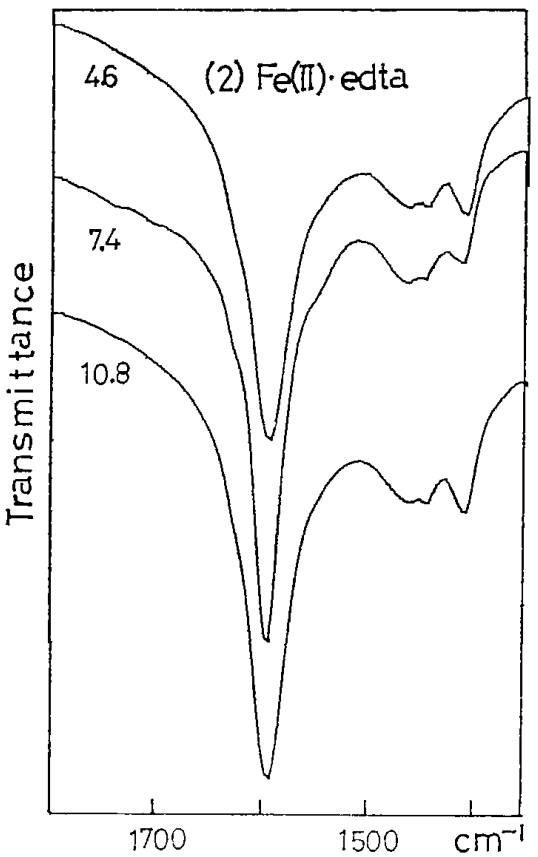

Fig-2-b

edta 錯体の νCOO, 特に ν_aCOO は錯体の化学構造，中心金属イオンなどの相違を反映して比較的大きなシフトを示すことが知られている。したがって，この吸収は吸収液中の錯体の化学構造を明らかにする上で，一つの手掛りとなる。標準的吸収液には，そのpD 範囲内で edta 錯体を形成しうる金属イオンとして Fe(Ⅱ), Mg(Ⅱ), が含まれており，また Fe(Ⅲ) の存在も予想され，さらには遊離した edta も存在しうる。またこれら錯体の化学構造は pD に依存し，したがってスペクトルも変化する。そこで 3.1 の考察にはまずこれらの錯体溶液についての νCOO の波数と

Table 2. IR bands of EDTA complexes in D_2O solutions. (cm^{-1})

Na_2edta	Mgedta	Fe(Ⅱ)edta	Fe(Ⅲ)edta	Assign[17]
1720		1725		$>NHCH_2COOH$, ν_aCOO
1625				$>\overset{+}{N}HCH_2COO^-$, ν_aCOO$^-$
	1625	1625		$>\overset{+}{N}HCH_2COO$–M, ν_aCOO
1580				$>NCH_2COO^-$, ν_aCOO$^-$
	1600	1595	1620	$>NCH_2COO$ $\diagdown$ M $\diagup$, ν_aCOO
1400	1405	1405	1395	EDTA, ν_sCOO

その pD 依存性を把握する必要がある。これらのうち，遊離の edta については中本ら[8] の，また Fe(Ⅱ)以外の錯体重水溶液については Sawyer ら[9] による報告がある。しかし，Sawyer らによるスペクトルは不鮮明であり，波数値の確実性に乏しい。

この理由から，上記各イオンの錯体重水溶液について標準的吸収液の NO 吸収前および後における pD値すなわち5.2〜8.0を含む pD 範囲で赤外吸収スペクトルの再測定を行った。

その結果を Fig. 2 に示した。(1)は Na_2edta の0.1 mol/ℓ 重水溶液であり，(2)，(3)および(4)はそれぞれ $FeSO_4$, $Fe_2(SO_4)_3$ あるいは $MgSO_3$ と Na_2edta のそれぞれについて約 0.1mol/ℓ になるように調製した混合重水溶液である。pD の調整には NaOH および H_2SO_4 を用いた。各スペクトルに添えた数値は pD 値を示す。νCOO の実測波数値をそれらの帰属とともにTable 2 に示した。

3.3 ^{15}NO シフトの測定

Fig. 1 で，1,775，1,260，1,230および 1,030cm^{-1} の各吸収は，NO 吸収反応生成物あるいは中間生成物によるものであることは疑いない。これらの生成物は窒素および硫黄化合物であることが予想される。その場合，窒素との結合が主として関与している振動の吸収帯では，窒素同位体 ^{15}N 化合物を用いると，十分に検知できる大きさの同位体シフトが予想される。そこで，^{15}NO ガスを吸収させた場合のスペクトルの変化を測定した。(Fig. 3)

その結果，1,775cm^{-1} の吸収は約 30cm^{-1} の低波数シフトを示し(1,745cm^{-1})，1,260，1,230および1,030 cm^{-1} の各吸収では検知しうるシフトは認められなかった。

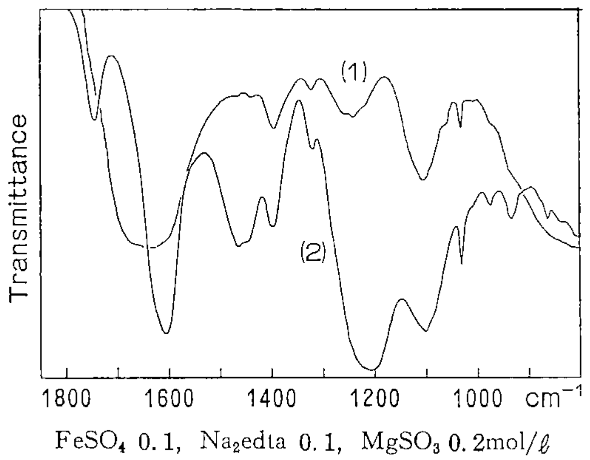

$FeSO_4$ 0.1, Na_2edta 0.1, $MgSO_3$ 0.2mol/ℓ
H_2O (1), D_2O (2) solutions.

Fig. 3. IR spectra of absorbing liquids after ^{15}NO was absorbed.

4. 考　察

4.1 吸収液のスペクトル

Fig. 1 の(1)で，νaCOO は 1,620cm^{-1} にごく小さな膨らみを持った 1,597cm^{-1} の鋭い1本の吸収帯として観測された。3.2の結果によると，1,597cm^{-1} の吸収は edta が Fe(Ⅱ)edta として存在するか，あるいは Mg-edta 錯塩と共存する場合にあらわれる。Fe(Ⅱ) および Mg(Ⅱ) の edta 錯塩安定度定数が，それぞれ14.33および 8.69[14] と著しく相違することを考慮すると，Fig. 1-(1) の実験条件下では，ほとんどすべての edta は Fe(Ⅱ)edta として溶解しているといえる。

SO_3^{--}による吸収帯 (935cm^{-1}) がスペクトル中に十分な強度として認められないことは，$MgSO_3$ があまり溶解していないことを示すものであり，このことは上述の結論と矛盾しない。

Sawyer ら[9] は 2 価金属イオンの edta 錯体に関する一連の研究を行い，それらの重水溶液に現われる 1,580〜1,595cm^{-1} の吸収が$>\underset{\underset{M(II)}{|}}{N}CH_2COO\diagup$によるものであることを示した。

このことから，1,597cm^{-1} の吸収は Fe(Ⅱ)edta のこの型の COO 基によるものと考えられる。この吸収が鋭いことは Fe(Ⅱ)edta のすべての COO 基が等価な状態にあることを示すものである。したがって，edta は Fe(Ⅱ) に対して6座配位しているであろう。

1,620cm^{-1} の小さな膨らみは，同じく Sawyer らの帰属から$>\overset{+}{N}HCH_2COO$–Fe(Ⅱ)型の COO 基によるものと考えられる。この溶液の pD (5.5前後) でこの型の結合がこの程度存在することは，Fig. 2 の Fe(Ⅱ)・edta の溶液に見られる pD=4.6 および7.4 における同じ吸収 (1,620cm^{-1}) の強度と比較して妥当である。Fe(Ⅲ)edta も 1,620cm^{-1} に吸収をもち，また吸収液中にて不純物として Fe(Ⅲ) が含まれうるが，pD=12.5で Fe(Ⅱ)・edta の D_2O 溶液のスペクトル(Fig. 2)にまったくこの膨らみが見られないことから，この膨らみが Fe(Ⅲ)edta の吸収である可能性はない。

4.2 NO 吸収後のスペクトル

4.2.1 1,775 および 1,600cm^{-1} 近辺の吸収帯

NO は多くの金属錯体と反応し，新しい NO 配位錯体を形成することはよく知られている。

1,775cm^{-1} の吸収は，その波数値，および^{15}N 置換

すると 30cm^{-1} の低波数シフトを示したこと，さらにシングレットであることなどから Fe(Ⅱ) edta の Fe(Ⅱ) に配位した NO の伸縮に帰属できる。2原子分子調和振動子として計算される NO 伸縮振動数の^{15}N シフト値は約32cm^{-1} であり，上の実測値と一致する。また，Fe(Ⅱ)edta に NO が配位すると，その νCOO に波数シフトが見られてもよいはずである。3.1で NO の吸収により ν_aCOO には 13cm^{-1} の高波数シフトが，また，ν_sCOO には 10cm^{-1} の低波数シフトが認められた。これらの事実も上述の帰属を支持する。

NO が金属錯体に配位する場合，M−N≡O$^+$，M−N=O$^-$，その他の多様な型をとることが知られており，錯体を触媒として NO を還元する場合，M−N=O$^-$ がもっとも望ましいとされている[15]。これらの配位 NO の伸縮波数は 2,300cm^{-1} から 1,000cm^{-1} 近辺の広範囲にわたっており，著しく高波数の場合は M−N≡O$^+$，著しく低波数の場合は M−N=O$^-$ であると見てよい。しかし，実測された 1,775cm^{-1} はこれらの中間領域にあり，波数値からどの結合型であるかを一義的に判定することはできない[11,18]。

NO 吸収反応における edta の役割を検索する目的で Fe(Ⅱ)–NO の NO 伸縮波数を測定した。$FeSO_4$ の 0.1mol/ℓ 水溶液に NO を導入し得られたFe(Ⅱ)–NO 水溶液で，配位 NO は 1,810cm^{-1} に吸収を示した。この結果両配位 NO の波数差は 35cm^{-1} であることがわかる。さきに述べたようにM−N≡O$^+$ と M−N=O$^-$ との波数差が 1,300cm^{-1} におよぶことと比較して，この 35cm^{-1} の差は非常に小さなものであることから，Fe(Ⅱ)edta に配位した場合と Fe(Ⅱ) に配位した場合とで NO の結合に著しい差異はないと考えられる。したがって，edta は NO の被還元性を高める作用は特に持たないものと考えられる。

なお，この結果は Fe(Ⅱ)–NO と Fe(Ⅱ)edta–NO の配位 NO を明確に区別でき，さらに両者の分別定量も可能なことを示唆している。このことは3.2に示された Fe(Ⅱ)edta と Fe(Ⅲ)edta の弁別など νCOO からの情報とともに，鉄 edta 系吸収液を用いる NO 吸収反応の研究に IR が有効な情報を与えることを示している。

ν_aCOO は NO の吸収により高波数にシフトを示すと同時に幅の広がりが認められた。これは1,620cm^{-1} 近辺に極大を持つ吸収が 1,610cm^{-1} の吸収に重なっているためと考えられる。この 1,620cm^{-1} 近辺の吸収については次のように考察される。Fe(Ⅱ) edta–NO 錯体で NO が Fe(Ⅱ) edta と1：1で配位し，かつ Fe(Ⅱ) が配位数6を取るものとすれば，

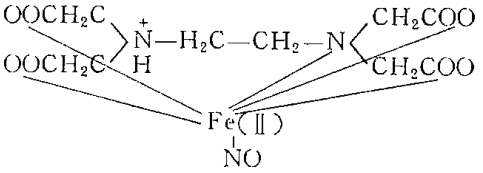

の型の錯体を形成していることが考えられる。その結果，$>\overset{|}{N}CH_2COO$–Fe(Ⅱ)–NO および $>\overset{+}{N}HCH_2COO$–Fe(Ⅱ)–NO の2種類のCOO基が存在し，それらがそれぞれ 1,610 cm^{-1} および 1,620cm^{-1} 近辺の吸収を与えているのであろう。pD＝7～8 の溶液中でこの酸性錯体が比較的多量に存在し得ることは，Fig. 2の(1)に示されたように pD=7.1での Na_2edta 溶液において酸性錯体 (1,625cm^{-1}) が相当多量に存在していることから推察される。

4.2.2　1,260，1,230および1,030cm^{-1} 吸収帯

Fig. 1－（2，4）に見られる 1,260，1,230 および 1,030cm^{-1} の吸収は，溶液中の最終生成物によるものであり，これらは窒素化合物，硫黄化合物あるいはN・S化合物であることが容易に予想される。そこで，多くのN，S化合物標準試薬について，水溶液およびこれら試薬を添加した吸収液のスペクトルを測定し，Fig. 1－（2，4）のそれと比較対照した。その結果，イミド・ジ・スルホン酸カリウム $HN(SO_3K)_2$ およ

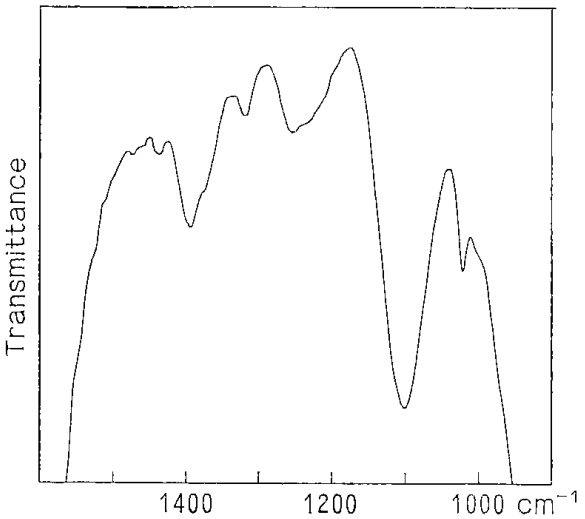

$NH(SO_3K)_2$; 10mg per 1 ml of $FeSO_4$ 0.18, Na_2edta 0.1, $MgSO_3$ 0.29 mol/ℓ D_2O solution.

Fig. 4.　IR spectra of $NH(SO_3K)_2$ dissolved in absorbing liquid.

びニトリロ・トリ・スルホン酸カリウム $N(SO_3K)_3 \cdot 2H_2O$ のスペクトルと酷似していることがわかった[16] (Fig. 4)。

したがって溶液中の生成物はイミド・ジ・スルホン酸塩または，ニトリロ・トリ・スルホン酸塩あるいはこれに類似した化合物であると考えられる。3.3において 1,260，1,230 および 1,030cm^{-1} の吸収は，いずれも検知しうる^{15}N シフトを示さなかったが，これらの吸収は前二者が $-SO_3^-$ の ν_3，1,030cm^{-1} は同じく ν_1 振動によるものと考えられるので，この事実は上述の同定と矛盾しない。

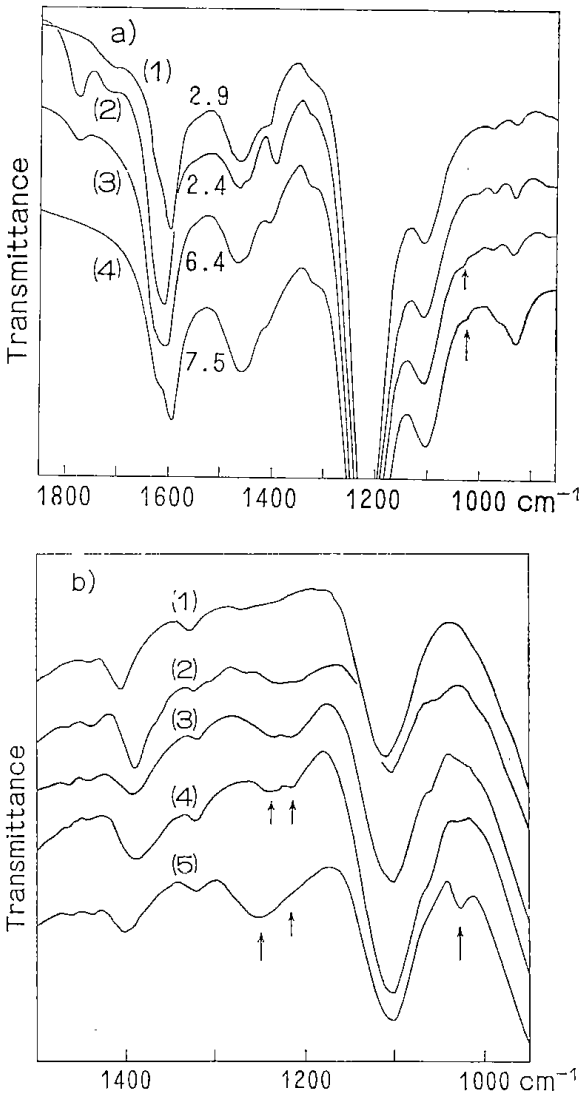

a): (1) : $FeSO_4$ 0.1, Na_2edta 0.1 mol/ℓ D_2O solution. (2) : (1)+NO. (3) : (2)+$MgSO_3$ 0.1 mol/ℓ, after 1.5 h. (4) : (2)+$MgSO_3$ 0.2 mol/ℓ, after 1.5 h. b); (1) : corresponding H_2O solution. (2) : (1)+NO. (3) : (2)+$MgSO_3$ 0.1 mol/ℓ, after 1.5 h. (4) : after 2.5 h. (5) : after 1 WeeK

Fig. 5 Spectral change in the reaction between coordinated NO and $MgSO_3$.

この液相生成物は NO–Fe(Ⅱ)edta と SO_3^{--} の反応により生成すると予想されたので，これを裏付ける目的で次の実験を行った。$MgSO_3$ を含まない標準吸収液($FeSO_4$，Na_2edta それぞれ 0.1mol/ℓ) に NO を吸収させ，その後，この液に $MgSO_3$ を添加して各段階のスペクトルを測定した。その結果をFig. 5に示した。(2)は NO 導入後のスペクトルである。この状態は安定であり，数か月保管してもまったくスペクトルに変化は認められなかったが，この液に $MgSO_3$ を添加すると配位 NO の吸収 (1,775cm^{-1}) が減少すると同時に，1,260，1,230 近辺および 1,030cm^{-1} に新しく吸収を生じるのが認められた。

これらの吸収帯，特に 1,260～1,230cm^{-1} 近辺のそれは時間の経過とともに多少のシフトと変形を示していることが図からわかる。この事実は最終生成物の生成に至る反応が何段階かの反応を経て，非常にゆっくりと進行することを示すものである。3.1において 1,260および 1,230cm^{-1} 近辺の吸収の再現性が必ずしも良くなかったのは，NO 導入後，スペクトル測定までの経過時間の相違か，あるいは何らかの微妙な条件の相違によって類似はしているものの多少異なった生成物を生成したためであろう。

液中生成物としては，上記物質の他に，3.1に述べたように NO 吸収により 1,100cm^{-1} の吸収強度が若干増加するので，SO_4^{--} が生成することも明らかである。

Fig. 5–(4)に 1,620cm^{-1}の吸収がかなりの強度で現われている。この吸収帯は，1,775cm^{-1} の吸収が認められないこと，およびこの液の pD が 7.5 であったことから $>\overset{+}{N}HCH_2COO$–Fe(Ⅱ)–NO，あるいは $>\overset{+}{N}HCH_2COO$–Fe(Ⅱ)によるものではありえず，したがって Fe(Ⅲ)edta の存在を示すものである。反応の経過中に Fe(Ⅱ)の一部が酸化され Fe(Ⅲ)が生成したことは明らかである。NO 中の不純物として導入された NO_2 のモル数は，吸収液中鉄イオンの 0.3% 前後であり，また実験中に空気が混入した可能性も小さいと考えられるので，おそらく，この反応系の何らかの過程を介して NO によって酸化され生成したものであろう。本実験の条件下では，SO_3^{--} が Fe(Ⅱ)の酸化防止剤としては十分機能していないことが明らかである。これは本実験の吸収液調製法では $MgSO_3$ の溶解度が小さいためであろうと考えられる。

文　献

1) 蓮井，押尾，大道，福寿，垂井，日本化学会誌，1978，(3)，447
2) 服部，河合，宮島，坂野，菅，斉藤，石川，菅野，公害，**12**，27 (1977)，**13**，35 (1978)
3) 田中，小泉，石原，電力中央研究所報告，275017 (1976)
4) T. Sekiya, Pro. Natl. Conf. Energy Environ. (USA), 5 th, 447 (1977)
5) K. Sawai and T. Gorai, Second Pacific Chemical Engineering Congress, 340 (1977)
6) 池田，福田，井戸川，三浦，安藤，化学工学協会，第43年会講演要旨集，E 106 (1978)
7) 佐藤，福田，井戸川，三浦，化学工学協会新潟大会，B-12 (1977)
8) K. Nakamoto, Y. Morimoto and A. E. Martell, *J. Am. Chem. Soc.*, **84**, 2081(1962), **85**, 309(1963)
9) D. T. Sawyer and J. E. Tackett, *J. Am. Chem. Soc.*, **85**, 314, 2390 (1963)
10) K. Mikkelson and S. O. Nielson, *J. Phys. Chem.* **64**, 632 (1960)
11) N. G. Connely, *Inorg. Chim. Acta, Rev.*, **6**, 47 (1972)
12) 服部久雄他，公害，**13**，1，35 (1978)
13) H. Sisler and L. F. Audrieth, *J. Am. Chem. Soc.*, **60**, 1947 (1938)
14) 吉野，藤本，水町，佐藤訳，コンプレクソン滴定，共立出版 (1958)
15) 長哲郎，大勝靖一，化学工業，**25**，1154 (1974)
16) $NH(SO_3K)_2$ および $N(SO_3K)_3$ の水溶液 IR スペクトルは，1,300～900cm^{-1} の領域において完全に一致した。
17) 文献 8，9) 参照
18) 増田勲，庄野利之，化学，**28**，859 (1973)

Infrared Study on NO absorption by Fe(II)edta · $MgSO_3$ Aqueous Solution. (I).

Masao HINO, Takashi FUKUDA, Junko NITTA*, and Yasuko HIRAMA

(Government Industrial Development Laboratory, Hokkaido. *Seishū Junior College)

SYNOPSIS:—Infrared spectra of $FeSO_4$, Na_2edta, $MgSO_3$–^{14}NO and ^{15}NO systems, and those of related substances were measured in aqueous solution phase. The results showed that EDTA present in the solution forming a complex of Fe(II) edta (ν_aCOO, 1,597cm^{-1}), NO is absorbed to the complex through the formation of NO–Fe(II) edta coordinate bond (νNO 1,775, ν_aCOO 1,610cm^{-1}), and that the coordinated NO react with SO_3^{--} to form imido-di-sulfonate or nitriro-tri-sulfonate and or compound analogous to them (νSO, 1,260, 1,230, 1,030cm^{-1}). Stretching vibration frequency of the coordinated ^{14}NO, 1,775cm^{-1}, suggests that the edta has no activity to promote the reduction of the NO. It was found that a part of the Fe(II) is oxidized to Fe(III) in the present reaction, which is considered to be probably caused from the absorbed NO. It should be also noted that Fe(II) edta–NO (1,775cm^{-1}) was distinguishably observable from Fe(II)–NO (1,810cm^{-1}), as well as Fe(II) edta (1,597cm^{-1}) from Fe(III) edta (1,620cm^{-1}) with the use of IR technique.

(燃料協会誌，第59巻第638号 (1980) pages 382～388)

北海道工業開発試験所報告
第 23 号

昭和56年3月10日　印刷
昭和56年3月16日　発行

発　行　所　工業技術院北海道工業開発試験所
札幌市豊平区月寒東2条17丁目2番1号
電　話　011 (851)　0 1 5 1

印　刷　所　富士プリント株式会社
札幌市中央区南16条西9丁目
電　話　011 (531)　4 7 1 1

REPORTS OF
THE GOVERNMENT INDUSTRIAL DEVELOPMENT LABORATORY, HOKKAIDO

No. 23 March 1981

Contents

Published by

The Government Industrial Development Laboratory, Hokkaido
2-Jo 17-Chome, Tsukisamu-Higashi, Toyohira-ku, Sapporo, Japan